Local Failure Induced By Greenwater Loading

Master Thesis

by

Filippos Kolovos

Student Number: 5623200

Chair:	Dr. ir. P.R. Wellens
Committee:	MSc. A.D. Boon
	Dr. A. Laskari

Date August 2024

Faculty Mechanical Engineering and Marine Technologies, TU Delft

Cover: Rogue Wave aboard the supertanker Esso Languedoc, taken by Philippe Lijour South Africa, 1980

TU Delft

Summary

The present Thesis contains a proposal concerning the graduation topic of the author, required for completing the Master's Programme "Offshore and Dredging Engineering" of the Technical University of Delft. The title of the Thesis is "Local Failure Induced by Greenwater Loading".

With the above topic the author aims to shed some light onto the green-water phenomena taking place in extreme weather conditions, which may lead to local failure. Even though these type of failures might not directly affect the global integrity of the whole offshore structure, they can lead to crack formation and propagation issues, and the introduction of corrosion entry points into the structure's interior. The aforementioned effects combined with fatigue loads throughout the life cycle of an offshore structure are the number one cause for structural health deterioration and vessel losses. Yet, most importantly there have been instances where greenwater induced failures have led to the loss of human lives. Therefore, the author considers the local failure caused by shipping of water events of significant interest from several perspectives, such as public safety, further technological advancement and improvement in the offshore structure design and financial gains.

The report is organized into seven chapters, beginning with the Research Objective section, which succinctly outlines the rationale, primary goals, and the chosen methodology for achieving the stated research objectives. The second chapter provides a review of previous literature related to green-water events and associated fields. The third chapter details the design process and calculations for the various components of the experimental setup utilized during the research. The fourth chapter describes the numerical environment and simulations employed in the design of the experimental layout and for comparing results with data collected in situ. The fifth chapter presents the findings from the experimental trials, while the sixth chapter offers an analysis and discussion of the results from both the experiments and the simulations conducted in this Thesis. Finally, the last chapter suggests potential improvements and alternative approaches that could enhance the current setup or explore scientifically interesting topics that were not thoroughly investigated in this study.

The Thesis was completed under the supervision of Assoc. Prof. Dr.ir P.R Wellens, and in cooperation with the Ship Hydromechanics Lab of the faculty of Mechanical Engineering and Marine Technologies of the Technical University of Delft.

I extend my deepest gratitude to all those who have provided their assistance and support throughout the duration of the thesis, both technically and interpersonally.

The author

Contents

List of Figures

List of Tables

1

Research Objective

1.1. Research Objective

Greenwater events remain a significant challenge for the scientific community due to their complexity and infrequent occurrence, making them difficult to fully understand. However, these shipping water events, often triggered by extreme weather conditions, can have dire consequences for the safety of passengers and crew during offshore operations. There have been a few documented cases of severe greenwater incidents leading to the tragic loss of human lives. Additionally, the substantial forces generated during such events can cause local structural failures or lead to micro-cracking and the long-term degradation of a structure's integrity.

It is evident that studying these shipping water phenomena holds substantial social and economic benefits. A deeper understanding of greenwater loading and the associated failure mechanisms could lead to the improved design of offshore structures and vessels, enabling them to better withstand these conditions and reducing the risk of accidents and casualties. Furthermore, by analyzing greenwater events, the primary risks to crew members and passengers on ships can be identified, resulting in improved safety protocols and procedures. Economically, minimizing the likelihood of damage during extreme weather conditions can yield significant savings in maintenance and repair costs while extending the lifespan of marine structures. This is particularly crucial in the long term, as cracking and corrosion progressing within hulls are the leading causes of marine structure decommissioning.

Existing literature primarily focuses on breaking down the mechanisms and phenomena associated with greenwater events and developing models to predict the loads generated by shipping water. However, to the best of the author's knowledge, no studies have specifically examined failure caused by greenwater loads. This Master's Thesis presents an opportunity to explore the topic of "Local Failure Induced by Greenwater Loading," an innovative and challenging area of research that has not been previously investigated. The research objective is to identify the dominant mechanisms during shipping water events that lead to material failure, as well as the parameters that influence them, and to draw connections between sea-state characteristics and the occurrence of failure.

1.2. Thesis Goal

The goal of this Thesis is to thoroughly analyze material failure caused by shipping water events by simulating and recording instances in a small-scale experimental setup. Additionally, numerical CFD simulations will be employed to test additional hypothetical cases similar to those produced under laboratory conditions, where all variables can be precisely controlled and monitored. The focus will be on comparing the results from both simulations and experiments. This approach will facilitate a parametric study that combines artificial and scaled-down real-life data to better identify the mechanisms that could potentially lead to failure. Moreover, the comparison and analysis of discrepancies between experimental and numerical results will shed light on the potential gap between predicted scenarios

and real-world applications. Ultimately, the Thesis will have achieved its goal if instances of failure are observed and graphs can be generated that correlate specific aspects of the incoming sea-state with the probability of material failure. In summary, the research question guiding this project is:

"Can material failure caused by greenwater events be achieved in experimental trials, and which are the wave characteristics that mostly affect the dominant mechanisms responsible for it?"

2

Background Literature

2.1. Greenwater Cases and Mechanisms

In extreme weather conditions due to the relative motion between a vessel and the sea state or due to tall waves reaching the structure, there can be instances of large bodies of water exceeding freeboard. This can lead to significant volumes of water going onboard crushing on the deck of offshore structures. These events are called shipping of water or greenwater events. The loads created by such phenomena can be rather large, often resulting in damaged equipment and superstructures on deck, or even in worse cases local failure of structural members.

Research focusing on different aspects of shipping of water events has noticeably increased during the last two decades. Although, several factors such as the strongly non-linear water flows that are generated during the greenwater processes, the high variability and the several factors affecting shipping of water events, as well as the extremely short duration and interaction of the mechanisms involved deem any accurate analytical and numerical solutions still a challenge.

2.1.1. Elementary Loading Processes

In principle, greenwater events can be categorized as a water impact phenomenon. From experiments conducted with unidirectional breaking waves investigating sloshing phemenona on a simple and a corrugated vertical wall, it was concluded that three main mechanisms determine the pressure distribution and the loads induced during water impact phenomena [39]. These mechanisms were named *Elementary Loading Processes* by the authors, because the behaviour of every fluid impact phenomenon, can be broken-down in a different pattern and sequence that these mechanisms appear, and interact with each other.

These mechanisms are connected with the physical processes of the pressure wave propagating through the liquid phase due to the liquid compressibility (*Direct Impact*), the sharp change of liquid momentum direction in front of an obstacle (*Jet Formation*) and the pressure oscillations of the entrapped or escaping gas due to the gas compressibility (*Pulsating Gas Pocket*).

2.1.2. Greenwater Cases

In shipping of water events there are usually four distinct stages. Firstly, the wave will exceed the free board of the structure, and the water goes on board in a manner that is heavily affected by the vessel's motion and the wave's characteristics. Then, an initial body of water will crush on board creating jet-type flows. Thirdly, the largest mass of the over-topping fluid will go onboard and will start propagating as a shallow water wave. Finally, the moving body of water will hit an on deck structures or equipment creating a second upwards travelling jet-like flow, until the gravitational pull overcomes the inertial forces of the fluid and the water spills of deck, designating the end of the phenomenon.

Although, the above stages are present in various types of greenwater events, the properties of each stage and the elementary loading processes involved may differ depending on factors such as the freeboard exceedance, the relative motion between the wave and the structure, free-surface instabilities and wave characteristics and others. So far, in the literature several categories greenwater event types have been identified which will be presented further below. This distinction between the shipping of water cases is used so that the water on deck features are examined in terms of incoming-wave and kinematic variables to fully describe the physical phenomena which are involved.

The first type of shipping of water category firstly identified was the dam-break. From observations made in [47], [14], Buckner in [6] was able to correlate the fluid properties and the flows created onboard from the water exceeding the freeboard to those taking place during a dry dam-break scenario. Thus, the first category was named dambreak (DB) green water event. In dambreak shipping of water cases the body of water flows onboard as consistent mass with a joint front, without any strong initial flow plunging onto the deck or air pockets formulating.

Bercelona et al. [2] conducted experiments investigating the water on deck during greenwater events. A single shipping of water event was simulated using with head-sea wave on a stationary vessel, using the focused wave train method. By altering the phase of wave components a small train of the waves was generated, where most of the energy was focused on a central wave whose properties can be calculated a priori, while the other waves are limited to small surface disturbances. For the experiments three bow geometries were used, two elliptical and a circular bow with the geometry corresponding to real life vessels. The results from [2] showed that the velocity of the on deck water flow at the centerline of the vessel, remains relatively unchanged for different rounded bow shapes, and thus doesn't depend on the shape. Moreover, it was observed that the first body of water that will most likely go onboard and hit deck structures is the one coming from the fore bow of the vessel. Both of these conclusions, suggested that a two-dimensional flow conditions can be used without great loss of accuracy, especially for highlighting the mechanisms and the different stages involved during shipping of water events, which are not overshadowed by 3D phenomena and are easier to observe at midline.

Greco et al. also investigated the effects of green water loading on a stationary barge-shaped vessel in head sea conditions using experimental and numerical tools [16]. For the experimental trials, the analytical equations used for describing the water flows, as well as the numerical simulations were conducted in 2D conditions. The aim of the investigation was to simplify the phenomena, so that a detailed description of the behaviour of the flow and the loads exerted on the structure could be provided.

Greco et al. in [15] continued their previous work examining stationary blunt bow vessels, by updating the numerical model for simulating shipping of water events and conducting additional experiments. During the experimental trials in [16], greenwater scenarios which did not match the (DB) events, that had been reported, but not accurately documented and categorized in literature before were recorded. The newly identified type of shipping of water events that were introduced were named plunging wave (PW), plunging wave with dam-break (PDB), and hammerfirst (HF) greenwater events.

Greco et al. also conducted a parametric study in [15] based on incoming wave kinematics for the different types of shipping of water scenarios. The results showed strong correlation between the type of green water loading cases and the steepness, ϵ, of the incoming wave, the maximum vertical velocity of the wave ,W_w, and the vertical velocity, W, at the bow of the structure.

It was observed that for small values of ϵ and a high ratio W_w/W, the shipping of water event will probably resemble a (DB) event.As the ratio steepness increases in value, or the ratio of W_w/W decreases the PDB case starts appearing. During PDB events an initial vain of water crushes onto the deck and the rest of the volume over-spills on deck trapping small amounts of air. The cavities formed during PDB events collapse while turning into bubbles aerating the flow and getting carried away by it.

For moderate to high steepness there is a threshold where for very high ratios of W_w/W, the plunging impact becomes the dominant mechanism and the PW greenwater case appears. During plunging

wave cases most of over-topping mass of fluid plunges rapidly on board creating a strong jet that propagates both forward onto the deck and backwards towards the bow, enclosing notable amounts of air initially, which break into numerous smaller air-pockets.

Finally, for very steep waves, meaning high ϵ values, the HF case appears with the phenomena being stronger as the ratio W_w/W drops. During the hammer fist cases the body of water exceeds the free board in a coherent column of water with unchanged direction and thickness. When gravity becomes the dominant force, the large body of water crushes on board in a uniform manner. The motion of fluid resembles a hammer impact, hitting the deck almost simultaneously, and enclosing small portions of air at the same time.

Even thought the HF cases are rarely observed in literature, they present unique features compared to the other shipping of water cased regarding the flow kinematics that are observed at the early stages of the event. After the incoming waves crushes on the hull of a vessel, a strong water jet is usually created leading to a run-up phase. This stage is over once the body of water surpasses the freeboard level reaching its maximum exceedance of the freeboard. The vertical velocities observed during the run-up phase during the HF greenwater events are rather high, and can be twice as large as those observed in other scenarios. Additionally, the horizontal component of the water velocity once the water reaches the maximum exceedance has a significant contribution to the overall velocity, whereas it is nearly zero and considered negligible for the other scenarios.

The water profiles for each of the mentioned cases, and the ratio W_w/W and steepness, ϵ, area for which they appear are presented below (Fig2.3). Case (e) is a case which does not correspond to a shipping of water event, but it is named 'whitewater'. During whitewater occurrences of spray effects take place and no substantial loads are exerted on the structure, as no significant water impact takes place.

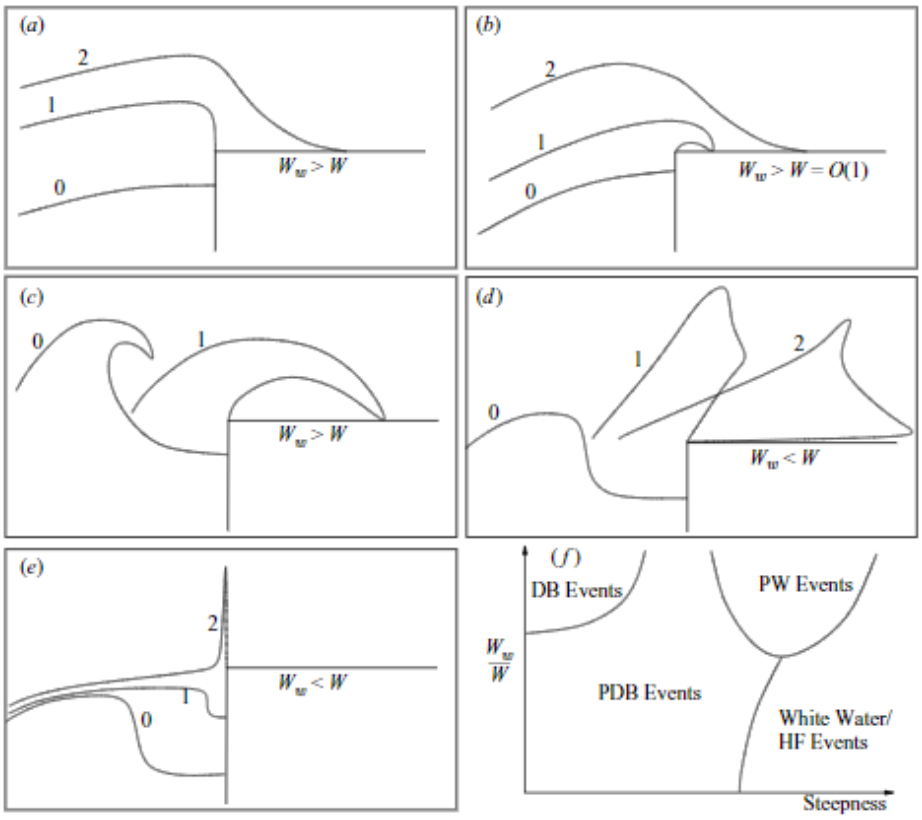

Figure 2.1: Greenwater water profiles and values of W_w/W and ϵ which generate them (Figure originally from [15]).

Zhang et al. [56] investigated wave over-topping on stationary 2D structures based on FPSO vessel during shipping of water events. They researchers conducted numerical simulations based on a VOF surface solver schemes continuing the work carried out in [57], while simulating additional loading scenarios using train waves that were generated by the concentrated wave train method. In the simulations they conducted, they were able to observe all the above greenwater cases that were described by Greco et al. [15]. Furthermore, Zhang et al. analysing the data of the recorded instances, proposed different criteria for classification of the shipping of water events, which underline more clearly the physics and parameters that involved in each shipping of water case.

The new classification was based on dimensions values of (A/λ_p) and (λ_p/D), where D the draft of the structure, A the wave amplitude which is denoted as η in the current research, and $_p$ which is denoted as L. This classification presents similar graphs as then in [15], but emphasizes on the local effects of the structure on the wave field (Fig. 2.2). From the simulations it was evident that HF type events occur when small wave length and large wave steepness are present. The DB events appeared for small wave steepness (regardless of the incident wave length), and PDB which are the most common form of overtopping and are more likely to be caused by waves of moderate steepness and intermediate wave length, or by long waves of large crest height. These same general trends appear to hold regardless of relative freeboard f/D, which is the freeboard devided by the draft of the structure. It is noted, that the freeboard does in fact have some effect on specific events. For example, DB type events become less common as the freeboard increases.

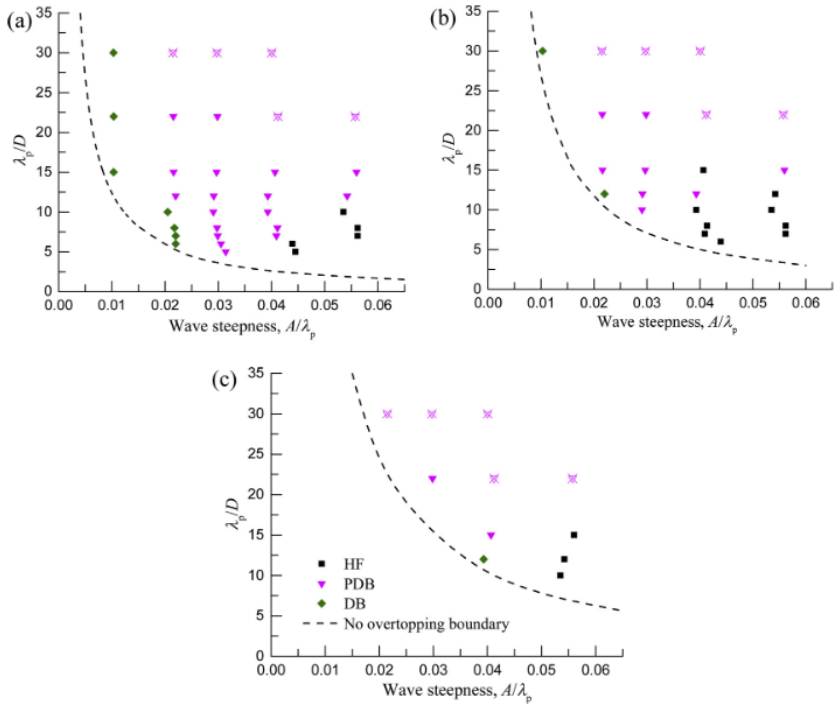

Figure 2.2: New greenwater event classification. The hollow shapes with an 'X' indicate slamming, which did not result in shipping of water events (Figure from [56]),

Hernández-Fontes et al. in [23] investigated the application of the wet dam-break method for describing the interaction of the generated bores with a structure, and the flow produced from it. Specifically, the research was focused on analysing the features of the air cavities formed during green water events, the spatial and temporal aspects of the incident flow and the water on deck, the effect of freeboard and downstream position to the shipping of water event, and establishing a relationship between the kinematics of greenwater with that of the incident bore.

By using four different ratios of upstream and downstream water depth, h_1 and h_0 respectively and

producing irregular waves instead of regular in [16], the researchers were able to simulate the DB and the PDB events similar to those described in [15]. Furthermore, they were able to simulate an event strongly resembling the hammerfist case. However, in the event that resembled the HF event generated in [23], a large cavity formation took place due to significant air entrapped near the edge of the deck.

Examining the kinematics of shipping of water events a new labeling was suggested by Hernández-Fontes et al. The PDB scenario was proposed to be renamed pludging dam-break with small cavity, PDB_{sc}. Finally, the recently observed case was named pludging dam-break with large cavity, PDB_{LC} ,and was categorised as a new separate greenwater scenario, different from the HF case. The PDB_{LC} case presents a coherent column of water formulation like the Hf scenario in the early stages. Then, a vain of water plunges initially onto the deck, creating a jet propagating in both directions, trapping a large ammount of air. In the end, the rest of the of the fluid mass spills onboard in a manner that resembles the PDB case. The above process can be seen in (Fig.**??**).

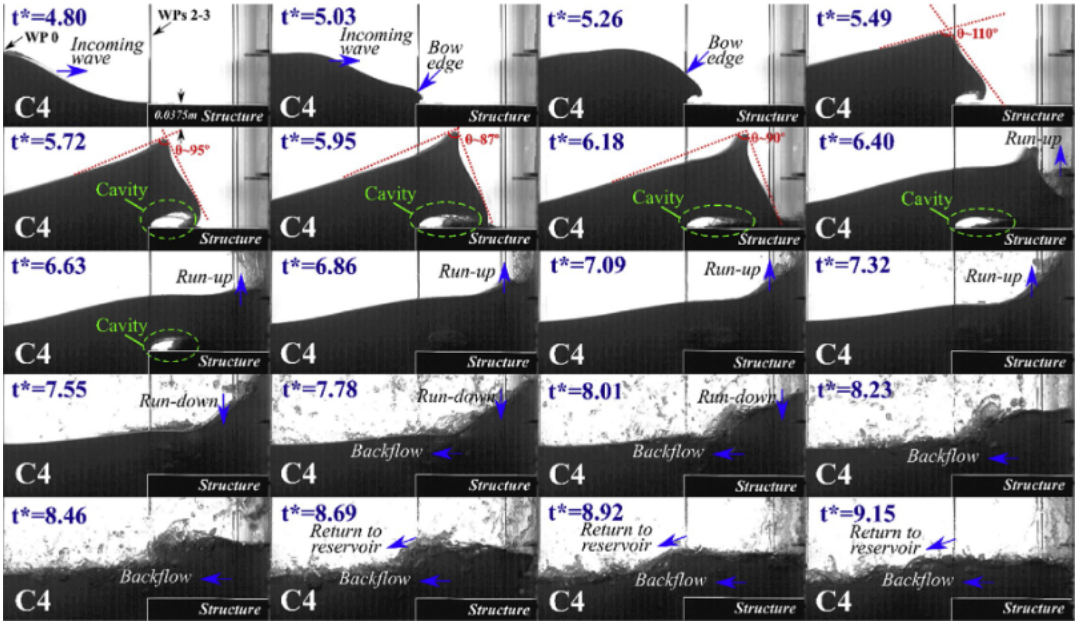

Figure 2.3: Greenwater water profiles and values of W_w/W and ϵ which generate them (Figure originally from [15])

2.2. Greenwater Loading Models

2.2.1. Flow Description

In the existing literature, there have been multiple efforts to derive semi-empirical or analytical formulations that can describe the mechanisms of the greenwater loading. Significant steps have been made to accurately describe the loads induced by shipping of water events. However, it is still a challenge to adequately describe the behaviour of the water once it exceeds the freeboard until the fluid spills off deck using the existing equations.

Dam-Break

The most widely found set of equations to describe the water flow on deck during shipping of water events were devised by Stoker [53]. Stoker expanded the work of Ritter, who was the first to analytically examine the problem of the water flow after a dam break scenario. Ritter's solution is only applicable in the case of a dry dam break , where the downstream water depth is zero, while assuming that the removal of the gate is instantaneous and the terrain is horizontal and frictionless.

Stoker's equations, like Ritter's, were derived by solving the Saint-Venants equations describing water flows in channels. Stoker was able to describe the flow created after the breaking of a dam, covering the whole range of downstream, h_0, to upstream h_1 ratio $0 \leq h_0/h_1 < 1$. The analytical solution by Stoker were able to describe cases such as the hydraulic jump which could not be described by Ritter.

The equations are based on three main assumptions. First assumption is that the dam gate vanishes instantaneously. This means that means that no upward velocity is introduced to the fluid thought the boundary layer, which is in contact to the opening gates in real life applications. Secondly, in Stoker's equations it is assumed that both the upstream and downstream parts extend in a semi-infinite plane each, down scaling the problem into a one dimension flow problem. This results to boundary layer effects from the side of walls or channels to be ignored. Furthermore, the upstream flow of water remains steady, as the upstream volume is infinite and the water depth is constant. Finally, it is assumed that the flow propagates into a horizontal and frictionless plane.

The dry dam-break solutions can describe adequately the flow during some greenwater events. The results offer a sufficient depiction of the fluid behaviour, after the wave have crushed initially on board and the water starts propagating, a few moments later as a swallow water wave on deck [40]. The equations for the most important quantities (Eq. 2.1-2.6) of the dry dam-break scenario applicable for $x/t < 2\sqrt{gh_1}$ are presented below:

$$h(x,t) = \frac{1}{9g}(2\sqrt{(gh_1)} - x/t)^2 \tag{2.1}$$

$$U(x,t) = \frac{2}{3}(x/t + \sqrt{(gh_1)}) \tag{2.2}$$

$$u_s = 2\sqrt{gh_1} \tag{2.3}$$

$$Q(x,t) = \frac{8t}{27}\sqrt{gh_1^3} \tag{2.4}$$

$$M_D(x,t) = \frac{4}{81g}(x/t + \sqrt{gh_1})^2(x/t - 2\sqrt{gh_1})^2 \tag{2.5}$$

$$M_{D_{max}} = 0.25gh_1^2 \tag{2.6}$$

, where h is the water depth, U the depth-averaged velocity of the created bore, u_s the velocity of the tip of the surge created before the bore, Q the volume of water flowing through the gate, M_D the moment flux the horizontal direction, $M_{D_{max}}$ the maximum moment flux in the x direction, t the time variable, and x the horizontal coordinate [45],[56].

Although, the influence of friction produces some deviations between the estimated flow properties and the measured flow on board. Yang et al. [55] conducted a series of experimental trials in a rectangular flume tank, examining the flow created from the dam-break problem for a wide range of downstream to upstream water depth ratios. The researches investigated the influence of bottom resistance on wave front profile for dry-dambreak scenarios, and the accuracy of exiting analytical solution on the wave height behind the wave front surge for wet-beds.

Yang et. al concluded that the bottom resistance exhibits significant influence on the wave front celery and mostly, on the wave front profile. The wave front slope increase when the upstream water depth ,h_1, increases, and decreases as the flow propagates further away from the position of the dam-gate (x=0), which is not accurately described by Stoker's equations. Similar observations were made by [6] where from the experiments conducted it was observed that the dam-break analytical solutions could not handle the found curvature in the initial water flow. Finally, Yang et al. verified that Stoker's solution can predict reasonably well the wave front celerity and the wave height behind the initial surge for all wave front profiles.

Zhang et al. in [57] examined the effect of blow flare angle on overtopping during greenwater events.

Using CFD simulations with a VOF surface capturing scheme, two dimensional fixed rectangular box representing an FPSO unit, was simulated with bow flare angles of 10,30, and 50 degrees. The waves used for the shipping of water events were generated using the focused wave train method, and a wide range of steepness and relative length are considered. The researchers compared the results with the analytical solutions to the dam-break problem derived by Stoker. They concluded that the classical dambreak model was seen to over predict the momentum flux, and at the same time under predict the overtopping volume in several cases.

Modified Dam-Break

Continuing the work of [57], Zhang et al. [56] conducted additional simulations based on greenwater overtopping on a 2D rectangular box. Moreover, the researchers identified multiple parameters that resulted in the variation between the theoretical values of the dry dam break problem and those calculated numerically. These variations were attributed to four factors mainly. First factor is that the greenwater over-topping has a finite duration. Secondly, there is a finite volume of water going onboard during each event. Thirdly. the local geometry at the edge of the bow affect the shipping of water events, and lastly, the horizontal momentum in the crest of wave that exceeds the freeboard can significantly differ from the analytical value. Zhang et al. proposed new modified dry dam-breaks equations (MDB) based on the solutions of Stoker, where the over-topping takes place on a structure with zero bow flare angle, and bottom friction is ignored.

In terms of the finite duration, the classical dam-break problem was extended to incorporate the limited duration of events, by allowing the fluid level exceeding the freeboard to vary in time. This was done by introducing a vertical input velocity on the fluid. Zhang et al. solving the swallow water equations for propagating waves concluded the vertical velocity is approximately sinusoidal in time, even for steep waves. The vertical velocity is given in (Eq.2.7) for $x \leq 0$&$0 \leq t \leq T_0$.

$$q(x,t) = \frac{\pi h_1}{T_0} cos(\frac{\pi t}{T_0}) \tag{2.7}$$

,where $2T_0$ is the time taken for the far upstream water depth to increase from zero to its maximum value and decrease back to zero, and h_1 the maximum water exceedance at the freeboard for a greenwater event, instead of the water height upstream for the dam-break problem. The water height upstream of the edge of the deck is given below:

$$h(x,t) = h_1 sin(\frac{\pi t}{T_0}) \tag{2.8}$$

Zhang et al. in [57] concluded that for estimating the severity during shipping of water events, besides the water height exceeding the freeboard, another quantity should be considered as well. This quantity was named relative duration ,T'. The relative duration given in (Eq.2.9) represents the ratio of the time for which the upstream water is available to flow through the dam, in the modified dam-break, or the time scale associated with run out for a classic dam break. In practise, if the relative duration is small, the MDB has a limited time for water to flow on to the dry bed. Thus, the momentum flux and volume of water that goes onboard, which affect the severity of the greenwater events, decrease with a decrease in the relative duration. When, T' is sufficiently long the properties of the fluid will resemble those of the classical dam-break.

$$T' = \frac{T_0}{\sqrt{h_1/g}} \tag{2.9}$$

The researchers in [56] analysing the results from the simulations, plotted the dimensionless numbers of relative overtopping volume and the transition zone normalized by maximum exceedance length, to the relative time. They observed that different overtopping types tend to cluster in different ranges of relative duration. The HF events tend to occur for T'$\tilde{<}$3.5, whilst DB events are more common for larger durations associated with T'$\tilde{>}$5-6, potentially producing a new system for categorizing greenwater events. Most importantly, Zhang et al. where able to observe that the transition length is between 0.6 and 1.6 times the maximum freeboard exceedance length for all scenarios. This is arguably the first quantitative estimate of the extent of this transient zone, and could be used in practice to determine

locations on deck where impact due to plunging may occur.

Regarding the finite crest width, an alternative way to introduce transient effects is to modify the dam so that it has a finite upstream width so the volume of the run out water is finite. This can be achieved by modifying the initial conditions such as:

$$h(|x + l_d/2| \leq l_d/2, 0) = h_1 \tag{2.10}$$

, where l_d is the width of the dam. With this conditions the time T' changes, along with the quantities that are calculated after integrating, such as the total volume of fluid that goes onboard. The physical meaning behind this limit is that that for small T', the finite crest width does not contribute to the transient nature of the overtopping events. The duration of the overtopping events is too short for the finite crest width to influence/limit the greenwater momentum flux or overtopping volume.

Accounting for the local geometry, a 'bottom step' , Δz was suggested from the position of the deck edge (x=0) and upstream. This bottom step is incorporated through (Eq.2.7). With this modification the fluid contributing to the dam run out results to a larger water level just upstream of the dam compared to the flat bed geometry, leading to an increase of the run out volume and momentum flux so that the MDB values become closer to the ones calculated numerically. However, no guideline is given on the Δz length.

Finally, for the initial horizontal momentum, Zhang et al. solved the swallow water equations. assuming the duration effect could be ignored, which means that a uniform depth averaged horizontal velocity, U_x, and upstream water dept, h_1 can be assumed. They derived (Eq. 2.11):

$$M_{D,max} = 0.25gh_1^2(\frac{Ux}{2\sqrt{gh_1}} + 1)^4 \tag{2.11}$$

The equation above was able to give a more accurate estimate to the maximum horizontal momentum flex compared to the one calculated using the traditional dam break equations. The maximum horizontal momentum flux showed significant variations in values compared with the equations of Stoker, especially in the case of waves with short wavelengths [56]. As observed in the simulations, short waves were fully reflected by structure, whereas for the case of very long waves compared to the size of the FPSO model vessel, the values estimated from the traditional dam break solutions, matched well with the ones acquired by the CFD simulations.

2.2.2. Horizontal Loading

The horizontal loads induced during green water events, have a very similar profile to those of bores crushing on vertical structures [6]. Several publications exist in fluid impact literature validating the profile of the loads exerted in the horizontal direction as presented in (Fig.2.4), where two distinct stages can be identified.

The pressure signals usually exhibit two peaks during the green water event. The first peak with a very short rising time is caused by the impact of the merged water front against the wall, and the second peak with a longer rising time is caused by the fall of the piled-up water, which resembles sloshing events. Pressure time histories show the typical church roof profile with a single, prominent peak immediately followed by a gradually decreasing pressure gradient.

The earliest stage of the horizontal loading is characterized by highly dynamic phenomena, where the water initially hits the ondeck structure and the water flow is fully deflected. As the main body of water follows behind the initial impact there's a pressure built-up, that is caused by the momentum of the incoming water mass. Due to the incomprensibility of water, the pressure is released in a form of a jet shooting upwards towards the wall of the superstructure.

Based on the relationship between the maximum pressure Pmax and the corresponding maximum kinetic energy ρU_{max}^2, the impact coefficient c_i varies from 0.22 to 1.28 without significant deviation

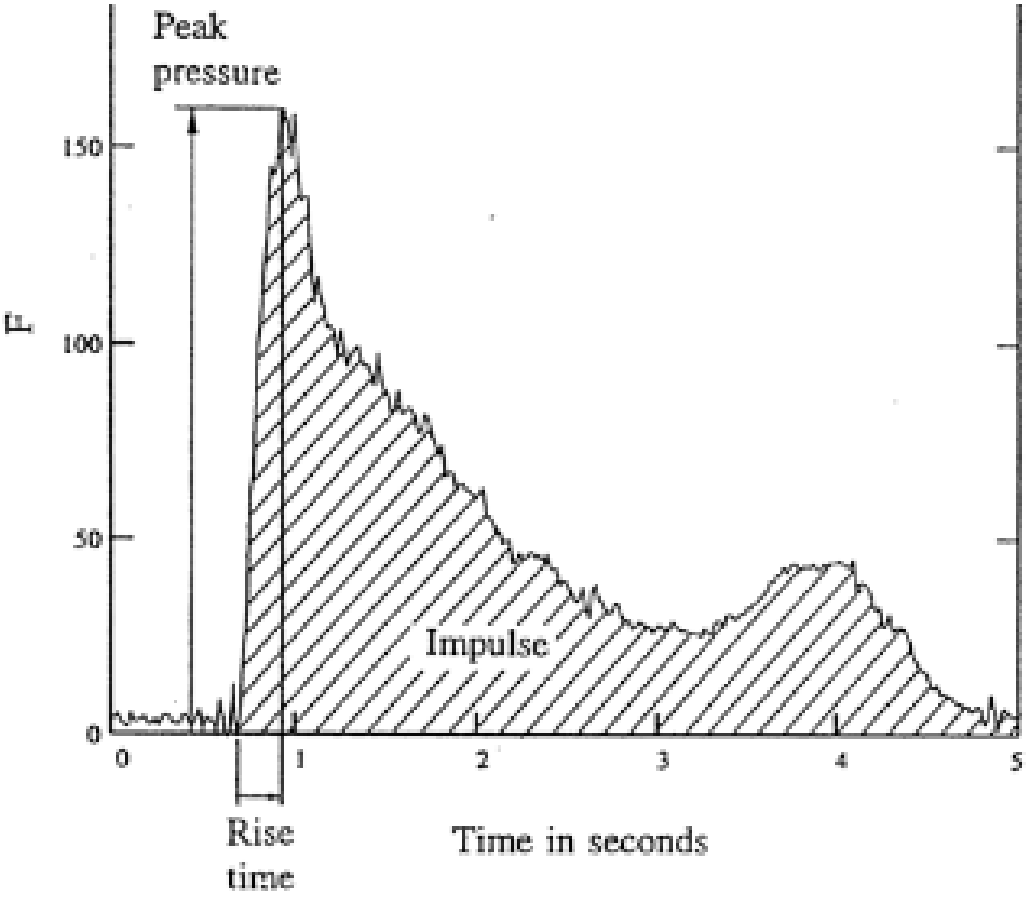

Figure 2.4: Horizontal forces profile during greenwater events (figure taken from [2])

from the mean value of 0.48. Similarly, the correlation between Pmax and ρC2 shows that the range of $c_i^{'}$ is from 0.29 to 1.58 with an average of 0.95 on all pressure measurements, and 1.54 based on maximum pressures recorded.. In practices the value of $c_i^{'} = 1.5$ may be used in practical applications

The maximum instantaneous pressures p_{max} were related to the pressure rise time tr with a relationship $p_{max} = 52t_r^{-0.91}$ that separates impulsive pressures from those with a relatively longer rise time, typically located near the deck surface. At the lower elevation above the deck surface the impact pressures may be less impulsive but the resulting peak impact pressures.

After most of the kinetic energy of the fluid has transformed to potential energy, the second stage of the horizontal loading begins. In this stage the flow is characterised by flow stagnation points appearing on the lower parts of the vertical wall referred to as the bouragge [6]. The gravitational force is starting to become larger than the inertial forces of the fluid, pulling the fluid back down, leading to a quasi-static type of load, resulting to a second peak in (Fig.2.14).

The pressures and therefore the loads exerted on the structure during both stages of a green water loading, are heavily affected by the location of the point along the superstructure. For the lowest parts of the wall it was found out that the impulse load is the dominant one in most cases. Greco et al. [15] observed that for the PDB and the HF events the interaction with a vertical wall on the deck caused the highest loads, with the highest pressures recorded at the centerline at the base of the wall, where the greenwater mechanisms are stronger and less affected by 3D phenomena. Similar observations were made by [2], who concluded that for horizontal loading the second quasi-stating loading cycle is weaker as the fluid is not restricted and is flowing off the deck, reducing the mass of water involved in

the phenomenon [2].

However, Greco et al. in [17] observed that when 3D phenomena affect the flow, specific cases of structure geometries and waves combinations, or upper parts of the vertical walls, the peak force resulting from the second stage of the horizontal loading can have a values similar to the first peak. In [15] the researches also noted that for upper parts of a vertical wall the experiments showed a second peak of the same order of magnitude in the evolution of the pressure along the wall. This peak appeared in the later stages and was caused by the falling water.

It is very difficult to formulate analytical equations that describe adequately the forces generated in shipping of water events, because the mechanisms involved are affected by a combinations of factors. Green water events are heavily influenced by the wave characteristics, and the structural properties of the system, contain highly sensitive and localised mechanisms, and interwind with other 3D phenomena.

Hamoudi & Varyani presented a simple method for calculating an approximation to the horizontal loads on a deck structure in head sea states [19]. The forces exerted in the horizontal direction are caused from the mass of water hitting the structure, with the most difficult task is identifying accurately the volume of water going onboard. In order to simplify the problem and liniarize it, the onboard volume of water is calculated by discretizing in a large number of rectangular cross-sections.

$$V = \int_0^L kB(x)Z(x)dx \tag{2.12}$$

,where L is the distance that the liquid covers from the edge of the deck until it hits some ondeck structure, k is a dispersion coefficient that takes into account the water and air mixture, B(x) and Z(x) are the width and height dimensions for each finite rectangular respectively as a function of the longitudinal direction. The force can be calculated as shown below:

$$F_{hor} = \rho V \frac{(U+C)^2}{L} \tag{2.13}$$

where ρ the density of the water, U is the vessel's forward speed, and C is the velocity of the incoming wave.

Further investigations on the horizontal forces induced during shipping of water events and specifically the maximum horizontal forces on deck structures, were conducted by Buchner in [8] and [7].For the designing process of new vessels and other maritime applications, the case of maximum forces during shipping of water is of high interest, and thus was the scope of focus in more recent studies.

The difference in the case of shipping of water events compared to other impact phenomena, is that maximum horizontal pressures and forces that are generated, come from the jet that is increasing in height in the early stages of the event, instead of the maximum loads generated by a solid impact in case of the latter. The horizontal loading increases in a form of consecutive impulses caused by the additional water height in each time-frame, until the height of the jet reaches the value of the maximum water height on deck, H_{max}, [8]. The maximum horizontal force per meter breadth is given by (Eq.2.14):

$$F_{peak} = \rho H_{max} u^2 \tag{2.14}$$

where u is the velocity of the water propagating on deck. For the above equation shallow waters are assumed for the on deck flow, and thus the velocity is assumed to be constant.

Buchner in [7], continuing the work of [8], in his PhD Thesis experimentally investigated greenwater events coming from the bow, the sides and the stern of a vessel. For the bow events, formulas based on semi-analytical equations with correction coefficients and data fitting were derived, describing the pressure profiles and maximum horizontal forces for deck structures with different shapes and geometries, based on the pressures and forces on a rectangular deck structure. However, because these formulations are not utilized in the current project are not presented.

2.2.3. Vertical Loading

The vertical loading exhibits a similar picture to the horizontal loading in terms of pressure formation. In greenwater events, the pressure distribution demonstrates two distinct peaks. The initial peak arises from the impact of the body of water on the deck, with its mechanisms and intensity contingent upon the specific circumstances of water shipping. The second peak occurs subsequent to the interaction between the body of water and the superstructure. After a water jet, propelled upwards, exhausts its kinetic energy, the water descends and strikes the deck for a second time.

Once more, the pressures exerted on deck are highly affected by the 3D phenomena, and case specific characteristics of the incoming wave and structure. Greco et al. [17] by placing pressure sensors on the deck of different three dimensional model vessels concluded that the primary significance lies in the initial impact loads. However, the experiments demonstrated that pressure peaks generated during the stage of gravity-driven dominant events can reach similar magnitudes, and thus cannot cannot be ignored.

The most reliable analytical solutions for calculating the vertical loads on a deck have been derived by Hernández-Fontes et al. [23]. A series of experiments were conducted where the wet dambreak method was used for generating isolated greenwater events in a 2D fixed structure. Using force sensors on the deck a vertical force balance was applied for the whole duration of the trials. The researchers conducted a validation study on the convolution motion, which proposed time series of shipping water elevations, to estimate time series of slow varying vertical loads on the deck. The goal of the research was to evaluate the potential of the advection-diffusion for estimating vertical loads on a structure using a time series of wave elevations onboard. For a solution to the advection-diffusion equation with Diricklet-type boundary conditions and constant advection and diffusion coefficients, mean shipping water velocity and bottom friction were able to be accounted for more easily aiming to produce more accurate results.

In the end, the analytical approach was compared with experimental measurements and results obtained with the analytical equations of Stoker for calculating the volume of water on deck. After the mass of water is known, only the static water head component of pressure was estimated using the momentum method. The findings showed that the new method yielded significantly more accurate estimates instead of using Stoker's analytical approach capturing well the trend and the peak time of the loading, but still overestimating the vertical loads up to 2.5 times.

The researches remarked that the advantages of the the proposed method is that, in contrast to the dam-break method which requires to impose the time to start the simulation, the convolution method allows using any time history of water elevations at the boundary as input. Additionally, the advection-convolution model could potentially be extended to estimate time series of vertical loads on moving structures by considering all the pressure components of the momentum method, which include the vertical motion of the deck and the rate of change of the water elevations. A detailed overview along with the analytical equations are presented in [23]. The full method is not recited in the current research as it out of the main scope and objectives of the current project. However, for a complete and broader discussion.

2.3. Crucial Parameters

In literature concerning greenwater events, several variables that affect the mechanics involved, have been identified by researchers throughout the years. These variables can alter several aspects of a shipping of water events, such as the type and processes involved as the phenomenon unravels, the amount of water on board, the response of the structure and the loads exerted on the vessel to name a few. The main factors involved in green water phenomena have been categorized and presented in

the following sub-sections.

The forces applied during greenwater events, and fluid mechanics in general, are equal to the flux of momentum of the fluid. All the variables that were identified correlate with one or both of the two main parameters connected to the flux of moment, which are the mass of fluid going onboard, and the relative motion between the structure and the body of water. For a better understanding and organizing of the main parameters, the variables that have been identified as crucial are organized in two groups. One group which is related to the geometrical and structural properties of the vessel, and the other with the environmental characteristics and properties of the waves before they reach the structure.

It is important to note, that the literature focusing on parametric study on the mechanisms of greenwater events is not very extensive. Moreover, some of the literature was published before sufficient understanding on the phenomenon was achieved, therefore not all factors described in the next subsections, will necessarily impact each greenwater case the same way or to the same magnitude. With each different scenario the sequence or nature of the mechanisms involved may differ, so when a crucial parameter is examined there is not a general rule that satisfies all cases at once, but results are based mainly on the greenwater scenario that was observed. However, most of the effects of variables presented, correspond to the dam-break (DM) or the plunging wave with dam-break (PDB), which are the most commonly found in both real applications [15], and experimental literature.

2.3.1. Environmental variables

Direction of Waves

First parameter examined is the direction of the incoming wave with regards to the ship's bow. Bernhault et al. [3] carried out a parametric study on greenwater events investigating the effect of wave height, ship motions, and bow shapes. For the investigation they conducted experimental trials with different bow geometries and wave directions on FPSO type of vessels in regular and irregular waves, along with numerical simulations which were compared with the behavior on board. The researchers concluded that the most severe cases took place when the waves invaded from an angle of 180degrees from the bow, in head sea conditions.

Moreover, the head-sea cases develop the strongest flows at the center line of the structure [32], and is least affected by 3D phenomena [2]. The stages of head waves over-topping from the bow can be seen in (Fig.2.5). A volume of water once it gets onboard, in most cases will start propagating forming a vain type flow. The water will exceed the freeboard and depending on the shipping of water scenario will crush differently on board. Then, the flows coming from the lateral directions will be pushed outwards along the centerline, while a blunt waterfront appears. In the next moments, a strong water tongue is formed at the midsection, and the lateral flows intensify. Finally, the water front resembling the case of a dam breaking propagates on board, with the lateral flows having stabilized and converged towards the center.

Kudupudi & Datta in [29] conducted CFD simulations using the VOF (Volume of Fluid) method on moving FPSO vessels with predetermined motions, in waves coming from different angles from the bow for multiple wavelengths. It was concluded that the direction of the incoming sea states alter slightly the mechanisms included in the shipping of water events. Most importantly waves coming from different directions induce different pressure profiles for waves with same height and steepness. It was observed that for the same locations the graphs of the pressure showed various rising time, different peak value, dominant loading stage, and a change in the phase of the phenomena involved. For all the cases, the head-sea state coming from an angle of 180degrees produced the largest pressures, in agreement with the finding of [3].

Finally, wave direction can have some secondary effects. Buchner in [7] observed that waves coming from the sides, might create forces that are not critical for the structural integrity of the vessel, but rather critical for the stability of the vessel, which becomes the main concern in these cases of shipping of water events.

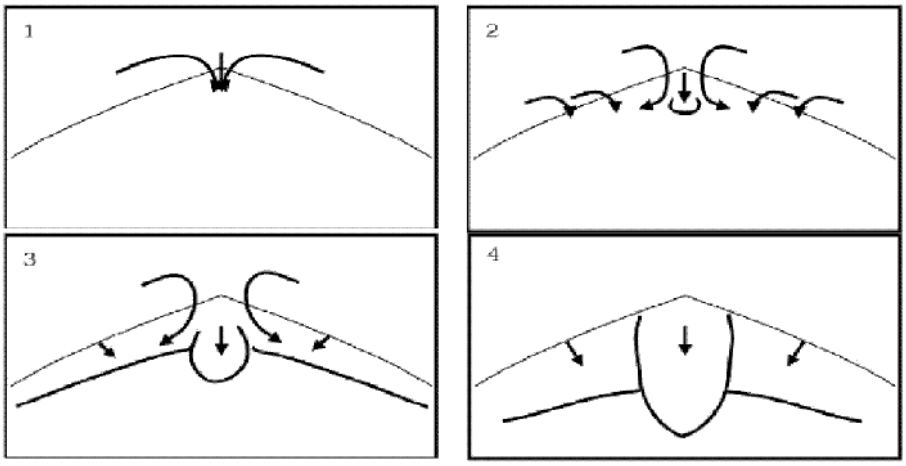

Figure 2.5: Horizontal forces profile during greenwater events (figure originally from [2]).

Wave Height

The height of the incoming wave is one of the most examined parameters in terms of greenwater events. The general trend is that the larger the wave height, the large the freeboard exceedance. This means, that more water gets onboard, usually larger water velocities are recorded, resulting to larger peak pressures.

One of the first to systematically investigate the effect of wave hight was Buchner in [6]. Examining greenwater events caused by regular waves in a moving FPSO vessel in head seas conditions, Buchner observed that there is almost a linear relation between the wave height and the water height on deck for the dambreak greenwater case, which was the only one recorded. This results in a larger volume of water going onboard and larger on board velocities which lead to larger peak pressures. However, it was concluded that due to high variety in the measured pressures due to small changes in the wave height no clear correlations could be made.

Fonseca et al. in a series of experiments focused on the responses of a structure in regular and irregular head-waves, which produced the most severe events with respect to the vertical responses [13]. The model was towed by a system which included two vertical struts, that allowed vessel to free heave, pitch, and roll, while the horizontal motions were restrained. Fonseca et al. observed that in regular waves impact pressures and forces present a trend of increasing almost linearly as the measured height of water on deck increases, although some dispersion in the data was reported. This was not the case with irregular waves where singificant dispersion was observed and no clear correlations could be made.

Lee et al. [32] conducted several trials where train of waves loaded different models based on FPSO-vessels with three distinct wave geometries in stationary head sea conditions. Each bow geometry was loaded with three cases of regular waves with varying amplitude (6-10cm in scale) with each case having the same amplitude but different wave lengths corresponding to a percentage of the total length of the model vessel corresponding to 75%, 100% and 125% of the wave length. The water front velocities, freeboard exceedance, and flow patterns were recorded with a high speed camera. Lee et al. observed that the maximum pressures were captured at the center-line which showed more complex behavior as wave amplitude increased. Additionally, at the bottom of the vertical wall at midline, the pressure peaks were correlated with the incoming wave amplitude for each wave length. The findings indicated a quadratic relation between the pressure peaks and velocity of the flooded water on deck.

Wave Length

Buchner in [6] observed that the pattern of the flow over the deck is dependent on the wave period. Shorter waves produced flows more concentrated around the middle of the deck. Moreover, for short waves in duration there a larger variation in the velocity of the flow over the deck than in the longer

waves was documented.

Buchner & Voogt [6] conducted experimental trials in weathervaning FPSO models is investigated. Based on a series of experiments conducted, different bow flare angles of 10,30,50 degrees were tested in regular and irregular waves. The results for all tested regular waves with lengths of λ/L=0.75, 1.0 and 1.25, where L is the length of the model vessel, showed that the freeboard exceedance and water height onboard is almost independent on the wavelength. This is also the case by the extensive model tests that were completed with irregular waves. On the contrary, Greco in her PhD dissertation observed that for regular waves, when steepness was constant the smaller wavelength the more reflection happened and less water climbed on board [17].

Fonseca et al. in [13] from the results of the experiments, observed that the highest pressure values are associated with the wavelengths in the regio of λ/L=1.20-1.40. From graphs constructed it was shown that the impact pressures and forces increase with the measured height of water on deck. Futhermore, there is clearly a dependence of the pressures on the on wavelength. For the same wave heights the measured pressures on deck were larger for the region around λ/L=1.20. Finally, observing the results for each wavelength, the pressure on deck seems to increase almost linearly with the height of water on deck, while the pressures and forces on the box seem to increase with a kind of a soft power curve.

Lee et al.[32] concluded that the main flow at the centerline showed complex behavior wave length increased. They observed that a threshold wavelength or threshold green water velocity which results in large peak pressures values on deck. These spikes in pressure values appeared for each bow geometry and each wave amplitude as the values of wavelength surpassed the threshold around λ/L=1.25.

Kudupudi et al. (2020): carried out a series of CFD simulations using the VOF method to conduct a parametric and a validation study for shipping of water events. The researchers compared the results yielded by the numerical model with the data recorded in [17] for 2D and [32] for 3D to experimental setups. They positioned monitoring points along the deck of the models to measure peak pressure. In the simulations regular waves with different steepness values and different bow angle variants were used. The impact pressure on the deck was investigated for different λ/L for two different Froude numbers, translating to different forward speeds, revealing that peak pressures during greenwater events peak are found to be maximum in the range $1 \leq /L \leq 1.2$. The peak pressure decreased at lower and higher λ/L values for both the Froude numbers.This shows the dependency of green water loading on wavelength since the same wave height is used in the computations.

Wave Steepness

The wave steepness, , is defined as the ratio of the water height, H, divided by the wave length ,. Even thought both of the previous parameters are examined separately, their combined effect is a one of the most crucial parameters in shipping of water events. This is why, many times in greenwater literature these parameters are examined as one through the wave's steepness.

The most important effects of wave steepness it that it can determine the shipping of water case that appears, and therefore the mechanisms that are involved in the processes. As mentioned in previous sections, in [16] and [15] four cases of green water events were namely the dam break *PB*, the plunging wave ,*PW*, the plunging dam break ,*PDB* and the hammer fist,*HF*. The researchers conducted a parametric study based on parameters affecting the greenwater event cases, and revealed a strong correlation between the type of green water types and the steepness, ϵ, of the impacting wave, the the maximum vertical velocity of the wave ,W_w, and the vertical velocity, W, at the bow of the structure. From (Fig. 2.3e) it is easily understood that while keeping the value W_w/W ratio constant, and by increasing the steepness, ε, of the incoming wave, single parameter can alter the succession from the PB to the PDB to PW cases, which have their on distinct features and mechanisms.

Greco conducted two dimensional experiments on a stationary FPSO model vessel in head-sea waves in her PhD dissertation while carrying out a 2D numerical study based on BEM (boundary element method) of computational fluid dynamic simulations for modelling the flow ondeck in her PhD disserta-

tion [17]. The aim of her Thesis was to do a parametric study on the main parameters of wet deckness during greenwater events, while trying to create a numerical method that accurately simulates the deck flow. In the experiments three bow flare angles of (-45, 0, +45) which could be attached and removed were tested. The waves generated were train of regular waves with a steepness of (0.04-0.08). The data was recorded using pressure sensors on the vertical wall and horizontal deck along with water level transducers both planes. Greco showed that as the wave steepness, ε, increased the volume of water on deck linearly for small values and non linearly for high values f/H, where f is the freeboard length. Additionally, Greco concluded that the steepness was the dominant factor for the severity and peak pressures on deck for wavelengths equal or larger the ones of the vessel.

Bercelona et al. observed in [2] that for a given geometry, as the steepness increases,for three dimensional cases the flows coming from lateral sides becomes stronger. Moreover, the three-dimensional effects interact with more with phenomenon, and the time needed for the shipped water to reach the vertical wall is shorter meaning higher on board velocities were meassured. Findings , were recorded by Fatilsen et al. [12] where for 3D cases, steeper waves produced more localized flows with non-linear phenomena flow phenomena involved. Also, the researchers noted that ondeck flow is more affected by the flow that takes place outside the bow. Finally, Barcelona et al. conluced that The maximum pressure increases as the incoming wave steepness increases for both elliptic and circular bow geometries that were tested.

Kudupudi & Datta [29] concluded that is a direct relation to the wave steepness with the maximum pressures on board. This conclusion was based on the results that were calculated for different steepness and heading angles for wavelengths equal to the models length, as most severe cases occur around this frequency, From pressure profiles plotted for a single point during the duration of the event, it was noted that there is a distinct jump in peak pressures as steepness increased. Similar findings were noted in [28]. Simulation results showed that for a 3D model vessel in regular head sea waves, most severe cases occured for a region of λ/L=1-1.2, where for the same wavelengths as the steepness increased the maximum pressure on deck also incresed in value. Additionally, Kudupudi & Datta observed that for the steepness of 0.05, amplitude of the maximum impact is nearly same for different heading angles. However, for steepness 0.06 and 0.07, maximum impact pressure is different for different heading angles. Meaning that as steepness increased more localized flows were created and stronger 3D flow phenomena took place on deck.

2.3.2. Geometrical & Structural Properties

This sections examines the impact of geometrical and structural properties of the vessel on the greenwater induced loading. These properties start affecting the mechanisms involved once the wave reaches the vessel throughtout their interaction, until the water goes offboard and the events are over.

Bow Shape

Bercelona et al. in [2] studied three types of bow geometries one ESSO-Osaka tanker, one circular,and one elliptical FPSO shape. The concluded that simpler two-dimensional bow geometries do not result to more simple two dimensional flows, and instead 3D phenomena are still present. However, they showed that the flow and the velocity along the centerline presents very limited data scattering regarding the bow geometry.

Lee et al. tested three bow shapes were tested in the series of 2D experiments they conduced on FPSO vessels [32]. A rectangular deck with a vertically straight stem , Rect0, a rectangular deck with as stem angle of 5 degrees, Rect5, and a rounded edge deck with a vertically straight stem, Round. The researchers observed that in most wave conditions, the Rect5 model showed reduced average deck pressures than the other two models (Rect0, Round). This could be explained as with a small stem angle reflected waves were produced with greater reverse velocity component, which suppressed the incoming wave energy in the Rect5 model case. Furthermore, the patterns for green water propagation on deck were visually observed. The shape of the water front was almost the same as that of the deck edge of each model. A diagonal form of water front from the corners of the deck front to the

bottom center of the vertical wall, which represents the merged water from the front and side edges of the deck, was seen more clearly with the Rect0 and Rect5 models than with the Round model.

Flare Angle & Stem Angle

Buckner conducted an extensive study of the mechanisms involved in greenwater events on a FPSO vessel weatherwaving conditions , with and without current, using regular and irregular waves for generating DB shipping of water events [6]. The results showed that the relative motions in front of the bow increase when flare angles, α, are present, whereas the water height on the deck decreases. Moreover, Buchner observed that with higher bow flare angles the wave elevation in front of the bow is increased. This is due to a larger pressure built-up at the initial impact on the hull of the vessel leading to a jet that pushes the water upwards but also forwards away from the bow.

Buchner and Voogt [8] in a series of experiments they conducted in 3D FPSO model vessels, concluded that he effect of the bow flare increases with the distance from the fore perpendicular. Moreover, they indicated that the velocity of the waterfront over the deck is proportional to the square root of the freeboard exceedance at the fore perpendicular and is unaffected by different bow shapes and flare angles. Finally, for the elliptical bows that were tested, the impact pressures and global loads decreased clearly with an increase of the bow flare angle.

Greco in [17] observed that a positive bow stem overhang reduces the relative amount of shipped water. This resulted from a larger wave reflection for the ship's bow. However, the deck wetness severity did not dramatically change in the cases of flare angles, $\alpha = (0, 45)$, which became more evident for larger freeboard to wave-height, f/H, values. Although, Greco noted that the stem-angle effect could have some importance, depending on the actual ship loading conditions and also, when multiple degrees of freedom are considered. A more local analysis showed that the water level for the cases cases of $\alpha = (0, 45)$ was smaller than in case $\alpha = -45$, while the water-front velocity was larger. Furthermore, Greco concluded that the loads depend strongly on the impact velocity,and thus on the wave-front velocity. In this respect, the water impact due to an inclined bow can be worse even if the amount of shipped water remains roughly the same.

Lee et al. [32] in the series of experiments they conduced, three bow shapes were tested. A rectangular deck with a vertically straight stem , Rect0, a rectangular deck with as stem angle of 5 degrees, Rect5, and a rounded edge deck with a vertically straight stem, Round . The researchers observed that in most wave conditions, the Rect5 model with a small stem angle compared to the other two models that had none showed reduced average deck pressures. The researchers concluded reflected waves were produced with greater reverse velocity component, which suppressed the incoming wave energy in the Rect5 model case, finding similar to those of [17].

Zhang et al. [57] performed numerical simulations in 2D stationary conditions in head sea states for several bow flare angles. The researches concluded a large bow flare angle has a more significant disturbance on the water profile around the bow, causing an obvious jet like feature which overturns away from the box back into the incident wave. The increase of bow flare angles also inhibits water shipping, leading to less shipped water flowing onto the deck and an absence of a visible plunging feature when the bow flare is 50 deg. Additionally, it was observed than an increase in α, reduced maximum freeboard exceedance and overtopping duration at the deck front. The effect of the bow flare angle on the freeboard exceedance was more evident for short waves than for longer waves. Finally, the Zhang et al. concluded tat the relationship between the momentum flux and overtopping volume (normalized by the classical dam break predictions) and the relative overtopping duration have been shown to collapse well for a fixed box with bow flare angle up to 30 deg. (i.e. up to angles well within that expected in practice). This observation implies that the local physics of overtopping are similar for different flare angles. relative water level elevation at the box edge can be computed accounting for flare angle, the local prediction of momentum flux and overtopping volume using this relative water elevation can proceed in the same way regardless of practical flare angles.

Kudupudi et al. [28] showed the dependence of peak pressure on bow rake angle for four different bow geometries with bow flare angel ranging from 0 to 30 degrees. For all the bow geometries and the

different forward speeds they simulated, it was observed that the impact pressure on the deck increases with decreases in the bow flare angle for all the values of Fn investigate, although the effects remained highly localized. Furthermore, the quantity of water shipped on the deck from the bow reduces as the bow angle increases. In all the sequences having different α, the incident wave gets splashed up and then overturns like the plunging wave breaker and impacts on the deck, as the previous literature also suggested.

Rigidness

Rigidness is the product of the moment of inertia, I, of a cross section times the modulus of elasticity, E. It is a critical component that affects both the static and dynamic response of the structure, and also governs the interaction between fluid and structure. Rigidness and hydro-elasticity have been examined extensively during slamming phenomena, however the existing literature for shipping of water phenomena is not very extensive.

Greco in [17] in the CFD simulations for modelling the flow on deck incorporated the hydro-elasticity of deck structure into the simulations. Greco conlcuded that the hydro-elasticity does not play an important role for the resulting maximum deflections on the wall. For rigid structures that the magnitude of hydroelastic results oscillates around a mean value close to and slightly larger than the corresponding quasi-steady value. This implies the unimportance of hydro-elasticity. Additionally, as confirmed from the test results with the rigid on ondeck vertical wall of the set-up, the experiments were not affected by elastic oscillations of the wall. This was evident because the pressure recordings did not show any suspicious oscillation frequencies. Thus, Greco suggested that the effect of hydro-elasticity during the impact on a deck house may generally be neglected.

Faltinsen et al. [12], in the numerical simulations they conducted for simulating the flow on deck considering 2D analysis, they incorporated they hydro-elasticity of the system using realistic parameters and examining the problem using several assumptions such as neglecting the gravity and approximating the problem as the impact of a fluid wedge for the deck structure, simplifying further the solutions, and by assuming either small or large interior angles of the impacting fluid wedge. The researchers concluded that the effect of hydro-elasticity during impact can be generally neglected.

Qin et al. [43] conducted numerical simulations on isolated freak waves crashing on deck. For the simulations three types of deck were tested, a fully rigid,an elastic deck, and elastic with intermediate supports. The surface elevations and sectional average velocities are compared with the theoretical results of a combined dam-breaking approximation for the global event progression. Moreover, the hydroelastic effect and the influence of the intermediate elastic supports are investigated by comparing the results of local pressures of the fluid on the decks and the deformation of the decks. The simulation results showed that although the elasticity of the deck barely influence the global evolution of the fluid motions, it effects the local fluid pressures significantly. The fluid weight and the collapse of wave would cause a global deformation of the deck, while the hydroelastic effects would cause local vibrations. Finally, concluded that for elastic structures the effects of hydro-elasticity should be taken into account, while for rigid structures can practically neglected.

Relative Motion

Buchner in [6] from the experiments that were conducted with moored FPSO model vessels with and without current concluded that the additional forward speed created by currents is significant and cannot be neglected. Most important contribution observed was that the current increased the wave length. Increased wave length resulted in larger relative motions between the vessel and the sea-state, and in general larger volume of water going on board, and larger peak pressures taking place on deck.

Zhao et al. [18] conducted experimental trials and numerical simulations using focusing wave groups to investigate the effect of DOF (heave and roll, and then heave roll and and sway) of a floating body on the maximum pressures on deck during agreenwater events. The results showed that the maximum peak pressure and green water overtopping mass varied for different degrees of freedom. It was concluded that the maximum pressure occurs when the body is fixed (0-DOF case). Meanwhile, the

peak pressure decreases rapidly with the increase of the number of DOFs, and the value of the peak pressure pressure of 0-DOF is over twice times as much as that of the 3-DOF case. Specifically, the researchers observed that a 3-DOF body, there was about20% reduction of impact pressure as compared to a 2-DOF floating body, while 40 and 60 % reduction compared to a 1-DOF and 0-DOF body, respectively. Therefore, the body with more DOF could experience green water phenomena less severally. Additionally, Zhao et al. conluded that different degrees of freedom do not affect the shipping of water events the same way, with the heave motion greatly suppressed by the body of water on board.

Kudupudi et al. [28] protted the results obtained from the simulations at the location of the foremost point on the deck from the bow edge which was kept constant for all the cases. The obtained results showed. These results showed that the peak pressure increased with increasing speed of the vessel for all the bow variants that were used, with different blow flare angles.

Position on Deck

Buchner & Voogt [8] in the serieis of experiments they conducted in weathervaning conditions for 3D FPSO models, concluded that the effects of geometry of the bow start becoming more evident as the distance from the edge of the bow increases.

Lee et al, [32] investigated the shipping of water loads to understand the physics of green water and quantify the pressure distributions on deck, in different part of FPSO model vessels in a series of experiments they conducted inside a towing tank. The researches concluded that the strongest pressures are recorded on the bottom of the vertical wall at the centerline where flows from the middle and rear merge. Moreover, concluded that both spatial and temporal pressure distributions between points varies significantly in both the horizontal and vertical plane, showcasing the highly localized nature of the shipping of water phenomena.

Song et al. [51] conduct a series of experiments of large scale experiments investigating extreme wave impacts in head-sea conditions on an offshore structure. They researchers measured the pressures on a 3D fixed box structure with a vertical wall, in head sea conditions with individual a train of waves with the focused waves method for each experiment. The pressures were recorded in 12 positions organized in 3 columns, while the wave propagation and the two-phase flow were recorded using a high speed camera with the bubble image velocimetry (BIC) technique. Song et al. concluded that the front velocity of the green water was the highest velocity in the entire green water flow before it reached the rear edge of the deck. Moreover, the transverse mean velocity was approximately zero, resulting in most of the flow creating a vain propagating at the same direction towards the deck structure. Finally, for the deck structure tested, the horizontal mean velocity reached a maximum magnitude of about 1.5 times the phase velocity of the wave near the center, half the distance between the edge of the deck and the deck structure, and stayed approximately constant until it reached the end of the deck (x=L). This indicated that a minimum distance is required before the properties of the greenwater flow on deck can be fully developed.

3

Experimental Setup

The methodology for achieving the goals mentioned in (Chap. 1) was based on utilising the experimental layout described below, so that an adequate number of repeatable and isolated greenwater events can be generated. By conducting these experiments, a significant amount of data was expected to be acquired which would be enable a systematic study and a statistical investigation, providing a better insight of the phenomena involved. The aim of the experimental layout was to produce and record instances of material failure caused by shipping of water events. The ultimate goal would be to produce curves that describe the probability of failure and be able to correlate it with the mechanisms that take place during green water events.

Brief Description

The experimental layout as shown in (Fig. 3.1) consisted of several pieces all working together to produce and record greenwater events. These pieces namely were; a water tank containing two bodies of water capable of producing repeatable solitary waves with varying characteristics, a 2-dimensional scaled-down model vessel based on the front part of an S175 container ship with a box on deck resembling a small structure which was connected to the deck of the model by pair of hinges, a release mechanism capable of almost instantaneously opening the water gate that separated the two bodies of water, and finally instruments and equipment for measuring and gathering data.

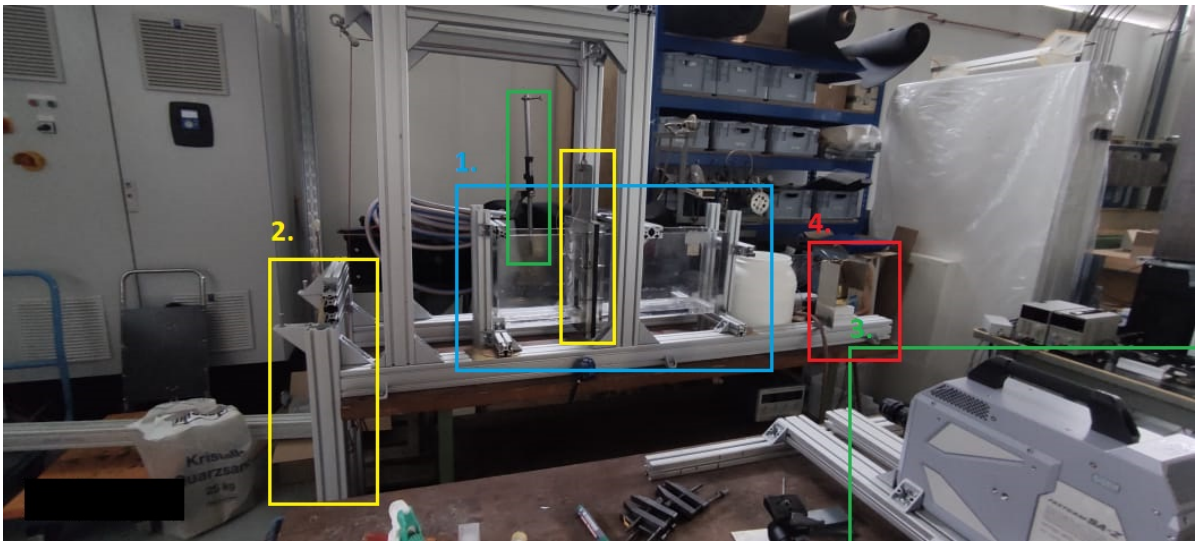

Figure 3.1: Experimental Setup (1. Water Tank, 2. Water Gate-Release Mechanism, 3. Measuring Equipment, 4. Model Vessel).

3.1. Setup Design

3.1.1. Wave Generation & Loading

Dam-Break Method

For the generation of waves the dam-break method was chosen. An individual wave ccan be created using two bodies of water separated by a dam gate. Upon opening the gate, the larger body of water is accelerated under the influence of gravity and pushes the smaller volume of fluid in a manner similar to a piston [52]. Flow characteristics such as the water elevation, the wave length and the steepness are determined predominantly by the ratio of the water depth downstream the gate, h_0, to the water depth upstream, h_1.

Nakagawa et al. conducted a large number of experiments generating waves with the dam-break method using a wide variety of h_0/h_1 values. They identified four different wave profiles for the whole range of downstream to upstream depth ratio. For the current application the range of interest is for the values of $0.56 \leq h_0/h_1 \leq 1$, for which a stable bore is created. The bore increases in height for a distance up to $4h_1$ from the dam gate, where it becomes fully developed, and after that point it starts reducing in height due to channel friction.

The dam-break wave generation method was selected for several reasons as it presents a lot of advantages for the application at hand. First of all, it is a tested and reliable method since extensive literature exists, like similar applications of generating individual greenwater events [34], [40]. Secondly, [53] derived the analytical equations describing the flow that is created upon opening of the gate. Although, the solutions of Stoker present considerable deviation for several quantities compared to experimentally measured values [38], they provide reasonable estimates, without having to resolve to any complex analysis. The most important advantage however, is that the dam-break method can create isolated, irregular and repeatable waves relatively easy without requiring any long duration time-series or create additional water flows that may affect the main greenwater event.

Loading

The two bodies of water as specified by the dam-break method were expected to start interacting in the tank creating individual irregular waves. The experimental trials started with the generated waves corresponding to 14m waves in real life ,increasing gradually in height, which can be considered as extreme weather conditions. These waves reached the model vessel producing individual greenwater events, and then loaded the box structure that was able to pivot from the windward side, signifying failure if the box opens.

For each wave height five consecutive trials were conducted with the same wave. The number of experiments for each wave height were based on a practice which was present in several publications that investigate water impact and hydrodynamic phenomena. The number of samples can be dictated as the minimum amount which is statistically required by the distribution to yield reliable results. However, choosing such a number of samples can be very consuming in terms of time and resources. Therefore, conducting five repetitions provided a reasonable balance between statistical significance and practical feasibility for the type of specific experiments.

After a set of six experiments with a single wave height was completed, the wave height was increased by 1m in prototype scale. This could easily be done in the water tank by adjusting the upstream and downstream water depth ratio. The experimental trials stopped where all the wave heights that caused greenwater events were produced, and five undisrupted and fully recorded trials were gathered. The values of h_0, h_1 ,and their ratio for each wave height initially estimated are shown in the below (Table 3.1). A first estimate of the values of the table that were calculated graphically, from diagrams provided in [38].

Waves	10m	11m	12m	13m	14m
$h_0(m)$	0.063	0.063	0.063	0.063	0.063
$h_1(m)$	0.078	0.0814	0.084	0.0866	0.0893
ratio	0.080	0.7742	0.750	0.7273	0.7059

15m	16m	17m	18m	19m	20m
0.063	0.063	0.063	0.063	0.063	0.063
0.0919	0.0945	0.0971	0.0998	0.1024	0.105
0.6857	0.6667	0.6486	0.6316	0.6154	0.600

Table 3.1: Upstream h_1 and donwstream h_0 water depths required for generating different wave heights.

3.1.2. Dimensionless Number

For calculating the dimensions and properties of every aspect of the experimental layout it was necessary to scale down the real life application in a way so that the prototype and the model could exhibit the same behavior. To achieve this all the quantities involved between the model and the prototype are related using dimensionless analysis with a non-dimensional number. The Froude number, *Fr*, was selected for the current applications, because is the most capable dimensionless number to describe hydrodynamic phenomena in open water flows [9]. Froude number relates the inertial forces with the gravitational forces in a system, and is defined as the ratio of the latter to the former.

$$Fr = v/\sqrt{gl} \tag{3.1}$$

,where v is the velocity of the flow, and l the length of the flow line.

In order to ensure that the systems will have the same behaviour hydro-dynamically, both systems should have the same *Fr*. Therefore by choosing a scaling factor, λ, suitable for the application at hand, it was possible to start estimating the values of the quantities involved based on those of the prototype. The ratio between the quantity of the prototype to the model based on Froude's dimensionless number are shown in (Table 3.2).

Quantity (SI)	Q_p/Q_m
L (m)	λ
T (s)	$\lambda^{0.5}$
M (kg)	λ^3
E (N/m^2)	λ
σ (N/m^2)	λ
F ($kg \cdot m/s^2$)	λ^3
a (m/s^2)	[-]
v (m/s)	$\lambda^{0.5}$
A (m^2)	λ^2
I (m^4)	λ^4
EI (Nm^2)	λ^5

Table 3.2: Scaling of quantities according to Froude number.

3.1.3. Scale

The water tank which the experimental trials that took place was already manufactured before the design phase,and its dimensions were known. The tank was constructed from see-through acrylic, with a wall thickness of 2.00 cm on each side. The inner dimensions are 28.00 cm height, 13.00 cm breadth, and 81.30 cm in length. The total length included the upstream part from the front wall up to the gate

equal to 31.10cm, the water gate was a built-in thin sheet of steel equal to 1mm in thickness, and the downstream length from the water gate up to the back wall measuring 50.10cm.

To calculate the dimensions of the model vessel, as well as the dimensions of the two bodies of water and the produced wave, an appropriate value for the scaling factor, λ, should be chosen. To decide the scaling factor a system of four equations (Eq. 3.2-3.5) were solved using a custom script constructed using the MATLAB mathematical toolbox. After solving the system the exact value of the scaling factor was found equal to 402.58(-) which was rounded down, so that the scale of the experiment would be 1:400.

$$h_0 = 0.6 \cdot h_1 \tag{3.2}$$

$$\eta = 0.48 \cdot h_0 \tag{3.3}$$

$$\lambda = \frac{12}{\eta} \tag{3.4}$$

$$4h_1 + 0.20 \cdot \frac{L_p}{\lambda} = 0.501 \tag{3.5}$$

,where η is the water elevation produced and L_p the length of the prototype vessel. In Eq. 3.2 the coefficient 0.6 was chosen because as indicated in [38] using the dam-break method with an ratio of $h_0/h_1 > 0.56$ a stable bore can be created, with the wave being more irregular as the ratios approach the value of 0.56. The coefficient 0.48 in 3.3 is also selected from [38], which is the relationship between the elevation of the water produced and the depth of the water in the downstream for $h_0/h_1 = 0.6$.

It is noted that the analytical solutions by Stoker, do not produce adequate results in real application due to the main assumptions being, that the water depth upstream h_1 stays the same throughout the the wave generation events, and out of plane dimensions expand to infinity, thus vertical wall friction is disregarded. Furthermore, the coefficient in Eq. 3.4 refers to a wave amplitude of 12m that comes from a 20m wave assuming an amplitude equal 0.6 of the wave height due to wave non-linearity. The 20m wave is the maximum wave that was generated during the experimental trials. Finally, in Eq. 3.5, $4h_1$ refers to the minimum distance for a steady undular bore to be fully developed according to Nakagawa et al. The coefficient 0.20 refers to the percentage of the total length of the vessel which the bow usually occupies in container-type vessels, and 0.501m is the measured distance from the water gate until the back wall.

3.1.4. Model Vessel

The 2D model vessel was constructed from several different parts, which will be presented separately into the following subsections. As shown in (Fig. 3.2) the main parts of the model vessel are the Hull, the Deck Structure, the Force Sensors, and the Support-Plates.

Material Selection

For the prototype and the model to exhibit the same hydro-elastic behaviour two conditions must be met at the same time. The first one is for the rigidness of the structure, EI, to be scaled down correctly, meaning the appropriate choice of material and dimensions should be made. The second one is choosing a liquid whose properties preserve the flow's compressibility between the real life application and the experimental layout. This means that both fluids must have the same Cauchy number [9].

$$Ca = \frac{v^2\,\rho}{B} \tag{3.6}$$

,where B is the bulk modulus elasticity.

The dimensions of the model have already been selected while using the Froude number to define the scale of the experiment. What remains is the selection of appropriate materials for the model to be

constructed, along with the appropriate fluid to reproduce hydro-elastic phenomena accurately in scale. However, there are two crucial issues that originate from the scale chosen so that every part could fit inside the limited space of the tank.

Firstly, with most of the common materials used for experimental models (steel, wood, plastics, fiber reinforced materials), the dimensions chosen give much higher rigidness values than the ones of the the prototype. Considering a small plate with dimensions 1000m x 10m of high strength steel for the prototype, the values of EI of the model become at least three orders of magnitude more than the theoretical value for accurate down-scaling. Vice versa, calculating the dimensions would lead to lengths that don't fit the experimental layout or are too thin to fabricate or work with. Therefore, accurately reproducing the stiffness of the prototype turns out to be not feasible with the current scale.

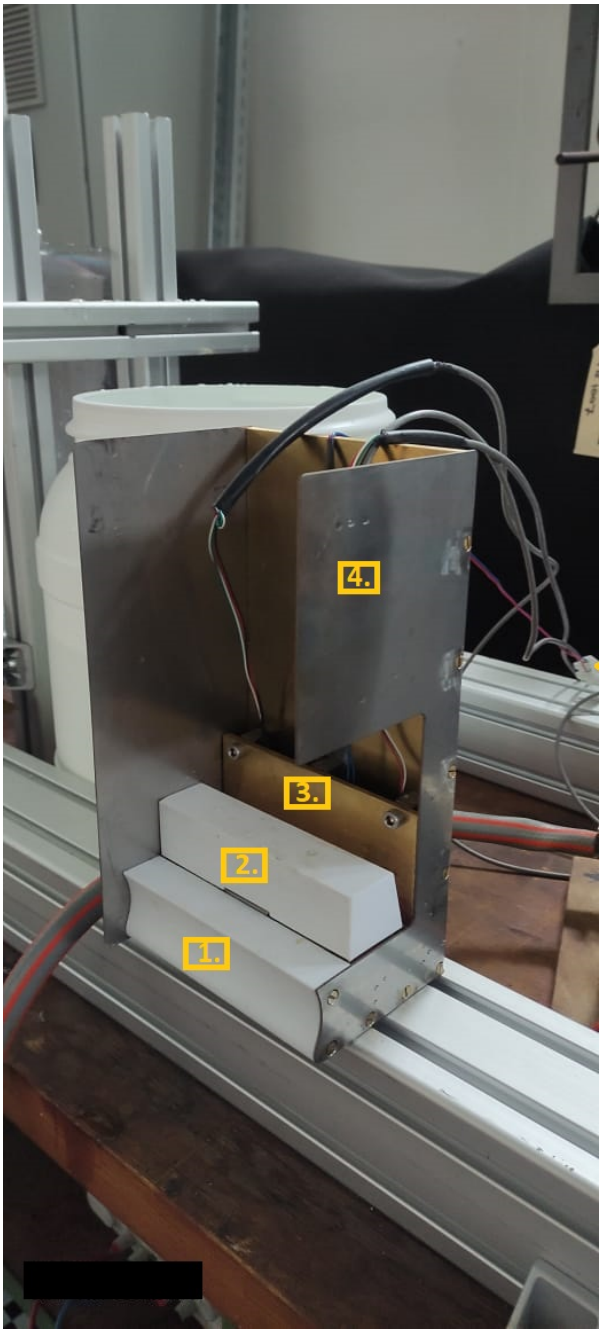

Figure 3.2: Model Vessel (1. Hull, 2. Deck Structure, 3. Force Sensors, 4. Support-Plates).

For the practical reasons of easier fabrication and data acquisition, it was decided to keep most of the dimensions accurate, and build the experimental setup for different materials depending on their purpose. The general notion is that for the model vessel should be rather stiff, corresponding to an almost rigid body in full scale. This choice is expected to create minor inaccuracies in the hydro-elastic behavior of the model and the physics involved with the greenwater phenomena, but as concluded in the previous chapter without significant impact in general behaviour during shipping of water events.

Secondly, the liquid needed for the exact representation of the hydroelastic phenomena based on the expected velocities of the generated wave and the scaling factor, requires a ratio between the density ,ρ and bulk modulus, B, of the fluid to be around 4. This ratio cannot be found with water based liquids that are inexpensive and safe to use. Therefore, tap water was selected for the experimental layout. This results to a compressibility around ($v^2 \approx \lambda = 400$) times more than the theoretical value. This issue cannot be avoided, although pressure values and variations, especially during impact phases where pressure waves take place are expected to be amplified.

Hull

The base of the model was designed using the Rhino7 commercial software for 3D drawings and models. The bow follows the shape and dimensions of the bow of the S175 container vessel scaled down. It is a solid one-piece block, which includes the hull of the model and part of the deck (see Fig. 3.2). Specifically, the middle cross-section of the hull of vessel was cut and stretched perpendicularly to the longitudinal axis to cover the whole width of the water tank. Due to the limited space of the tank, only the first 20% of the total length of the vessel was used for the experimental setup.

The model was chosen to be 2-dimensional for simplicity reasons. As concluded in [2], in 3D setups it is inevitable to avoid additional flows and phenomena alienating the effects of the main mechanisms that take place at shipping of water events, and making things more complicated in general to study. However, Barcelona et al. remarked that 2D models could resemble very well the behaviour and highlight the main mechanisms acting during greenwater events that take place around the centerline. As the researchers observed in the experimental trials they conducted, the effects of greenwater phenomena at the mid section are stronger while intrusive flows are minimized. This property makes 2D setups very relatively easier to design and more convenient regarding practical matters of the experimental trials for the purpose of researching shipping of water phenomena.

The thickness of the walls was designed equal to 1cm. This decision was on the conservative side for a couple of reasons. Firstly, the hull is responsible for receiving the initial loads coming from water impact phenomena and is not of much interest, as the scope of the current Thesis is to examine greenwater impacts which take place after the wave overtopping and spilling over the deck. Due to the complicated geometry of the hull and cost-effectiveness the base was 3D printed. Thus, the thickness was chosen so, for the model vessel to be able to withstand the hydrodynamic loads from first wave contact, while retaining structural integrity. Secondly, the choice of increasing the material thickness of the base was chosen for the model to be rigid enough. While increasing the thickness and therefore the moment of inertia, the stiffness of the base increases without having to use a stiffer material. This way the hull does not develop significant deflections that can affect the data gathering equipment. The dimensions of the hull can bee seen below (Table 3.3).

Hull Dimensions	**[cm]**
Length (20%)	8.77
Breadth	13.00
Freeboard	1.15
Draft	2.34

Table 3.3: Model dimensions in 1:400 scale.

Deck Structure

To measure material failure an on-deck structure of a rectangular shape was selected. The box shaped structure was responsible for resisting the impact and the horizontal pressures induced by the greenwater events. The dimensions of the structure were chosen 35mm in length with regards to the direction of the loading, 30mm in height measuring from the deck, and 130mm in width. Furthermore, the deck structure was connected to the rest of the model vessel by two hinges and a vertical magnet. The hinges were acting as pinned supports, that were screwed onto the back wall of the box on the one end, and onto the deck on the other. Moreover, the electric magnet was able to produce a vertical pulling force, which could be adjusted by increasing or lowering the electrical current passing through it. The magnet was positioned mid span of the bottom part of the front wall.

With the box structure described above, a system was designed where failure could be visually observed and recorded during experimental trials. Moreover, besides offering a way to easily capture and reproduce material failure, the system served another important purpose. Creating an occurrence of failure would be of little significance if the mode of failure and the force that resulted in it were not known a priori. Both of the these parameters were taken into consideration in the preparation phase.

The design of the experimental layout was made in such a way that greenwater flows and loading could remain the main topic, without diving too deep into topics of structural engineering. The way in which failure occurs in the experimental setup does not correspond to a realistic mode of failure of a deck- on-board structure system. Reproducing failure in a system of plates would require, on the one hand accurate modelling of the system including weldings and secondary elements like stiffeners, and on the other hand scaling down system properties such as the geometry and stiffness, and quantities such as stresses and forces. This is not possible while using Froude's number for scaling down all the properties accordingly.

For calculating the force that causes the box structure to pivot around the hinges and open, the water elevation which corresponds to the 20m wave full-scale, was chosen as the design wave. This choice was made arbitrarily considering that it would be sufficient to create a greenwater events strong enough to produce micro-cracking in real vessels. As can been seen in (Fig.3.3) the system is statically determined. This means that the system can be solved using the three equations of equilibrium $\Sigma F_x = 0, \Sigma F_y = 0, \Sigma M = 0$ at any point of the system to find all the unknown forces and reactions.

The design wave was able to go onboard and load the box structure. The horizontal forces exerted on it by the green water event were estimated using a commercial CFD software, named ComFLOW. Thus, the only parameter that needed setting up in the box-structure system was the magnet, responsible for resisting the hydrodynamic forces. Besides, being a restoring force the force of the magnet was used as an indicator that the design force was exceeded and failure was achieved.

The pulling force of the magnet was adjustable, and could be altered by the electric current allowed to run through it. To find the maximum required pulling force that could be overcome by the force created by the 20m as an initial estimate and then fine-tune the pulling force of the magnet, the system was dynamically modeled and solved analytically. The force from the greenwater events was modelled as a impulse using the Dirac delta function. The Dirac delta function can be seen as the derivative of the Heaviside step function, and it has a fundamental property which makes it ideal for mathematically expressing impulse loads, shown below in (Eq. 3.8).

$$\int_a^b F(t)\delta(t-m)dt = \begin{cases} F(m) & \text{if } a \leq t \leq b \\ 0 & \text{elsewhere} \end{cases} \tag{3.7}$$

where, t, is the variable of time, $\delta(t-m)$ is a definition of the Dirac delta function, and M(t) is the shape function of the overturning moment responsible for the pulse.

The shipping of water induced forces for the purpose of designing the experimental layout were calculated numerically using CFD simulations. ComFLOW was able to estimate the forces with a timestep of dt=0.001sec (with automatic adjustments for numerical stability) and store the values for a time interval

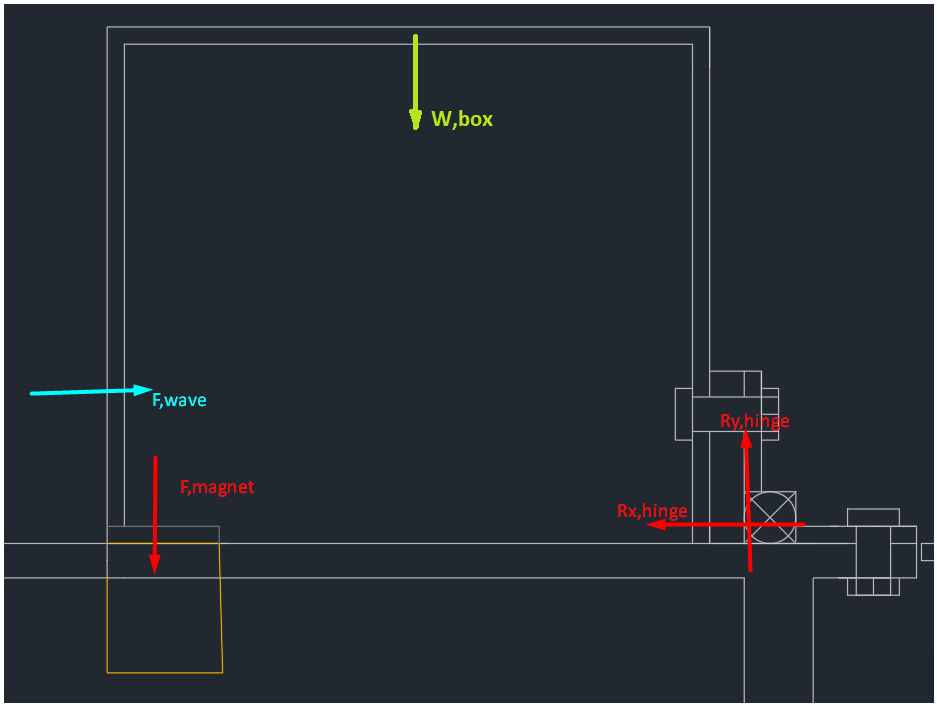

Figure 3.3: Sideview of the deck structure system.

of t=0.05sec during the designing phase. For determining the required pulling strength of the magnet the values for the overturning moment acting on the box-structure due to the 20m water height were used (Tabl. 3.4). The overturning values have been correlated with regards to the time of the loading and not the time of the simulations, this is why the first value is given for $t = 0\ sec.$

Time (sec), T	**Overturning Moment (Nm),** M_y
0.0	0.000
0.05	0.001313
0.10	0.000994
0.15	0.000595
0.20	0.000847
0.25	0.000244
0.30	-0.000012785

Table 3.4: Overtuning moment for several time marks obtained for the 14m wave height in ComFLOW.

The polynomial describing the overturning moment induced by greenwater loading, can be used for defining the shape of the pulse loads acting on the box structure for the whole duration that the system is dynamically examined. The Laplacian polynomials were used for extrapolating between these values. Using Matlab's command library for determining the coefficients of each term of the time function, the moments can be accurately described with a fifth order polynomial equation given in (Eq. 3.8).The plot of the polynomial describing the moment created by the greenwater events can be seen in (Fig. 3.4). It is easily observed that the shape of the function resembles the curves describing characteristic greenwater loads found in previous literature as presented in (Ch.2).

$$M(t) = -37.76t^5 + 13.4067t^4 0.40733t^3 - 0.051368t^2 + 0.051368t + 1.8 \cdot 10^{-7} \tag{3.8}$$

The only translating mass of the system is the mass of the box. Thus, it becomes possible to describe the behavior of the system by using a point load located at the center of gravity of the box. The dynamic equation of motion for the box-structure system can be reduced to a single degree of freedom system.

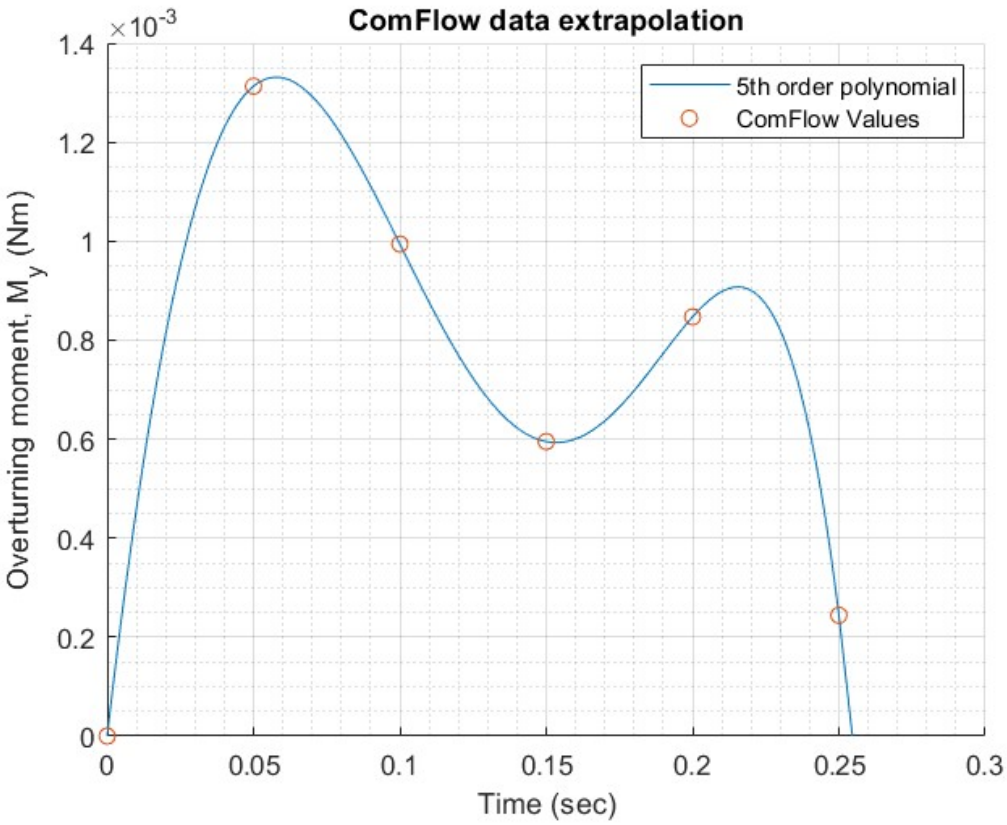

Figure 3.4: Extrapolation between the values of the overtuning moment given by ComFLOW

Every force acting on the box can be re-written as a function of the clockwise rotational degree of freedom, $\theta(t)$, that takes place around the hinge at the back support as the box is able to pivot around that location. The equation of motion expression as the sum of moments acting on the body given below (Eq 3.9).

$$[EOM] \;\; J\,\ddot{\theta(t)} = \int_{0}^{+0.30} M(t)\delta(t-T)dt - m\;g\;r\;\theta(t) \tag{3.9}$$

where, t, is the variable of time, J is the rotational moment of inertia, h the height of the box, and r is the distance between the center of gravity of the box and the hinge. The rotational mass moment of inertia of the box rotating from its bottom right corner can be calculated using equation equation (Eq. 3.10).

$$J = l \cdot (\frac{\rho\; b\; h}{12}(b^2+h^2) - \frac{\rho(b-2t)(h-2t)}{12}((b-2t)^2+(h-2t)^2) + \rho\;(b\;h\; -(b-2t)(h-2t))\;r^2) \tag{3.10}$$

,where h is the height of the box, b the breadth box, l is the width of the experimental layout, t the wall thickness, and ρ is the density of the box materials. The values for all the properties of the system used for defining the differential equation are given below (Table 3.5).

For formulating the equation of motion a few assumptions were made. Firstly, the rotations of the system are generally accepted as small, so $cos(\theta) \approx \theta$. Secondly, the system is considered to be undamped. This simplifies the response, and the thus the formulas describing the system and their solution. Finally, the equation of motion is only solved as the boundaries of the the integral for a window of $t = 0 - 0.30\;sec$. The polynomial describing the load derives numerically by intersecting real values, and therefore is only applicable and valid for the duration that recordings of the overturning moments take place. Furthermore, it is assumed that if the box has not opened, showing sings of failure, during

Quantity	Value
h	$0.030\,\mathrm{m}$
b	$0.035\,\mathrm{m}$
l	$0.130\,\mathrm{m}$
t	$0.005\,\mathrm{m}$
r	$0.023\,\mathrm{m}$
A	$0.00055\,\mathrm{m^2/m}$
ρ	$1350\,\mathrm{kg/m^3}$
m	$0.097\,\mathrm{kg}$
J	$0.0077\,\mathrm{kg/m^2}$

Table 3.5: System Properties

the duration of the loading, then it is physically impossible to open at a later stage of the phenomenon.

The equation is a second degree ordinary differential equation with regards to the time variable,t. This means that in order to get an exact solution two initial conditions must be used. The initial conditions to solve the differential equation were the zero initial rotation, $\theta(0) = 0$, and the zero initial angular velocity, $\ddot{\theta}(0) = 0$. Using the commercial software for symbolic math, Maple 2022, the exact solution describing the rotational degree of freedom of the box is given in (Eq. 3.11).

$$\begin{gathered}\theta(t) = +\,0.0045\cos(44.55t) - 0.018\sin(44.55t) - 611.69t^5 \\ 217.18t^4 + 6.17t^3 + 4.45t^2 + 0.81t - 0.0045\end{gathered} \tag{3.11}$$

With the equation describing $\theta(t)$ known, the inertial force of the box can be easily calculated. The resulting moment is equal to the moment caused by inertial forces $M_{inertia} = J\ddot{\theta}(t)$.The values of the moment equilibrium are presented in (Fig. 3.5). As can be seen in the figure below, the maximum moment acting in the box structure takes place just before the loading impulse maximum acting on the box structure. After that time mark around 0.10sec after contact between the flow and box structure, the sum of moments becomes negative, meaning that the restoring force of gravity is dominating the behaviour of the box.

Finally, to design the force of the magnet the moment needs to be translated in a force. Assuming that the magnet will be attached on the inner part of the windward side of the box structure, having a leverarm equal to $(b-t)$ from the hinge support, the force of the magnet can be estimated as $F_{mag} \leq \frac{M_{y.max}}{(b-t)} = 0.311$N. This value is rather low for a magnet to be used, since the weight of the box is sufficient to resist the greenwater loads up to the 20m wave height. However, a choice of installing a small electric magnet into the experimental vessel was made. This choice was made taking into account uncertainties in numerical results, which could be fine-tuned during experimental trials by adjusting the magnet's force if required.

Mounting Mechanism

The system of the box structure described in the previous section is responsible for receiving the initial horizontal loads, and making instances of failure easy to observe. However, the system is not able to record accurately the forces that are acting on the model vessel. For this reason a different mechanism was suggested. This mechanism worked complementary to the box structure, and was responsible for housing the deck system while measuring the actual forces during greenwater events.

The mounting mechanism consisted of two parts. First part is a stiff joint made out of steel plates (Fig. 3.6, *shown with purple colour*). The joint acted as the base of the box system having a horizontal plate of 6mm thick, with a cut-off section for tightly fitting in the magnet, and holes for bolting the hinge joints that were connected to the deck structure. The horizontal plate was connected to a vertical plate with a thickness of 4mm. In order to ensure that the system would be stiff enough so that the plates would practically deflect as one rigid body, and no alienation of the force measuring would be introduced to the system, two plates of 6mm each acting as stiffeners, were placed perpendicularly to

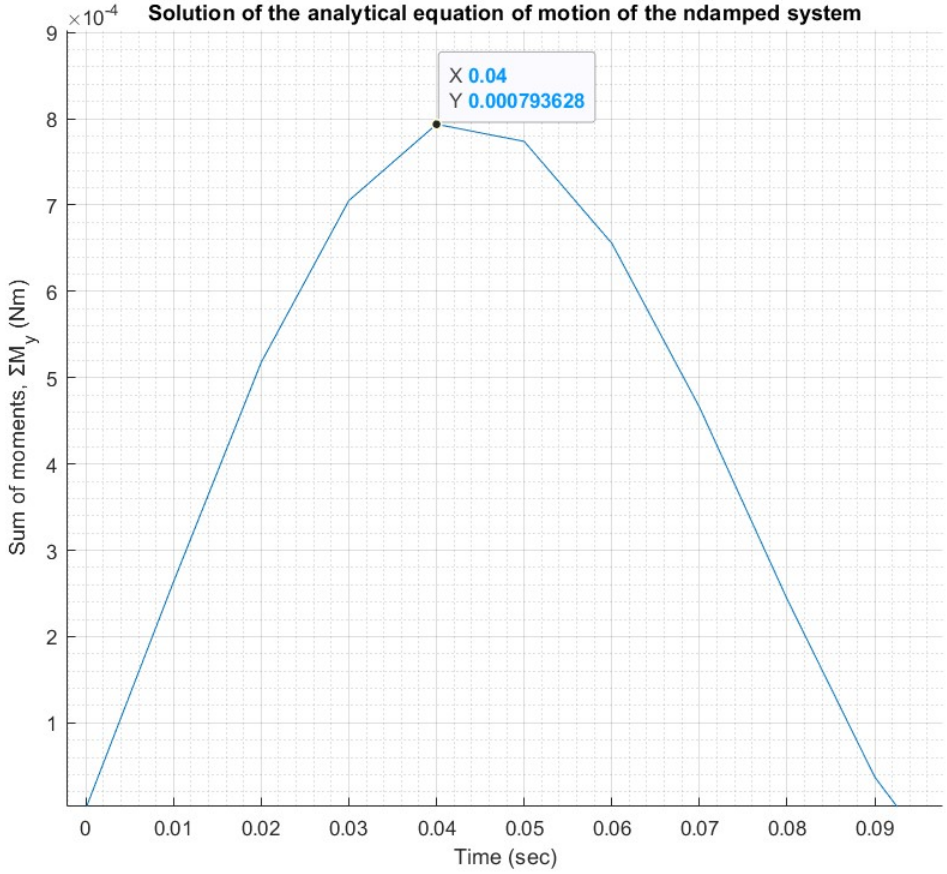

Figure 3.5: Estimated sum of moments acting on the box structure for the 20m wave height

the direction of the horizontal and vertical plates (Fig. 3.7).

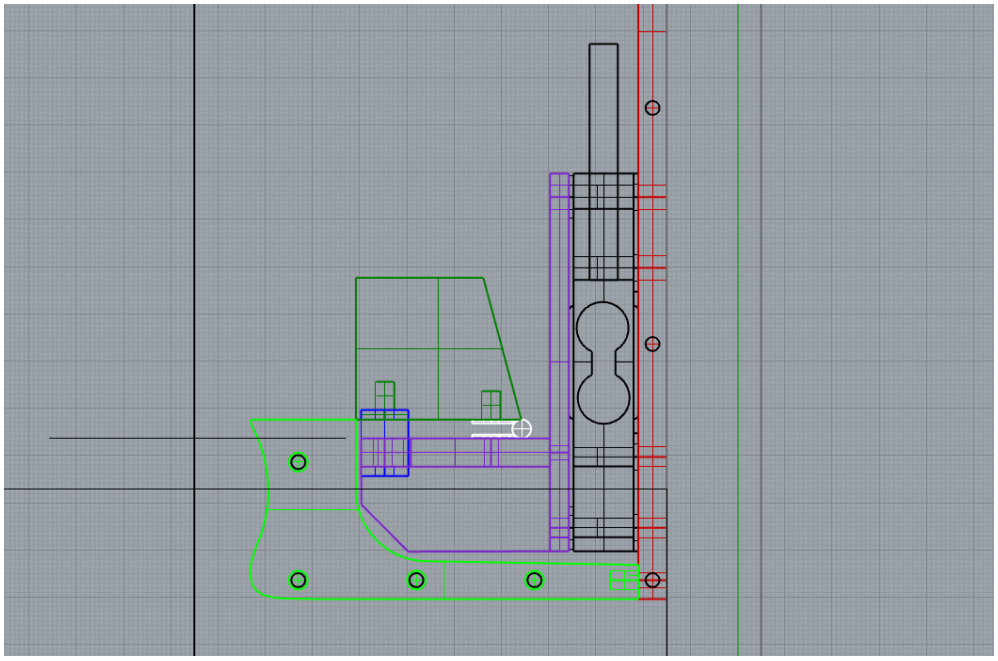

Figure 3.6: Sideview drawing of the experimental model model.

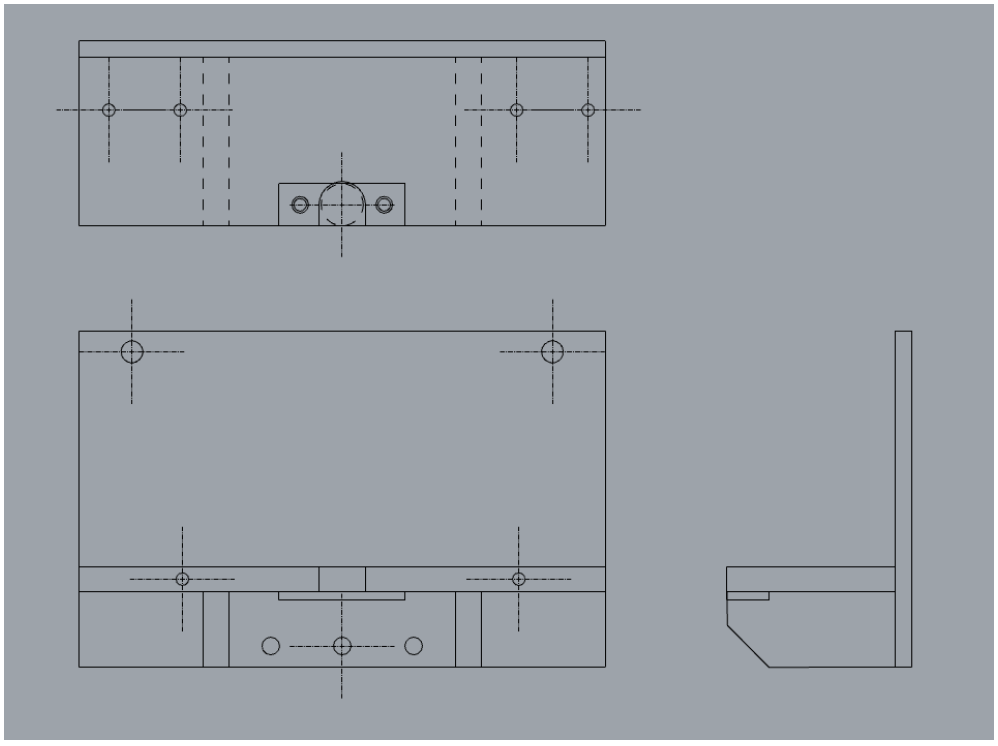

Figure 3.7: From left to right: top view, front view, and side view of the plate-joint.

Second part of the mounting mechanisms were the force sensors used for accurately measuring the forces acting on the system. The plate-joint and the box structure system were all held in place by a layout consisting of three force sensors. The force sensors were bolted from one end to the vertical plate and to the other on a stiff plate acting as the back surface of the experimental model. Two force sensors were connected to the upper left and right corner of the vertical plate and one at the center below the horizontal plate between the two stiffeners.

The number of force sensors was chosen, because three is the minimum number required for being able to measure the forces and moments in each direction reliably. The horizontal forces that acted on the deck structure, can be calculated by finding the mean displacement of the three sensors, as the horizontal force is distributed between all of them. Furthermore, the vertical forces caused during the experimental trials were neglected as the system was unable to record them for two reasons.

The axial stiffness of the force sensors was too large for any vertical deflection to take place, plus the force sensors are only able to measure in one direction, which is the one perpendicular to their longitudinal axis. This limitation does not reduce scientific interest in the collected data.With the numerical simulations conducted using ComFLOW, the vertical forces due to friction between the liquid and the box structure were at least two orders of magnitude smaller, compared to the horizontal forces for each wave height, and therefore were considered neglectable. Finally, the moments acting on the deck structure can be calculated, by finding the center of gravity of the plate joint system. With the lever-arms known for each row of magnets, the force system produced from the moments can be found finding the difference between the deflections of the top and bottom row of magnets. Then, the forces acting on the CoG of the plates can be transferred to the box-structure system. It is mentioned that for the top rows the deflections used for the calculations are the averaged of the two sensors, meaning that any 3D effects are ignored and assumed that the system works in two-dimensions only.

Support Plates

Last component of the experimental model were the support plates. The support plates consisted of three plates acting as the side walls of the model vessel. The back plate was made from steel 6mm thick, with a width of 128mm and a height of 240mm measuring from the top of the tank walls up to the kneel. It served as rigid plane, where the second end of the force sensors were bolted, and could be considered as a clap support, meaning the sensors were unable to deflect at this end.

The side walls were thin steel plates of 1mm which. The back plate was reinforced with the two steel side plates of 1mm thickness each, 100mm width and 240mm of height. Due to the geometry of the back plate acted as one-way slab transferring most of the loads to the side planes. The side planes were able to resist any bending of the back plate, as of their vertical dimension they could easily resist bending with regards to the y-y axis. Finally, the loads were transferred from the side planes onto the walls of the experimental tank, using two mechanical clamps on side. The width of the model vessel was almost 130mm as the inner width of the experimental setup. Using the clamps adequate compressive force could be produced on each side so that the system remained in place without experiencing any traslational or rotational displacements.

The benefits of using the setup for the support plates was that it allowed to easily unclamp the model and shift its position with regards to the dam-gate. As mentioned in the previous sections, when generating waves using the dam-break method, for waves with an upstream to downstream water death ratio of $0.56 < h_0/h_1$ the theoretical distance for the bores to become fully developed, without any energy loses starting to take place, is four times the downstream water depth $4h_1$. This is the design distance from the gate up to the bow of the model, considered for selecting the position of the vessel for each different wave height during the experimental trials. For placing the model on the same elevation during each repositioning, two wooden splines were used. These splines were measured to be precisely 39.6mm in height, and were place under the model until it could be evenly clamped on both tank walls. Then the splines were removed and the experimental setup was reset for a new series of experimental trials.

3.1.5. Measuring Equipment

Water Level Measurements

One of the most important parameters in the experimental layout is the upstream, h_0, and downstream, h_0, water depth. These values and their ratio are the main parameters that affect the type and properties of the generated bore, and thus the type of greenwater event that will take place. For accurately measuring the level of the two bodies of water analogue needle level indicators were used.

Needle level indicators are mechanical instruments which are based on very accurate visual inspection for measuring water levels. The indicators are metal tubes with a thin rod inside that has a very small and sharp 'needle' type of edge. Once the tip of the rod comes in contact with a still water surface a very small wrinkle-dot appears. This is because the sharp edge pierces through the surface, and due to the tension of the fluid capillary phenomena take place, making the entrance of the needle edge visible. The rod of the level indicator is controlled by small gears that can be manually raised or lowered. The distance that the tip shifted is marked on the rod, and can be controlled with an accuracy of 0.1mm.

During the experimental trials two needle level indicators were positioned vertically on the walls of the tank pointing down. One was place for the upstream and one for downstream part of the tank with regards to the gate. Each indicator was then lowered to measure zero elevation at the bottom of the empty tank. Then, having conducted test runs to measure the required water depths for achieving the design water elevations, the indicators were set to the desired level accordingly. After the indicators were set, each part of the tank was slowly filled with water. After, the water had settled down, fine-tuning could take place determining whether more water should be added or removed from each part, until the small wrinkle-dot appeared. Finally, before the trials started the needle indicators were raised so that their tip would not interfere with the flows. The process was repeated each time a new trial was run.

Load Cells

For precise measurements of the horizontal forces during greenwater events analog force sensors were used. Analog force sensors, also known as load cells, are devices designed to measure and quantify physical forces applied to them. Load cells were chosen for their ability to provide continuous, real-time data output in an analog format proportional to the applied force. The analog data is typically in the form voltage or electrical current, and is received and stored using a data acquisition system. Force censor measurements rely on the deformation of a sensitive material when subjected to mechanical loads. Having attached strain gauges on the sides of the sensor's material, the differential deformation between two points on the sensor, caused by the hydrodynamic loads would produce a change in the electrical resistance of the strain gauge, which was then converted into an analog voltage signal and was recorded.

Before selecting the force sensors that can properly function in the experimental setup, several parameters needed to be investigated. First of all, it is crucial to determine the expected range of forces expected to appear during trials. The range of expected forces in the experimental layout was assessed through ComFLOW simulations, where the whole range of the design wave heights were tested. This investigation indicated an estimated range of forces between 1N to 10N, equivalent to 0.102kg to 1.02kg. Secondly, another significant consideration is the resolution of the data acquisition system (DAS). Data aquition systems feature an Analog-to-Digital Converter (ADC) that samples continuous analog signals, voltage from sensors in the current application, and convert them into digital values. In this case, the data acquisition system includes a 16-bit resolution, which translates to diving the full measurement range into $2^{15} = 32,768$ equally spaced increments, while the 16th bit is used for the sign. For instance, in a 0 to 5-volt input range often used in experimental setups, each increment represents approximately 0.00015 volts or 0.15 millivolts.

The sensors that were selected were the Zemic 1HM 5kg sensors, which can be seen in the figure below (Fig. 3.8). The load cells have an effective measuring range of 0-5kg and a precision of 1.5mV for every increment. This translates to approximately to a maximum resolution of 0.015N for each increment based on the capabilities of the sensors. However, the noise of DAS that was used is three times the resolution of the data aquition system, based on experience using the DAS. Without, reducing the input voltage range of the system, which increases the resolution while also increasing the noise of the recordings, the final resolution of the system is approximately 0.020N for a range of 0-5V. This resolution was considered accurate enough for depicting the forces caused by the different mechanisms taking place during greenwater events.

(a) Force Censor Zinac 1HM 5kg

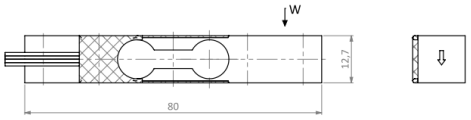

(b) Force Sensor Side and Front View

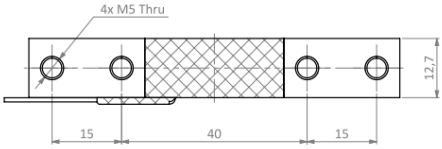

(c) Force Sensor Top View (Pictures taken from Zemic 1HM specification Sheet)

Figure 3.8: Overall caption for the three images.

The shipping of water induced loading is predominately dynamic in nature. To avoid secondary strains on the sensors that would alienate the force measurement recordings, the dynamic properties of the system were preliminarily compared to those of the loading, so that resonance effects could be minimized. The natural frequencies of both the the mounting mechanism and the sensors were calculated. The sensors were connected with a single bolt on the rigid back plate on one side and to the stiff joint on the other. Each sensor was subjected to a point load, can be found using equation (Eq. 3.12), where l_c is the length of the cantilever, and a is the distance from the support up to the location of the load. Moreover, the fundamental natural period of the system, T_o, which is the largest and most dominant natural, and thus the one most likely to produce some data distortion, is given by (Eq. 3.13), where M is the mass of the element.

$$K = \frac{6EI}{a^2(3l_c - a)} \tag{3.12}$$

$$T_o = 2\pi\sqrt{\frac{K}{M}} \tag{3.13}$$

For estimating the fundamental natural frequency of the mounting mechanisms, the volumetric mass of the deck structure and the stiff joint with were calculated and then were added to the the mass of the the three sensors. The stiffness was calculated as three times cantilever stiffness given above, resulting to fundemental natural period of the mounting mechanism $T_{o,m} = 0.0043sec$. For a single load cell the fundamental natural period was calculated using the mass of a single sensors and the stiffness of a cantilever, $T_{o,c} = 0.00078sec$. Comparing the fundamental natural frequencies of the system with an average rise time during shipping of water events, $t_r \approx 0.1sec$, is clearly concluded that for each component, the fundamental natural period, is well outside the period of the loading, and resonance occurrences that can potential distort the collected data will not take place.

High Speed Camera

The duration of the green water events as is the case for water impact phenomena is very short in duration. In previous literature many researchers have investigated the duration of the different stages of shipping of water events. The rise time ,t_r is the time between the initial interaction between the fluid and the structure up until the maximum pressure appears. From previous literature, takes around 0.10sec-0.30sec [6], [15], but depending the case specific properties there have been records where t_r can be as low as 0.05sec [44].

The very short duration of the mechanisms involved, requires recording instruments with a very high

sampling rate. For visually capturing the greenwater events the *Photron FASTCAM Sa-Z* high-speed camera was selected. *FASTCAM Sa-Z* can go up to 480K frames per second and includes built in software for post image-processing (IP) capable of measuring distances fro the videos recorded, track particles of fluids, apply thermal recognition algorithms and many more functions. For the current project the speed of the camera was set equal to the sampling rate (10kHz), which matches the sampling rate of the other components of the experimental layout,and translates to 10K frames per second. With a 10k FPS rate the *Photron FASTCAM* has a 1024x1024 resolution, with a shutter speed automatically set to 1/10163 sec. Because, the shutter speed of the camera, in order to capture 10,000 pictures every second was set to minimum required, an additional source of light was required. Complementary to the camera high power LED lights were used capable of producing up to 20,000lumen each. However, the for best image quality the LED were set to half their maximum power output.

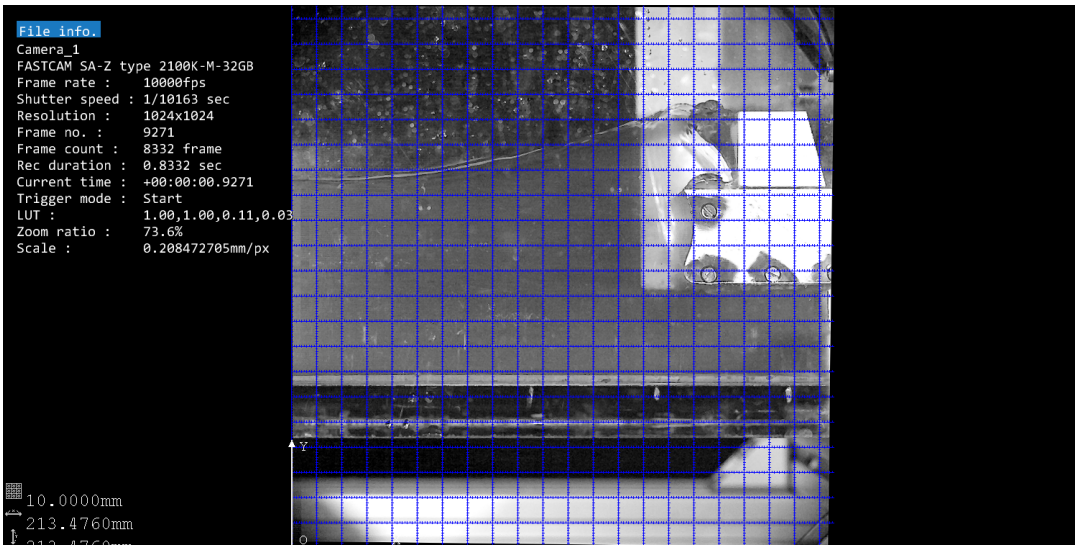

Figure 3.9: Image captured with the *Photron FASTAM-SaZ*

Before, using the camera to record the experimental trials, a lengthy configuration process was required for setting different aspects of the camera. First step was calibrating the camera. *Photron FASTCAM* was fixed in place on a sturdy horizontal surface perpendicular to the longitudinal direction of the tank around 1.50m from the side wall of the tank. The curvature of the lenses introduces small distortions on the recorded images, which increase as the distance from the center of the camera view increases. To counter this effect a procedure shown in (Fig. 3.10) was followed. Using PFV4 built in software used for configuring the *Photron FASTCAM* and playback the recording, the image distortions were captured and fine-tuned. The camera was able to recognize points on a calibrated grid where the dimensions between consecutive lines in each were known. Thus, the images once recorded, were automatically adjusted according to grid measured corrections. Furthermore, because of the short shutter time, the images were sensitive to ambient light differences. Before, every recording sessions a shade calibration was conducted through the *Photron FASTCAM*, where the camera recorded the level of ambient light, and adjusted the same level of blackness uniformly to all pixels, reducing bright and dark spots on the playback video significantly.

Besides, the main calibration taking place to deal with physical practicalities that affect the quality of the image, several filters and settings provided by PFV4 software were used for fine-tuning and improving the recordings of the experimental trials. These settings are briefly mentioned below:

- Median Filter : This filter removes all isolated spots with black or white pixels which are image capturing noise (salt-and-pepper effect).
- Edge Enchantment filter (*LEVEL3*): Increases the contrast locally, amplifying the contour of objects in the images.

- Zoomer interpolation: This setting interpolates between neighbouring pixels with very different colours for smoother image quality for large magnification.
- HDR (*LEVEL4*): High Dynamic Range is responsible for automatically enhancing the dark section, while reducing the contrast of bright areas at the same time, increasing significantly the quality for images where very bright and dark areas co-exist.
- LUT (*manual*): The Look Up Table is a graph , where at the X-axis has the input brightness and the Y-axis contains the output brightness. With this graph the RGB (Red Green Blue) channels and monochrome image can be manually tuned to improve the image quality depending the specific recording situations.
- Keystone Correlation (*manual*): With this setting the PFV4 software can correct small inclinations, due to missalignments between the camera and the object of interested can be corrected.
- Calibration Tool (*manual*): This tool can adjust a grid on the playback image where 1 pixel is correlated to its real size, offering length measuring in pre and post capture images.

With all the calibrations processes completed, and with filters and tools applied, the quality of the captured images is shown in (Fig.3.10).

Figure 3.10: Lens carvature calibration

3.1.6. Gate Release

Using the dam-break method for generating waves, a mechanism that releases the the dam gate almost instantaneously is required. In Stoker's equations which describe the dam-break flows the gate vanishes at earlier stage when $t = -t_0$ and the pressures which the equations derive from are considered to be hydrostatic. This unfortunately is not the case in real life.

As it was observed in [52] the releasing time of the gate affects significantly the water flows that are created once the gate starts rising and the two bodies of water interact. The pressures and boundary layer effects of the fluid are especially sensitive as the scaling factor of the experiment and the ratio of h_0/h_1 increase. Lauber and Hager suggested that the effects of the releasing time, t_{rel}, are minimized when $t_{rel} < \sqrt{2h_1/g}$, [30]. For the trials conducted, the largest upstream water depth was equal to $h_1 = 0.11m$, thus requiring an opening time less than $t_{rel} < 0.145sec$.

A mechanism similar to [40] was proposed. With this mechanism when the system was triggered at the beginning of a trial an electric magnet is switched off. The electric magnet released a weight which was connected by a rope string through a pulley system to the gate separating the two bodies of water. Once, the string was fully stretched, it transferred a violent impulse to the water gate causing it to rapidly open. The whole pulley system was connected through a system of rigid frames, which transferred its loads directly to main beams supporting the whole setup. Additionally, due to the strong nature of the impulse created from the string reaction, two aluminium legs were placed for compensating for the moment created by the horizontal force of the pulleys at the top frame and for reducing the unwanted vibrations created from dropping the weight. Finally, a bucket filled with sand was placed beneath the dropping weight to safely break the fall, without causing any damage to the surrounding area. The complete gate releasing mechanism can be seen in (Fig. 3.11 & 3.12).

The two main parameters affecting the opening time is the slack of the string translating into end velocity of the weight and its mass. An initial estimation of the required velocity was made using the free falling and change of momentum equations. However, the friction from the plastic frame waterproofing the cross-section between the two tanks resulted in significant difference between the estimated values and the ones measured in practise. In the end, an iterative process of fine-tuning was used and the mass of the weight ended up equal to 32kg with a slack of 20cm for rope. The opening time of the gate was measured using the high-speed camera and was equal to a little over 0.01sec.

3.1.7. Force Sensors Calibration

Force sensors measurements translate into change in the voltage of the circuit within the load cell. To extract the forces from the recorded signal of the sensors, and also to be able to reliably correlate the measured voltage changes into force values the load cells needed to be calibrated before they were used in the experimental trials. The calibration process involved determining the relationship between the sensor's output signal and the applied force and is separated into two main parts parts.

The first part of calibrating the sensors was manually loading them with an already known load and correlate the output to the force applied. For this step, the force sensors were bolted onto a solid and steady surface on the one edge, while a hook was connected and suspended from the other free end. With a time interval of 30sec, a weight increment of 200gr was added to the hook until the maximum weight suspended was 2kg in total. Then, the same steps were repeated by removing the weighted plates from the hook for every time interval until no weight, beside the hook was suspended from the free end of the sensor. This process was followed twice for every load cell, once using the indicated side where the deflections are designated as positive, and once for the opposite side, where the deflections of the sensors are recorded as negative. The recorded signal of the sensors can be seen in (Fig. **??**):

Second step in calibrating the force sensors, was processing the recorded signal. The mean value of the voltage recorded for every time step was used, after the mean value of voltage corresponding to only the hook hanging from the free end of the load-cell was subtracted from the rest. After that, the

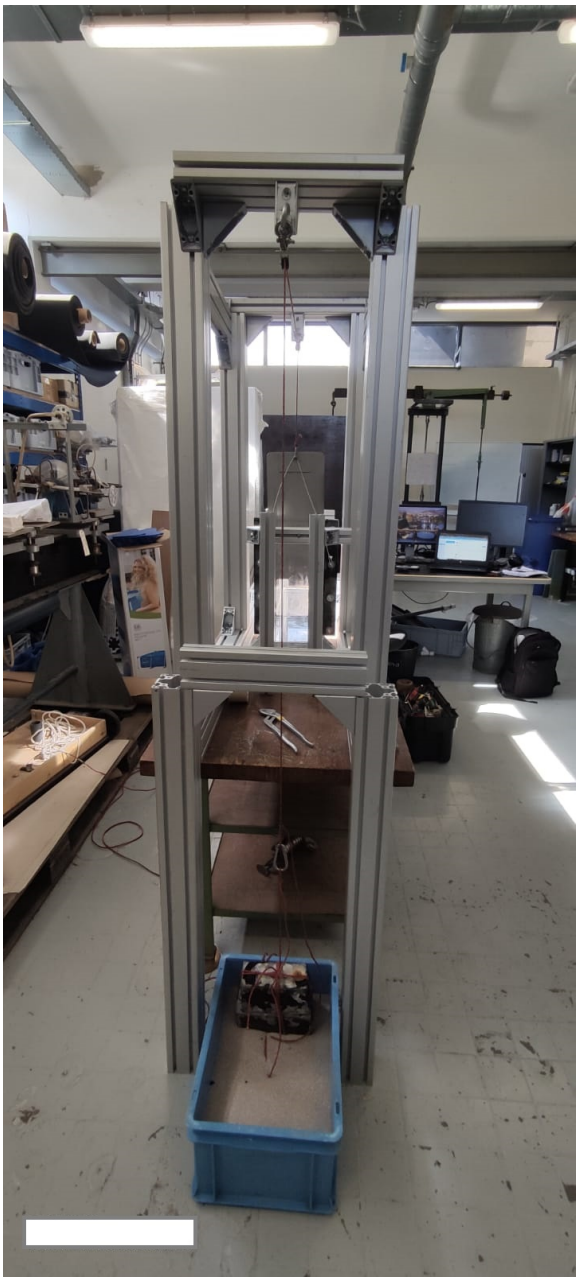

Figure 3.11: Gate Opening

Figure 3.12: Caption for Image 2

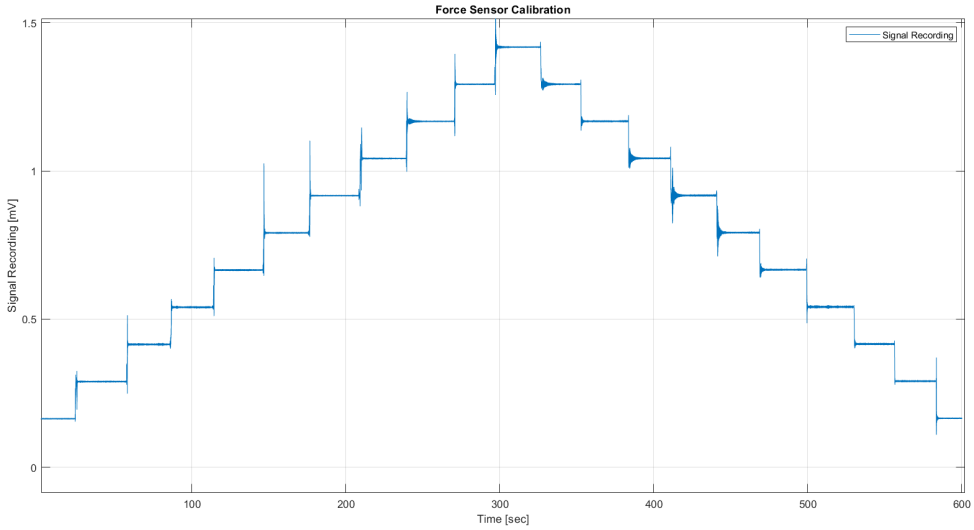

Figure 3.13: Positive direction ladder incremental loading of force sensor

weight of the calibrated plates was divided with the corresponding potential difference value for each increment and then, their mean value was estimated. The mean value of the weight divided by the voltage is known as the calibration factor, and it was used for converting the voltage into a force signal linearly, which was not the case for the complete meassuring range of the sensors.
Finally, to verify the reliability of the sensors the normalized residual error was found. The values calculated by using the calibration factor were subtracted from ones recorded by the sensors, and then were divided with the largest voltage value in the measurements. The maximum residual error was found equal to 4% of the recorded value, therefore the sensors were deemed reliable enough to be used for the experimental trials. The same process was conducted once for each sensor and the values for both the negative and positive sides for producing the calibrations factor were used for each sensor.

Sensor	Calibration Factor [N/V]	Maximum Residual Error [-]
Sensor 1	15.657	0.04
Sensor 2	15.856	0.03
Sensor 3	15.355	0.01

Table 3.6: Sensor Calibration Data.

4

Numerical Simulations

4.1. ComFLOW

Numerical simulations were conducted using the software ComFLOWdf. ComFLOW is a commercial CFD (computational fluid dynamics) software that specializes in violent free-surface flows. ComFLOW was firstly developed for viscous two-phase flows based on the Volume-of-Fluid method, using a Cartesian-grid for defining the liquid and solid domains. Additionally, one of the strengths of ComFLOW is that it utilizes a combination of domain descretization and numerical solutions algorithms, that can provide a description of complex and violent free-surface flows with reduced CPU usage and high accuracy results, making ComFLOW an ideal software for the current project.

4.1.1. Mathematical Expressions

For most CFD software first step is creating a simulation domain, let it be Ω. The domain is then discretized into small volumes known as computational cells. The properties of the fluid within the simulation domain can be described by quantifying the properties of the fluid at several points at center and boundaries of each computational cell. To connect and quantify the properties of a fluid on a single point the Navier-Stokes equations can be used. For the case of a two phase flow, including a incompressible viscous fluid and a compressible viscous fluid the Navier-Stokes equations are given below:

$$\frac{\partial \rho}{\partial t} + \nabla \cdot (\rho u) = 0 \tag{4.1}$$

$$\frac{\partial \rho u}{\partial t} + \nabla \cdot (\rho u u) = -\nabla p + \nabla \cdot (\mu \nabla u) + \rho F \tag{4.2}$$

,where ρ is the density, μ is the the dynamic viscosity of the fluid, F the external forces acting on the simulation domain, and $u = (u, v, w)$ the velocity vector in space.

The incomprennsibility of the flow is expressed through (Eq. 4.1), which is known as continuity or conservation of mass equation. The first term represents the rate of change in density in the fluid withing a point, (very small finite area for a physically sound interprentation), of Ω and the second term the divergence of mass entering or leaving this finite area. For incrompressible flows the first term can be set equal to zero as density remains steady, meaning that the flux of the amounts of the incoming mass should be equal the outgoing one.

The viscosity of the flow is expressed through (Eq. 4.2), which is known as the momentum or conservation of momentum equation. This equation describes the force balance on a point marrying together

the external forces acting on it with the internal changes taking place in the volume. The first term it the inertial force, the second term is the convective acceleration describing the interaction of fluid particles and the change of flow within a field, the forth term is the pressure forces, and it describes the viscous forces within the fluid, and the last term describes external forces acting on the computational cell.

Moreover, there is a need for an additional equation to properly describe the behavior of the gas phase . The equation used for incorporating the compressibility of the gas within the flow is shown below (4.3):

$$\frac{p_g}{p_{ref}} = (\frac{\rho_g}{\rho_{ref}})^{\gamma} \tag{4.3}$$

,where p_g and ρ_g is the pressure and density of the gas in the two-phase flow and p_{ref} and ρ_{ref} is the ambient pressure and density, which is assumed equal to the atmospheric pressure and density of the air, unless specified otherwise.

Finally, ComFlow is able to model the interaction with an object withing the simulations domain. The flow around an object induces forces on it that result from two main things. The first is a force that is created due to pressure acting perpendicular to the the object's surface, S, and the second force is created due to the viscosity of the fluid and acts parallel to surface of the object. However, the later forces are neglected in ComFLOW as they are typically much smaller in magnitude compared to the pressure forces. For calculating the forces on an object (Eq. 4.4) is used, where p is the scallar value of pressure and n is the unit vector perpendicular to the surface, S.

$$F_p = \int_S p \cdot n \, dS \tag{4.4}$$

4.1.2. Boundary Conditions

To numerically solve the system of the differential equations two types of input needs to be defined. Firstly, restrictions that concern the boundaries of the simulation domain, and secondly, conditions that describe the state that the system is at the beginning of the simulations. The former are called boundary conditions and express properties of the system that derive from its geometry, whilst the latter are called initial conditions and determine who the behavior of the system will unfold through the duration of the simulation.

For two-phase flows boundary conditions need to be applied only at the boundaries of Ω. For boundaries in contact with solid objects two main conditions are applied by ComFLOW. First condition is known as the impenetrable boundary condition, meaning that the velocity of the fluid perpendicular to a solid boundary is always equal to zero, as the fluid cannot pass through the object. Second condition is known as the no-slip boundary condition, meaning that velocity along the solid boundary is also zero, as the fluid sticks to the wall because of its viscosity.

For the free surface in two phase flows, ComFLOW incorporates capillary forces describing the interaction between liquid and gas through the last term describing external forces on the fluid in (Eq. 4.2). Furthermore, to model the interaction of gas and fluid within a computational cell, the software averages the density and the viscosity by cell-weighted averaging the values, between the fractions of a cell open for flow,F_b, and filled with liquid,F_s, (Eq. 4.5-4.6). Lastly, the the edge of the cells the density is averaged between neighbouring cells, and ensuring that the interface at a free surface is smooth, and no artificial velocities are created from inconsistencies.

$$\rho = \frac{F_s}{F_b}\,\rho_l + \frac{F_s - F_b}{F_b}\,\rho_g \tag{4.5}$$

$$\mu = \frac{F_s}{F_b}\,\mu_l + \frac{F_s - F_b}{F_b}\,\mu_g \tag{4.6}$$

, where ρ_l and μ_l are the incompressible liquid density and dynamic viscosity, and ρ_g and μ_g are the compressible gas density and dynamic viscosity.

4.1.3. Cell labeling

To describe the computational domain Ω, ComFLOW uses a Cartesian grid, with variables measured at a specific location in the simulation space. In this arrangement, cell centers is the location where the pressure values are being sampled from, while velocity components are measured along the wall of computational cells boundaries. To describe the behaviour of the two-phase flow around complex structures within the computational grid, cells of different types are introduced. These cells interact with each other through edge and volume apertures.

The introduction of edge and volume apertures enables the assignment of geometry labels to cells. This geometry can represent which part of the cell face or cell volume is open to flow. Describing the nature of a cell within the simulations, fluid cells, boundary (B) cells, and exterior (X) cells are defined. For describing the free surface, the fluid cells are further organised in empty (E) cells, Surface (S) cells, and fluid (F) cells. An example representing the labelling system in ComFLOW is given in (Fig. 4.1).

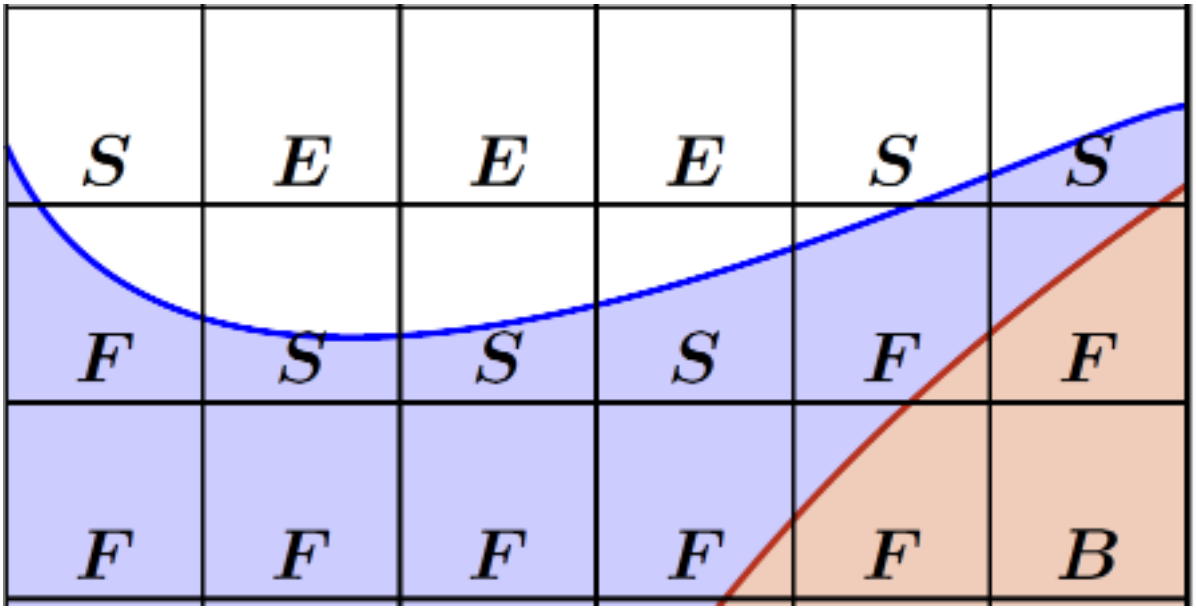

Figure 4.1: Geometry cell label system (*taken from the ComFLOW manual*)

4.1.4. Discretization

As described in the previous subsections to describe the behaviour of the flow the discretized in time and space Navier-Stokes equations are used. In the iterative algorithm used for the numerical simulations the pressure and velocity terms are decoupled. The velocity solution of the Navier-Stokes formulas for each direction is used by ComFLOW for calculating the pressure gradient using a Poisson equation, and then with the calculated pressure values, the velocity field is updated in order to satisfy the continuity equation for each time step. After all the velocity and pressure values for each computational cell have been calculated, the free surface is displaced using the VOF-method combined with a local height function depending on the type of computational cell and its surroundings as identified above. The discretization and extrapolation schemes used by ComFLOW for calculations all the required quantities during each time-step are presented in (Tabl. 4.1), and are briefly explained below.

- Forward Euler (First-Order) : numerical method of solving ordinary differential equations with ini-

Discretization	Method
Time	Forward Euler (first -order)
Spatial	User defined mesh size
Numerical Stability	CFL-condition
Volume of Fluid (VOF)	PLIC/Youngs
Advection	Macho
Convection	B2 Scheme (First-Order Upwind)
Velocity Extrapolation	Linear
Pressure Extrapolation	Linear
Density	Gravity consistent averaging
Step Termination Criterion	Low residual error/Maximum number of iterations

Table 4.1: Discretization settings used for the simulations in ComFLOW

tial conditions. After the independent variables have been decoupled into a system of ordinary differential equations, the variables for next step are expressed as a functions of the quantities of the current step, using two locations.

- The Courant-Friedrichs-Lewy (CFL) condition: is a necessary condition for convergence of partial differential equations, and it can be summarized for a 2D case as:

$$CFL = \frac{u_x \Delta t}{\Delta x} + \frac{u_y \Delta t}{\Delta y} \leq CFL_{\text{max}}$$

  The time step Δt is adjusted automatically according to the spatial step and the velocities for both directions to satisfy the CFL-condition during each step. Limiting upper and lower values for the simulations were set as CFL $\in$ [0.25 0.75] as suggested in [27].

- Multi-dimensional Advective Conservative Hybrid Operator (MACHO): is a explicit method for calculating the advection in one direction based also on the advection on transverse directions, using operator splitting techniques. The flux in one direction is calculated initially, while intermediate steps are reconstructed for treating the other directions,

- Piecewise Linear Interfrace Calculations (PLIC) is a method of VOF where for surface cells (S) a straight line segment (normal vector to the surface and a constant value for offset) is used to approximate the gas-liquid interface. Young's method is local height function where the interface normal vector is calculated in the computational cell's corners and then is averaged for calculating the vector normal to the cell's interface.

- B2 scheme: is an option for introducing artificial diffusion to stabilize the discretization method. It employs a first-order upwind scheme where two positions whose location is determined by the direction of the convection are used to descritize the convection equation and define the value of the convected quantities for the next time-step.

- Linear extrapolation for estimating the pressure and the velocity quantities at grid interfaces between cells based on their respective values at the center of the neighbouring ones.

- A gravity consistent averaging method, where the density is calculated at the center of the computational cell and is coupled with the cells filling ratio. To avoid the spurious velocities the averaged density is used in the momentum equation without the presence of a flow, thus the pressure gradient is equal the gravitational forces, allowing for a discrete averaged density by satisfying this condition $\nabla \times (\rho \mathbf{F}) = 0$, [54].

4.2. Simulations

To be able to design some aspects of the experimental setup described in 3, and to be able to compare and examine specific aspects of the experimental setup in an exactly repeatable way and draw conclusions, simulations were conducted for all the wave heights that were to be tested in the experiments. Two dimensional simulations following the design of the experimental layout were chosen. The simulation domains consisted of a single plane, where out of plane phenomena were ignored. Furthermore, by reducing the simulations space a greater refinement in spatial disecretization could be implemented, thus achieving convergence of results with also significantly reduced computational power and time efficiency, while maintaining similarity and being able to compare the experimental configuration, by assuming the same behaviour throughout the width of the setup, ignoring therefore 3D phenomena.

The numerical simulations consisted of three different parts which were defined separately. First element was the simulation domain, Ω, which was the same for all simulations. It consisted of a vertical plane with dimensions of 813mm x 280 mm. The boundaries of the simulation were walls except for the top which was ambient air. Second component was the bodies of water responsible for creating the individual bore that generated the greenwater events. For all the simulations the upstream body of water was the same, measuring from the x=+312mm to x=+813mm (where x=0 is the location of the water gate), and with an upstream water depth $h_0 = 65mm$. However, the downstream water depth, h_1 differs with each wave-height and was selected so that the ratio of h_0/h_1 could produce the desired wave height.

Last piece of the numerical simulations was the vessel model. The model vessel was constructed using several 2D quadrilateral elements (same as the bodies of water) by defining the four vertices corresponding to the elements corner clockwise. The box structure was incorporated to the top of the deck with the whole model represented as a solid stationary object, which was fixed in position for all degrees of freedom, and thus unable to move or rotate. For each consecutive wave height, the model was positioned at a distance of $4h_1$ from the water gate in the longitudinal direction, where the maximum wave height and the generated wave was expected to be fully developed.

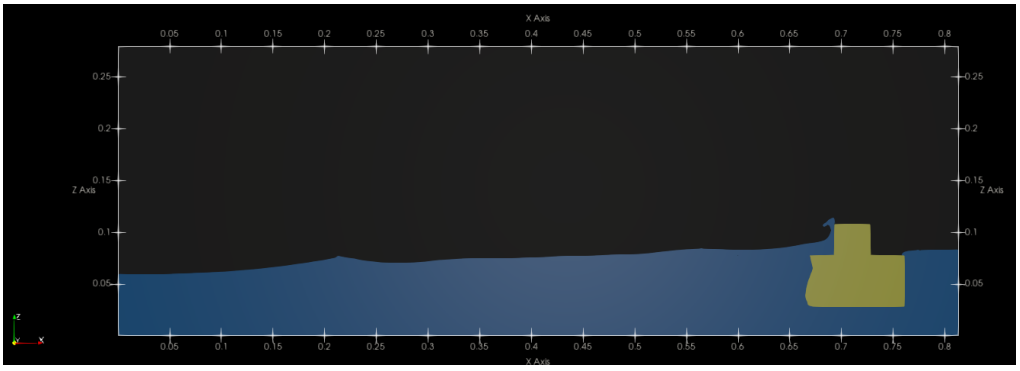

Figure 4.2: Simulation domain using ParaView for vizualization.

Finally, the properties of the gas/liquid phases defined are presented in (Tabl. 4.2). For all quantities ComFLOW uses the SI units.

4.2.1. Convergence Study

As mentioned before with numerical simulations, the simulation domain is ”dissected” into smaller pieces or computational cells, where the differential equations describing the physics are expressed. Generally, the smaller the cell size the more accurate the results are, theoretically estimating the exact solutions when the cell size becomes infinitely small reducing to a point. However, this is not computationally and mathematically possible, and a finite mesh size is used accompanied by inevitable discretization error residuals.

Quantity	Value
Liquid density [kg/m^3]	1000
Gas density [kg/m^3]	1
Liquid viscosity [$Pa \cdot s$]	0.01
Gas viscosity x 10^{-3} [$Pa \cdot s$]	0.17
Isentropic expansion factor [-]	1.40
Gravitational acceleration [m/s^2]	9.81

Table 4.2: Gas-liquid phase properties

The investigations of the the discretization errors are considered acceptable and the refinement level of the computational grid is called convergence study. The estimated results, as the computational cells become smaller and smaller and the grid becomes denser, show minor differences in values meaning that decreasing the element size will present an asymptotic behaviour in the numerical simulations output. Therefore, the goal of a convergence study is to determined the grid size where the results present asymptotic behaviour and convergence has been reached.

To carry out the convergence study the Grid Convergence Index (*CGI*) method proposed by Roache [46] was used. The GCI method is a widely used straightforward method, which can easily and accurately show the convergence of the mesh, by examining a single parameter of the simulation. The CGI method is based on the Richardson extrapolation where the exact solution of a dense grid can be approximated by (Eq. 4.7), where p is the order of convergence, r is the ratio between the size of two consecutive grids, f_{exact} the exact value of the quantity, and f_i, f_{i+1} the numerical results for the two consecutive simulations.

$$f_{exact} \approx f_i - \frac{f_i - f_{i+1}}{r_{i+1,i}^p - 1} \tag{4.7}$$

A practical way for checking simplifying the grid convergence index method is to choose a steady ratio between the size of consecutive grids. If the the ratio of the mesh size remains steady between the successive simulations the order of convergence can be calculated using (Eq.4.8). The grid convergence index values can be estimated using (Eq.4.10), after first defining the relative error of the consecutive simulations given in (Eq. 4.9). The coefficient F_s is the safety factor which is used to multiply the relative error value when three simulations are used to investigate the asymptotic behavior of numerical solutions, which is based on experience using CGI as recommended in [46].

$$p = \frac{log(\frac{f_i - f_{i+1}}{f_{i+1} - f_{i+2}})}{log(r)} \tag{4.8}$$

$$e_{i+1,i} = |\frac{f_i - f_{i+1}}{f_i}| \tag{4.9}$$

$$GCI_{i+1,i} = F_s \frac{e_{i+1,i}}{r_{i+1,i}^p - 1} \tag{4.10}$$

In the current convergence study three simulations, Simulation 1-3, of the 20m waveheight range were used with a steady refinement step by reducing the cell dimensions in a 2D domain by half in each direction for each consecutive trial. For the first simulation Simulations 1, 4mm x 4mm elements were used with an increasing number of elements by a ratio of four,$r = 4$. The quantity that was chosen for investigating was the horizontal force, F_x, on the box structure at a specific time instance (t=0.625sec) with the measurements acquired by ComFLOW built-in functions. The values of all the parameters mentioned above that are using for calculating the CGI can be seen in the table below (Tabl. 4.3).

From the values of (Tabl. 4.3) that between horizontal forces between the two most refined simulations

Quantity	Abbr.	Simulation 1	Simulation 2	Simulation 3
Number of Elements	$-$	14,210	56,850	227,640
Ratio of grid size	$r_{i+1,i}[-]$	-	4.001	4.004
Order of Convergance	$-$	-	-	3.36
Absolute Error	$e_{i+1,i}$ [%]	-	26.2	0.34
Horizontal Force	$F_x \cdot 10^3$ $[N]$	9.046	6.676	6.654
Grid Convergence Index	$GCI_{i+1,i}$ [%]	-	3.127	0.004

Table 4.3: Convergene study related quantities

that the relative error was very small, while the CGI value could be considered practically zero. Therefore, the mesh size of Simulation 3 consisting of 1mm x 1mm elements was considered converged and the results yielded by such a refined mesh could be used for designing for the experimental setup and for further result interpenetration.

The CGI presents a qualitative measure of how far away the results yielded by the simulations from the asymptotic numerical value are. Intuitively the lower the CGI values are the the closest the numerical solution is to the actual value. As an index it provides an estimate of the amount of discretization error in the finest grid solution compared to the fully converged value, but not the exact solution which remains unknown.

However, as shown in [48] the safety factor F_s could be considered as representing the 95% confidence bound on the estimated relative error. Based on the above a confidence interval could be defined using the CGI in (Eq.4.11), while using Richardson's interpolation an estimate of the fully converged solution, f^* can be found from equation (Eq.4.12) using the solutions of the most refined simulations.

$$[f_{i+2}(1 - CGI_{i+2,i+1}), f_{i+2}(1 + CGI_{i+2,i+1})] \tag{4.11}$$

$$f^* = \frac{r^p_{i+2,i+1} f_{i+2} - f_{i+1}}{r^p_{i+1,i} - 1} \tag{4.12}$$

4.2.2. Validation

After setting up the simulations and selecting the appropriate grid size, the next essential step is to conduct a validation study to ensure that the computational environment can accurate describe the real life application. There are several methods to validate a software for a specific application, such as comparing the results yielded numerically, with the exact solution of a problem. Another method is comparing the results with benchmark simulations yielded by other validated software, and finally by comparing the results with data acquired through experimental trials. For validating the results obtained by ComFLOW the latter method was used. A similar experimental layout, where greenwater events were reproduced, was used for as the basis for validating the results, before the experimental trials of the current project could begin.

For comparing the performance of ComFLOW a specific quantity at a specific location was used, which was monitored for the whole duration of the simulation. This quantity was the elevation of the water at the location of a pressure sensor in [34]. Hernández-Fontes et al. conducted a series of experiments where the dam-break method was employed for generating different types of individual green-water events. A wave probe, $WP1$, which measured the water elevation was placed in the middle of the tank upstream the water gate. The experimental layout presented in [34] was reproduced using the ComFLOW software. A monitoring line was positioned for custom measuring the water elevation from the location the WP1 probe used in the experiments of Hernández-Fontes et al. would be placed inside the simulation domain. The results of the ComFLOW simulation and the wave elevation measured by Hernández-Fontes et al. can be seen in (Fig. 4.3).

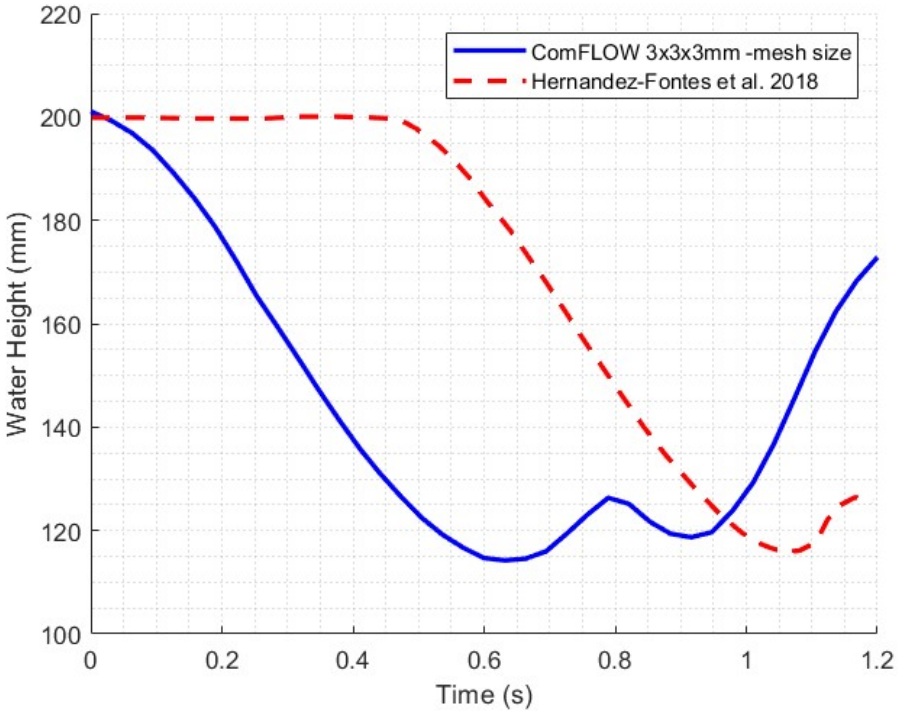

Figure 4.3: Wave height calculated by ComFLOW and measured by Hernández-Fontes et al. (2018)

The results obtained using ComFLOW present an accurate estimation of the behaviour of the free surface as the water gate is lifted and the bore develops. The water elevation calculated is within the values measured from [34], with extremely small deviation between the experimental and numerical results, whereas the shape of the curve is almost identical. The only difference is a significant time shift of around 0.5 sec from the moment the water height starts changing at the location of WP1. This time lag is attributed to the way the water gate opening is modelled.

In the ComFLOW simulation the water gate vanishes at t=0 at the start of the simulation. This translates to the body of water collapsing on itself as the boundary pressure at the position of the watergate becomes equal to the atmospheric pressure and the gravitational pull takes effect. However, in the experimental layout the lifting of the watergate takes a finite time. During that time the pressure is equal to the hydrostatic pressure for every level that is still in contact with the gate. Additionally, the movement of the watergate introduces an upwards velocity in the fluid at the boundary layer which propagates inwards the body of water due to the fluid's viscosity. Thus, the inertial forces and the pressure difference that cause the body of water to collapse, acting as a piston creating a wave, take effect later in the experimental layout compared to the numerical simulation. Finally, another practical issue is that trigger mechanism for the data capturing system in experimental setups is not instantaneous as in the simulation domain. From the momment that the recording time starts running and the trigger signal is sent, there is a time lag until the actual releasing of the gate. For all the above, it is concluded that ComFlOW is able to produce accurately the behaviour of the experimental layout of [34], and therefore suitable for simulating the experimental setup of the current project.

4.2.3. Simulation Output

For post-processing the results from the CFD simulations are automatically saved in a VTK (Visualization Toolkit) format. These files formats provide the possibility of storing a large amount of data for several time-steps, while at the same time enabling visual representation of several quantities using commercial post-processing software.

ComFLOW can create snapshots using the vtk file format, where the initiation time, time interval, and the simulations duration for collecting output can be explicitly defined. The output files include information about the velocity field components (u, v, w), pressure field, also include details regarding the geometry and the simulations domain, and liquid distribution over the computational cells. Specifically for the two-phase simulations, gas density and pressure information is also incorporated in the files. To calculate additional quantities like forces, or record quantities at a specific location not coinciding with cell center or boundaries monitoring points can be used. ComFLOW provides the option for several types of monitoring options, however only the two used in the current project are mentioned.

First monitoring method is the relative wave height lines. These are vertical lines that can be set manually at a specific location and for a given length. Relative wave height lines calculate precisely the water height, and are more precise compared to simple fill boxes which meassure the water height and store the information in the VTK files. Relative water height lines consider the actual liquid distribution within grid cells through a piecewise linear reconstruction (PLIC) aglorithm. Monitoring lines were defined in two positions along the downstream part of the simulations domain; one at a steady position within the simulation domain and another one just before the bow of the vessel, which corresponded to monitoring points selected for comparison with the experimental trials.

Second monitoring tool used were the force boxes. Force boxes are defined by stating the start and end point of the box in each direction. They calculate the total forces and moments acting on the box, by integrating the pressures in the domain defined from all pressure contributions on all closed cell segments. For each simulation a single force box was defined around the windward side of the box structure so the total forces acting on that front surface of the deck structure could be calculated. The results of the maximum water elevations for both monitoring points, η_1, η_2 respectively, and the maximum force and moment for each wave height can be seen in the table below (Tabl.4.4).

Quantities	**14m**	**15m**	**16m**	**17m**	**18m**	**19m**	**20m**
Elevation Location 1, η_1 [cm]	2.48	2.49	2.72	2.93	3.21	3.92	4.07
Elevation Location 2, η_2 [cm]	3.57	3.78	4.07	4.32	4.37	4.59	4.87
Max. Horizontal Force, F_x [N]	0.51	0.72	0.92	1.27	1.40	1.50	1.85
Max. Moment, M_Z x 10^{-3} [Nm]	0.47	0.55	0.82	0.90	0.95	0.99	1.31

Table 4.4: Maximum values of simulations results for all the wave heights simulated

For all simulations the a grid of 227,640 elements was used with an element size of 1mm x 1mm. The simulations time was set to t=1.2sec. For the ".vtk" files the recording frequency was 200Hz or t=0.05sec, due to the dense information and large data . while for the capturing the values of the water height at the monitoring locations and for the forces measured by the force box a sampling frequency of 1000hz or t=0.001sec was used. Moreover, it is stated that for the 2D simulations the ComFLOW results are expressed in the SI units normalized by a meter length. Therefore, the values of the forces and moments presented in (Tabl.4.4), are multiplied by the experimental tank width (0.130m) to match the values that are expected during trials.

5

Experimental results

5.1. Monitoring Points

The measuring instruments used in the experimental trials collected two types of data. First type comes from the force cells and was used for measuring the horizontal forces acting on the deck structure during the later stages of the greenwater events. The sensors captured the change of voltage, which was caused by the change of resistance in the sensor's circuit, when the horizontal loads were applied and the sensors deformed, thus mechanically changing the resistivity of the system. The output signal was then collected and stored in ".tdms" format files by the console used for synchronizing and running the different components of the experiment.

Second set of data was collected through the high-speed camera. With the Photron camera the shipping of water phenomena were captured in video. Combined with the camera's post processing software the data could offer visual inspection of the physical mechanisms involved in the greenwater event, while allowing for gathering information on the properties of the incoming wave and the resulting on-deck flow that was taking place in the early stages of the greenwater events.

With the data measuring the greenwater loads the monitoring points were known and corresponded to the location of the sensors. With the properties of the mechanical system known, a correlation between the forces recorded by the sensors and the forces and moments acting on the on deck structure could be made. Meanwhile, for the video recordings the camera image covered a wide area of the experimental setup. Therefore, for this type of experimental input, monitoring points needed to collect information about the incoming wave at specific locations of interest. Two points were selected to collect information on the incoming wave where the water elevation was measured.

The high-speed camera was bolted on a steady and leveled table and was not relocated for the whole duration that the experimental trials took place. The image was placed in a distance where the field of view (FOV) could cover an area with dimensions of 21.3cm x 21.3cm. Both of the selected points were located at different positions for each series of experiments. This choice was based on the on the properties of each wave height simulated and the layout of the experimental setup.

The first point corresponded to the location of the edge of the model vessel's deck. This monitoring location was selected to measure the elevation of the exceedance height of the freeboard. This point slightly varied in location depending on each experiment, since the main purpose was to capture the maximum elevation of the body of water from the deck level. Freeboard exceedance is affected from both the type of greenwater event occurring and the specific trial, so no strict location for measuring was required, unlike the second monitoring point where an exact position was determined.

For determining the second monitoring point finding the properties of the generated wave was used the parameter justifying the above choise. The dam-break method that was used for generating non-linear

Wave height	Design wave height	Dispersion Coefficient	Wavelength	Ursell Number
$[m]$	$H[m]$	$K_s[1/m]$	$L_s[m]$	$Ur[-]$
14	0.035	10.246	0.6132	52.638
15	0.0375	10.606	0.5924	52.638
16	0.04	10.953	0.5736	52.638
17	0.0425	11.291	0.5565	52.638
18	0.045	11.618	0.5408	52.638
19	0.0475	11.936	0.5263	52.638
20	0.05	12.246	0.5131	52.638

Table 5.1: Incoming wave properties based on the full scale design values.

and non periodic wave which can not described by the equations from Airy theory for linear waves. Boussineq and later Rayleigh were able to derive the equations for solitary waves. Solitary waves can be considered an extension of cnoidal waves, that are waves which can be described as a summation of a finite series of waves (cnoidals), where the velocity potential and the surface properties are based on the ratio of amplitude over depth called the beta parameter, which is raised in ascending order for each succeeding term used. The cnoidal wave theory is used for ratios larger than $\frac{H\,L^2}{d^3} \approx 26$ for intermediate and shallow waters, where the Stokes theory is not applicable. As the water depth decreases the wave crest sharpens and the through flattens. For very small depths the wavelengths compared to the waterdepth tend to reach very large values ($L \approx$ inf), which are called solitary waves solitons [24].

Madsen et al.[33] in the research they conducted based on tsunami waves simulated the evolution of initial rectangular shaped spans of water propagating large distances over constant depth. In their investigations they derived simplified equations to describe both cnoidal and solitary waves in steady water depth with very good agreement compared to previous literature. Madsen et al. showed that for high Ursell numbers ($Ur > 51$ where $Ur = \frac{H\,L^2}{d^3}$), which is a dimensionless number used for evaluating non-linearity of long waves on a fluid layer the cnoidal wave equations coincide with the solitary waves equations. The analytical equations for the dispersion coefficient ,K_s, wavelength L_s, the wave celerity, c_s , and angular velocity, Ω_s for solitary waves:

$$K_s = \frac{1}{d}\sqrt{\frac{3H}{4d}} \tag{5.1}$$

$$L_s = \frac{2\pi}{K_s} \tag{5.2}$$

$$c_s = \sqrt{g(d+H)} \tag{5.3}$$

$$\Omega_s = K_s c_s \tag{5.4}$$

,where H is the wave height, and d the water depth equal to h_0 for the wave propagating downstream of the the water gate.

These equations were initially tested using the design values of the the waves to calculate the properties of the generated waves which were then compared with the properties of the generated waves. These values are presented in (Tabl. 5.1). The lengths of the design waves were captured by the camera, before the experimental trials took place, where waves for each wave height range were generated on an empty tank.

As can be seen in the snapshot from the the camera feedback (Fig.5.2) the estimated wave weight showed good agreement with the recorded wave length. The design value of half a wave length was equal to $\frac{L_s}{2} = 25.6cm$, showing a difference of 1.4cm or 5.6m in full scale on one side, while the generated bores showed a slight left skewness, meaning that the difference is potentially less on the other half. Therefore, it was concluded the solidarity equations could adequately describe the produced waves for the requirements of the current research.

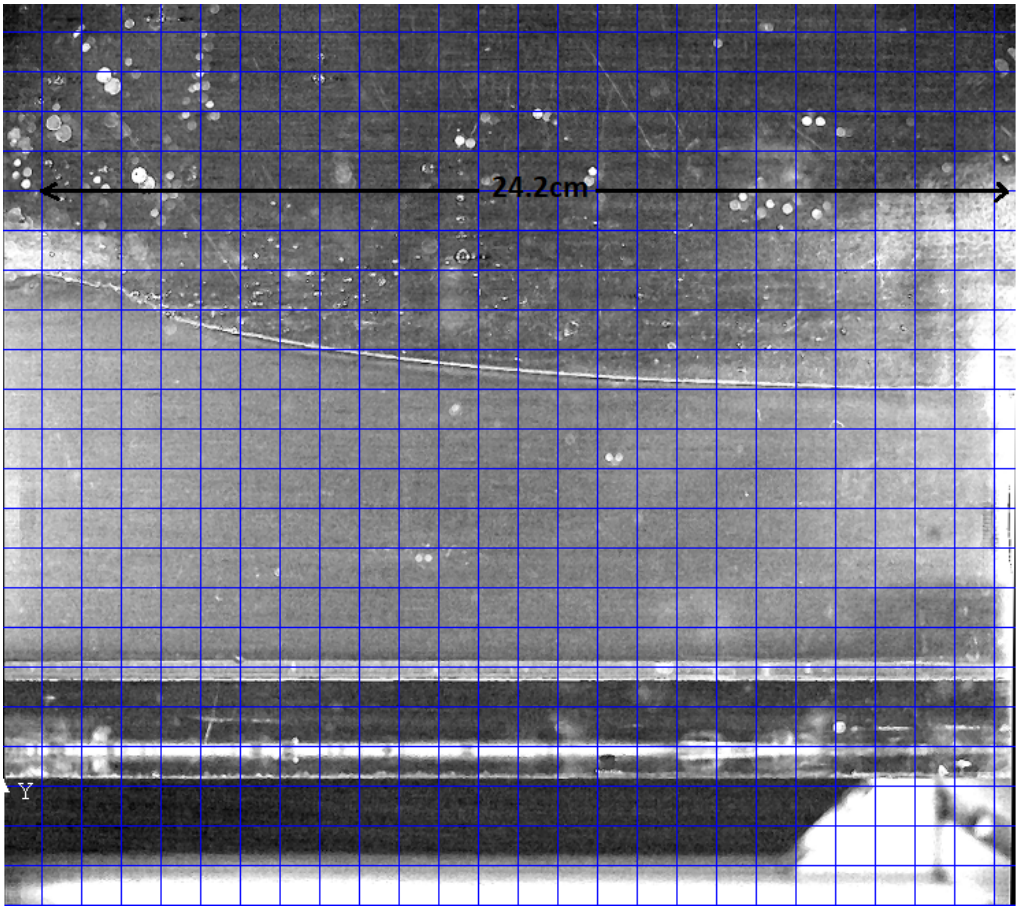

Figure 5.1: Half wave length captured during wave generation trials for the 20m wave

The problem for selecting a second measurement point laid into two factors. First factor was that due to the limited space and the design behind the experimental configuration, the location where the wave would be fully developed at a distance of $4h_1$ based on [38] coincided with the location of the edge of the model for each wave height tested. Secondly, even though the design water elevations were successfully achieved while running trials without the model vessel placed in the tank, significant reflection took place while the model was positioned in place for the experiments, especially near the locations where the incoming flow would reach its maximum development.

Finally, to overcome these difficulties the second monitoring point was positioned at a fix location 2mm downstream from the left edge of the field of view of the camera. That positioned was chosen for two main reasons. First, of all the it was observed that not significant reflection took place at that location for any of the wave heights tested, whereas for locations closer to the model vessel bow an exponential growth in the water elevation was observed during experiments. Secondly, from that location the peak of each wave could be clearly seen. The water elevations measured were smaller, although remained close to the design values. This meant that the waves were not fully developed yet, however that location presented a reference point, where the water elevations could be used without significant loss of accuracy, while the values could be compared with each other.

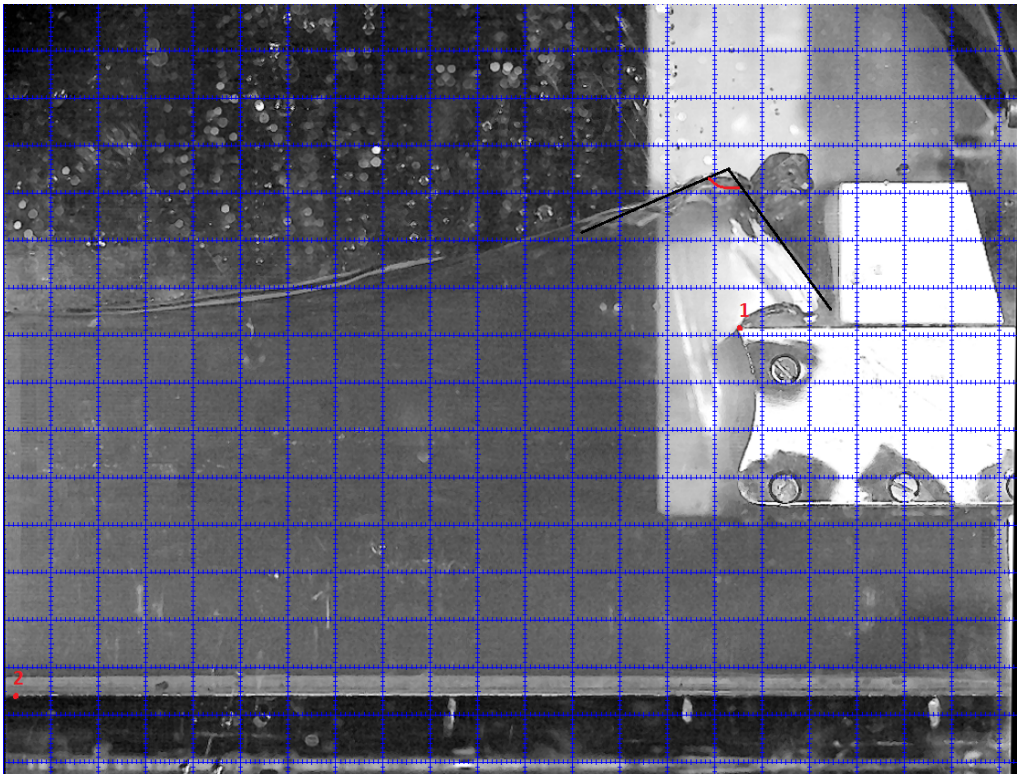

Figure 5.2: Monitoring points selected fro the video recordings.

The values recorded for the wave elevation and freeboard exceedance can be seen in (Tabl.5.2). The H_i correspond to the water elevations measured from the bottom of the bottom of the tank, minus h_0 which is considered a constant for all trials, and h_e the freeboard exceedance height measured from the elevation of the deck. The last two columns correspond to the numerator and denominator of the Ursell number respectively, and are used for identifying the type and therefore the theory that best describes the properties of the waves. Examining the values on the table above it can be concluded that the solitary wave theory could adequately describe the behaviour of the generated bores. The values presented indicated that the waves are in intermediate waters, as expected, while the dimensionless numbers position them around the solitary wave area of (Fig.5.3) with some values exceeding above or below the boundaries of the that region, but with the majority of the produced waves falling into the solitary wave category.

Trial	H_i [m]	h_e [m]	L_s [m]	$\frac{U}{gT^2}$ [-]	$\frac{d}{gT^2}$ [-]
20m - trial 2	0.024	0.0332	0.00395	0.00395	0.01021
20m - trial 3	0.025	0.0337	0.00429	0.00429	0.01069
20m - trial 4	0.020	0.0301	0.00247	0.00247	0.00785
20m - trial 5	0.026	0.0333	0.00453	0.00453	0.01102
20m - trial 6	0.026	0.0324	0.00437	0.00437	0.01080
19m - trial 1	0.021	0.0294	0.00272	0.00272	0.00829
19m - trial 3	0.019	0.0302	0.00236	0.00236	0.00765
19m - trial 4	0.021	0.0279	0.00281	0.00281	0.00844
19m - trial 5	0.022	0.0287	0.00322	0.00322	0.00910
19m - trial 6	0.020	0.0284	0.00241	0.00241	0.00775
18m - trial 1	0.020	0.0286	0.00255	0.00255	0.00799
18m - trial 2	0.016	0.0281	0.00238	0.00238	0.00770
18m - trial 3	0.019	0.023	0.00158	0.00158	0.00614
18m - trial 6	0.018	0.0265	0.00233	0.00233	0.00760
18m - trial 7	0.017	0.0254	0.00197	0.00197	0.00693
17m - trial 2	0.017	0.0232	0.00173	0.00173	0.00646
17m - trial 3	0.017	0.0243	0.00185	0.00185	0.00670
17m - trial 4	0.020	0.0249	0.00233	0.00233	0.00760
17m - trial 5	0.020	0.0243	0.00247	0.00247	0.00785
17m - trial 6	0.017	0.0217	0.00169	0.00169	0.00637
16m - trial 2	0.018	0.0238	0.00209	0.00209	0.00717
16m - trial 3	0.016	0.0239	0.00164	0.00164	0.00628
16m - trial 4	0.016	0.0244	0.00160	0.00160	0.00619
16m - trial 5	0.019	0.0233	0.00214	0.00214	0.00726
16m - trial 6	0.017	0.0228	0.00176	0.00176	0.00651
15m - trial 2	0.016	0.0221	0.00158	0.00158	0.00614
15m - trial 3	0.016	0.0224	0.00162	0.00162	0.00623
15m - trial 4	0.016	0.0213	0.00147	0.00147	0.00591
15m - trial 5	0.019	0.0208	0.00217	0.00217	0.00731
15m - trial 6	0.016	0.021	0.00147	0.00147	0.00591
14m - trial 1	0.016	0.0184	0.00160	0.00160	0.00619
14m - trial 3	0.015	0.0182	0.00147	0.00147	0.00591
14m - trial 4	0.017	0.0188	0.00164	0.00164	0.00619
14m - trial 5	0.016	0.0185	0.00150	0.00150	0.00552
14m - trial 6	0.016	0.019	0.00173	0.00173	0.00605

Table 5.2: Measurements for the monitoring locations for each experiment along with the properties for each generated wave.

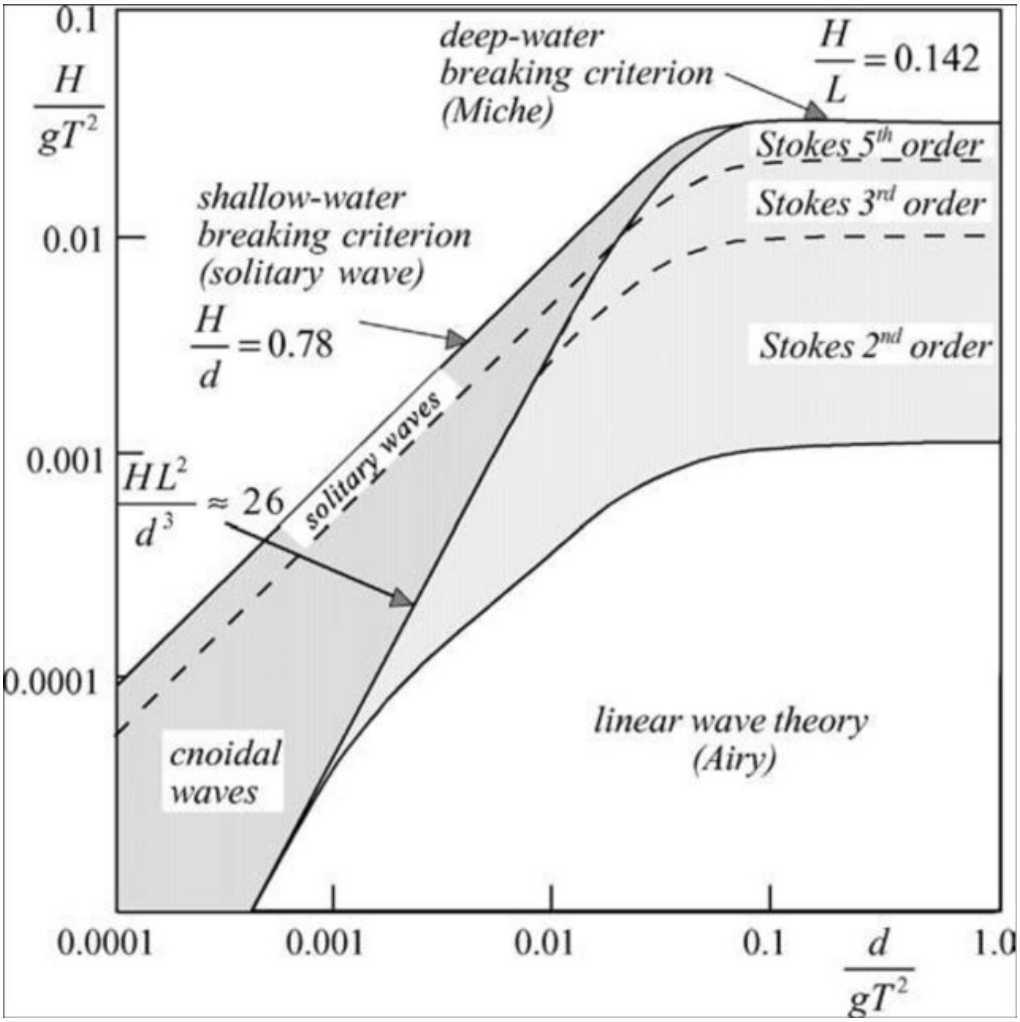

Figure 5.3: The ranges of applicability of the various wave theories taken from [24].

Finally, it is highlighted that for the freeboard exceedance height only the exceedance of the main body of water was marked down ignoring local flow instabilities. This was more evident for the higher wave height ranges tested and for the cases of the HF and PDB_{LC}, where at the position of the maximum exceedance the waves showed an angle was close to 90 degrees, as has been also observed by [22]. In the cases of HF, PDB_{LC} and some PDB, A vein of liquid formed a secondary smaller wave on the crest of the main wave. A similar phenomenon was observed by van Meerkerk et al. in [36].

The researchers investigated the variability in the pressures during plunging breaking waves impacts on a vertical wall. In their study the surface behaviour of the wave was examined and analytical equations describing the behaviour of the large air pocket under the plunging wave were produced. Continuing their work in [35] the researchers investigated the pressures induced during plunging breaking waves impacts on a vertical wall, but the focus was shifted on the global and local behaviour of the gas flow around the plunging wave. In [36] van Meerkerk et al. observed that the gas inside the large pocket of the pludging wave accelerated as the phenomenon progressed, with the tip of the wave acting as a roughness element causing disturbance, flow separation and the development of a shear layer. The separation of flow led to the creating of a gas vortex which propagated to the leeward side of the wave. The gas velocity near the wave crest was observed to be significantly higher that the bulk velocity of the gas. The high shear stresses on the surface between the gas and the water resulted to the development of a Kelvin-Helmholtz instability that caused a small amplitude wave formation on the crest of the produced wave [36], similar to those appearing during the experimental trials of the current research.

A secondary wave forming can be also seen in (Fig.5.2) moments before impact. This additional

freeboard exceedance height was not considered into and ignored from the measurements from two reasons. First of all, as explained above, the Kelvin-Helmholtz instability is a local phenomenon, and in most cases the secondary wave forming at the crest did not span for the whole width of the experimental layout. Because, the experimental setup consisted of a 2D model the properties across the tanks cross-section were considered steady, which was not the case with crest instabilities. Secondly, considering the result interpretation as showed in [36] the instabilities introduced high variability. Similarly in the current project, the secondary wave forming introduced significant scatter of data,which in the author's discretion took the focus out of the main parameters of interest and was therefore not considered in the measurements.

5.2. Repeatability

Since the 17^{th} century, scientists had observed that during execution of the experimental trials there was a strong need for the conditions of the experiments to remain the same as much as practically possible. It was observed that ensuring that crucial elements of the setup could be replicated significantly minimized possible sources of errors in the results. Ensuring that repeatability in experiments is met, can be considered a method for verifying that the data collected during the trials is reliable for further investigating and drawing conclusions from analysing them.

Nowadays, the scientific community has distinguished discrete phases as defined by the the Joint Committee for Guides in Metrology (JCGM). First step is the repeatability as a condition of measurement, which is defined as keeping the conditions of measurement fixed while performing two or more measurements over a short period of time. Second step is evaluating the measurement uncertainty, which is the evaluating the measured values obtained under defined measurement conditions by the means of statistical analysis [26]. With these two steps an initial validation of results is conducted, making sure that the data are suitable for statistical analysis.

Repeatability in measurements involves consistently following a specific protocol or methodology each time an experiment begins. To establish repeatability, it is common practice to verify that certain conditions are met. These conditions as recited by the JCGM include using the same location, employing the same measurement procedure, involving the same observer, utilizing the same measuring instruments, ensuring identical conditions, and conducting repetitions within a short time frame.

The initial step in establishing the repeatability of the experimental trials has been successfully taken, as all the specified conditions were met. The experiments were conducted within a brief time frame, during which the experimental setup remained fixed in place, including the recording instruments which remained the same for all trials. A single individual operated the setup, and the initiation of the experiments ,the operation, and the sampling frequency of the instruments were automated using a unified console system connected to all data collecting equipment. Lastly, the crucial factor in the experimental process and the only aspect of the setup which was manually handled, the water height in each tank, was measured with high precision during each experiment. The instruments employed could be mechanically adjusted to measure water elevation with an accuracy of a tenth of a millimeter. Thus, it was ensured that the ratio of upstream and downstream water heights which significantly influenced the fundamental properties of the generated bore and consequently the type and intensity of the green-water event was reliably reproduced.

For the next step, which is evaluating the measurement uncertainty a proper method for statistically analysing the results should be chosen. Different physical quantities follow different distributions and are prone to different degrees of variation. In the current project emphasis was given in the water elevation generated with the dam-break method and the maximum freeboard exceedance during shipping of water events, where the former can be adequately described by the Rayleigh distribution [24], [50], while the latter can be best described by the Weibull distribution [50]. Because, for each experimental trial a single observation was collected during each experiment a method based on evaluating the standard deviation of the two separate quantities was selected. The values of the statistical properties of the wave elevation and freeboard exceedance height based on the samples collected for each ex-

Statistical Property	Abbr.	20m	19m	18m	17m	16m	15m	14m
Expected Value [cm]	μ	2.53	2.07	1.93	1.74	1.70	1.63	1.62
Standard Deviation $x10^{-4}$ [cm]	σ	25.1	11.7	15.7	14.3	10.7	12.0	3.5
Coeff. of Variation [%]	CV	9.9	5.66	8.11	8.22	6.32	7.42	2.15

Table 5.3: Water elevation, H_i

Statistical Property	Abbr.	20m	19m	18m	17m	16m	15m	14m
Expected Value [cm]	μ	3.32	2.87	2.65	2.43	2.38	2.13	1.85
Standard Deviation $x10^{-4}$ [cm]	σ	14.1	9.0	23.5	12.7	6.1	7.0	3.2
Coeff. of Variation [%]	CV	4.4	3.1	8.5	5.2	2.6	3.3	1.73

Table 5.4: Freeboard Exceedance Height, h_e

periment are presented respectively in (Tabl. 5.3-5.4).

The method for evaluating the standard deviation that was chosen was the Coefficient of Variation, CV. Coefficient of variation as an index is used in evaluation of uncertainty expressing the standard deviation as a percentage of the mean value (Eq.5.7). The advantages of the CV approach is that can be used for several different distributions including the Rayleigh and Weibull distribution, it is dimensionless so it can be used for comparing different quantities that don't belong in the same distribution, but most importantly it is an index expressed as a percentage making it easy to interpret and recognize patterns in the sampled data.

$$\mu = \frac{1}{n}\sum_{i=1}^{n} X_i \tag{5.5}$$

$$\sigma^2 = \frac{1}{n}\sum_{i=1}^{n}(X_i - \mu)^2 \tag{5.6}$$

$$CV = \frac{\sigma}{\mu} \tag{5.7}$$

For drawing conclusions on the repeatability of the experiments, after the CV value has been calculated for each different wave height range (Tabl.5.3-5.4), it then needs to be compared with a threshold value. A common threshold value used in practise, which shows high repeatability in the samples and consistent values as a common practise is $CV = 0.10 = 10\%$. For each wave range tested it can be easily seen that for the wave elevation and freedboard exceedance values the CV numbers are lower than the threshold value. This statistically means that the consecutive experiments were successfully conducted under reproducible conditions, thus ensuring that the data collected could be used for further physical investigation.

5.3. Categorization

For the greenwater events the simplest and the most reliable way of identifying the type of a shipping of water occurrences is by visual inspections. The five categories as were distinguished and defined initially by [6],[17], [15], and then expanded by [40], are the dambreak (DB), the plunging wave (PW) the plunging wave with dambreak (PDB), the hammerfist (HF), the plunging dambreak with large air cavity (PDB_{LC}). Each category ,as was presented in 2, has characteristic features that result from the interaction of the critical sub-mechanisms or elementary processes [39] taking place during greenwater events.

For an initial categorization of the greenwater occurrences that took place during the experimental trials the visual recordings using the Photron Fastcam software were utilized. The result from the videos showed that four out of the five cases appeared during the experiments. The predominant case was the pludging dambreak with large air cavity with 12 occurances (34.3%), then the dambreak case with 11 (31.4%), the pludging dambreak with 9 (25.7%) and finally the hammerfist type with only 3 occurances(8.6%) . The PDB_{LC} case appeared for the mid to high water heights tested (18m-20m), the PDB for around the middle-low tier wave heights (15m-18m),and the DB for the lower to mid water heights (14m-16m), and the HF appeared for in the 17m and 18m trials.

The flow patters and the dominant elementary processes taking place in each greenwater category are distinct. However, system characteristics like the geometry of the vessel, environmental conditions like wave reflection and 3D phenomena alter the features of the main sub-mechanisms. For that reason the type of shipping of water scenarios that occurred during the trials were assessed for different time frames throughout the event development. This enabled for a more reliable categorization, since the greenwater events were evaluated over their general behaviour and not from specific instances where a sub-mechanism might have been emphasized. The time-lapses showcasing the features of each category as recorded during the experimental trials can be seen in the figures below (Fig. 5.4-5.7).

The DB shipping of water events were categorized for two distinct features. Initially, due to the reflected part of the bore and the shape of the bow of the model vessel the momentum built pushed the fluid upwards and forwards towards the deck (Fig. 5.4. A body of water then started over-spilling on the deck while the maximum freeboard exceedance was reached. This happened without trapping any air and creating air cavities in the process, a characteristic of the DB case. After this point, a water tongue was created that started propagating with a steady and distinguishable shape which can be described by Ritters's dry dambreak solution (Eq. 2.1).

The PDB case started similarly with the previous case where the momentum built-up led to a body of water exceeding the freeboard. However, in the present case the wave elevations were higher and the wave length shorter, thus the horizontal velocity component of water pushed the fluid further inwards, toward the aft of the model (Fig. 5.5). The main future of this greenwater event case, is that before the maximum water exceedance was achieved, a significant volume of water deviating from the main body of water plunges onto the deck. The momentum of the vein releases into a double jet forming with one end traveling backwards trapping small pockets of air between itself and the remaining body of the incoming water, while the other jet travels forward hitting the ondeck structure and preceding the main impact. At the same time, most of the exceeding volume that followed behind, over-spilled onto the deck in a similar fashion to the DB case.

The HF case was characterized by the rectangular body of water or fluid arm reaching the ship deck with unchanged direction and thickness until gravity starts to play a role. In the early stages of the event, the momentum built-up focused at the bow between the incoming wavefront and the wave trough resulting to the hammerfist shaped body of water. This body of water initially moves in a coherent volume before crushing onto the deck. Additionally, while the gravitational pull prevails and the fluid arm starts collapsing with the air managing to escape successfully. Therefore, for the HF cases practically no air cavities in the resulting ondeck flow are formed (Fig. 5.6).

The last shipping of water case that was observed was the PDB_{LC}. This scenario has a lot of similarities with the HF case, where again a rectangular body of water exceeded the freeboard. Strong horizontal velocity components shoot the volume of water forwards while the water elevation above the deck was increasing. While the fluid has reached maximum exceedance, a fluid vein escapes at the lower corner of the water arm. Like the PDB and the PB a double jet is formed as the fluid vein impinges on the deck propagating forward and backwards at the same time. The backwards jet flow traps large quantities of air unable to escape under the body of water that has exceeded the freeboard. The cavities trapped in the collapsing volume of fluid near the deck edge stayed at the same place for almost the whole duration of the event, where the water started flowing off the model vessel. The cavities contracted and expanded changing shapes from slender ellipsoid to almost circles observing

from the sides, before collapsing themselves into bubbles and mixing with the flow.

In general, as the water-heights that were tested increased and so did the steepness while the freeboard elevation was the same. The sequence of shipping of water events generally transitioned from PB, to PDB, to PDB_{LC}, with a few occasions of the HF cases. Moreover, as the greenwater types progressed the location of the maximum freeboard exceedance changed. For the DB the maximum exceedance took place in front of the bow of the vessel, for the PDB event at the edge of the deck, while for the HF and PDB_{LC} type the maximum elevation over the deck appeared further aft the vessel. Both of these trends are well in agreement with previous literature [15], [56] in both experimental trials and simulations, with the PDB ,including the PDB_{LC} being the most common shipping of water cases.

Additionally, during the experiments it was observed, that for all the greenwater event types the overtopping flow presented features similar to the fluid arm taking place for HF and PDB_{LC} scenarios as described in [15], [40]. As the momentum built-up took place and the body of water exceeded the freeboard the water mass formed an angular shape during all trials resembling the top part or tip of a fluid arm. The top corner reached angles around 90degrees close to the position of the maximum on-deck elevation, while turning to obtuse angles at later stages as the flow progressed inwards, with the mechanism being more visible depending on the shipping of water case, the intensity and the water volume that exceeded the freeboard.

This flow pattern was possibly attributed to two main reasons. First one are scale phenomena which are going to be further explained in (Chapter 6), and the second reason is the geometry of the experimental model. The shape of the bow of the model vessel consisted of two curves. The bottom part of the bow, reflected the wave backwards and upwards, hindering the release of pressure build up towards the keel of the model. When the waves got closer to the model vessel, the bow with the geometry that changed from a concave into a convex curve, acted like a stagnation point. This means locally a strong pressure field was built, which released mostly shooting a jet upwards, as the jet was met with lower pressures near the surface and therefore less resistance. That jet travelled upwards and away from the bow of the vessel meeting the incoming wave. The combination of the propagating wave and the upward jet moving in the opposite direction created a flow with a high vertical velocity component and a low horizontal one, which is evident examining (Fig. 5.4-5.7). For all type of shipping of water events the front part of the wave had an almost linear profile just like the top part of the fluid-arm. Moreover, while the freeboard exceedance height was almost doubled comparing the 14m and the 20m trials, the location where the maximum exceedance was achieved further aft the deck, stayed within a range of less than a centimeter for the wave height ranges tested, emphasizing the difference in the vertical and horizontal velocity components.

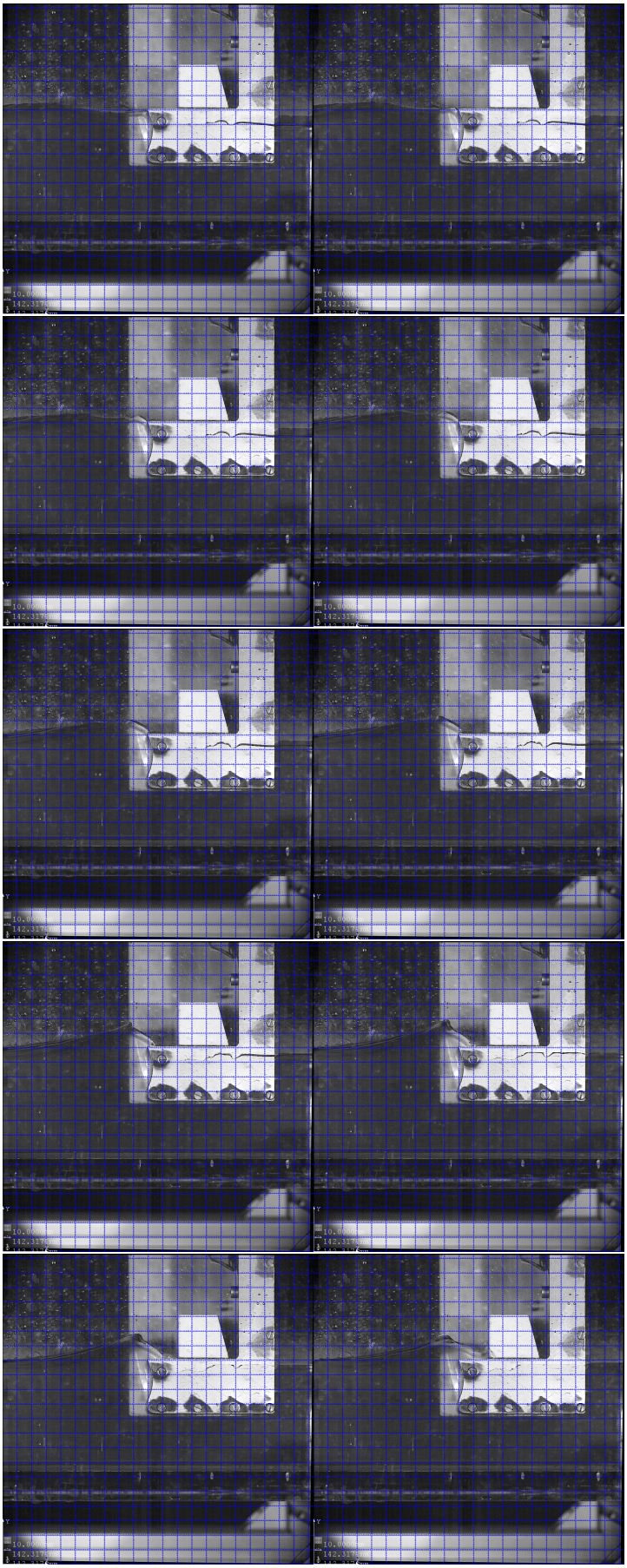

Figure 5.4: Timelapse of a DB greenwater event taken from the 14m wave fifth trial

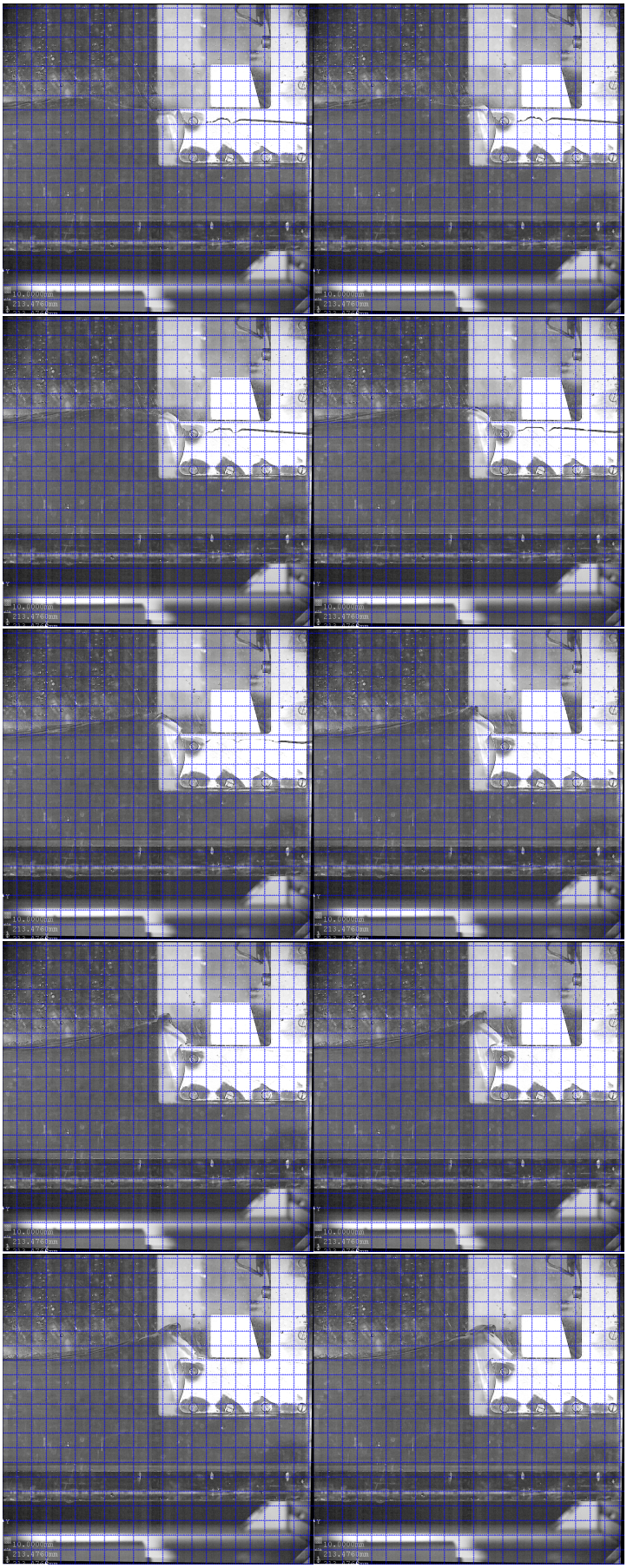

Figure 5.5: Timelapse of a PDB greenwater event taken from the 16m wave second trial.

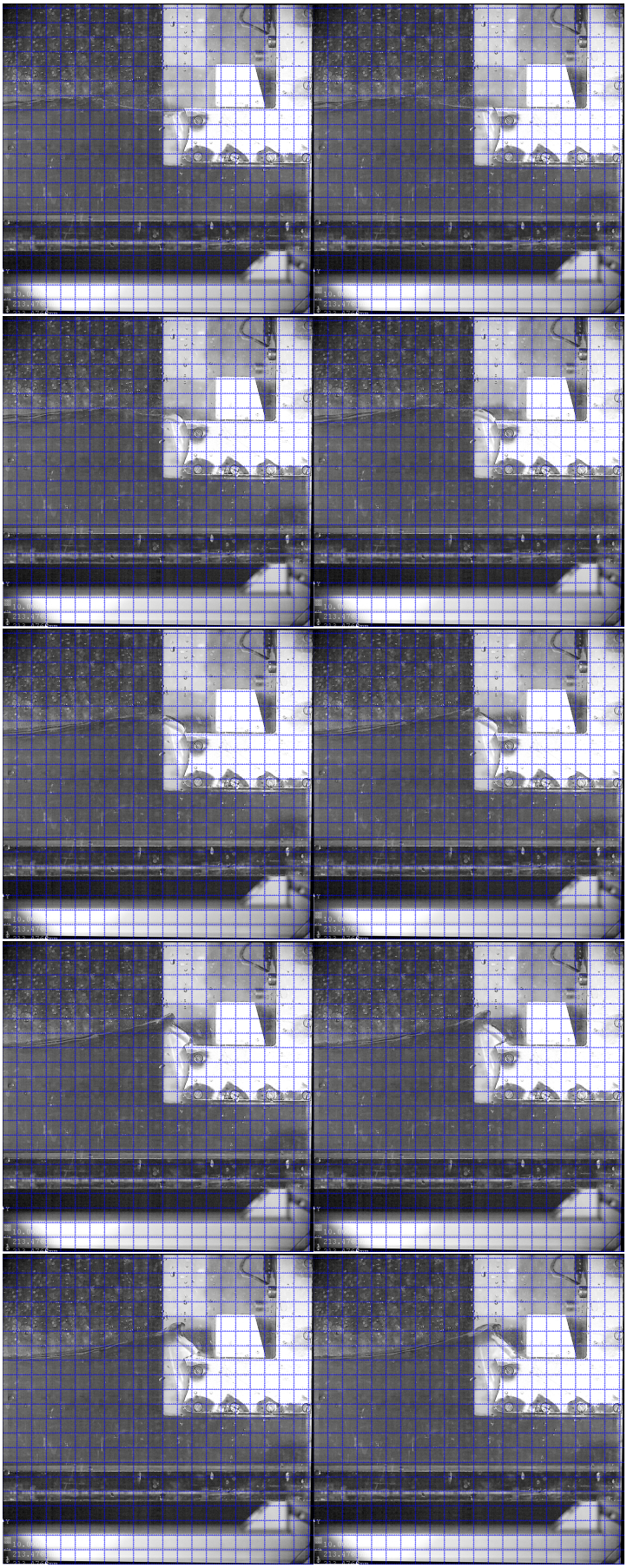

Figure 5.6: Timelapse of a HF greenwater event taken from the 17m wave third trial.

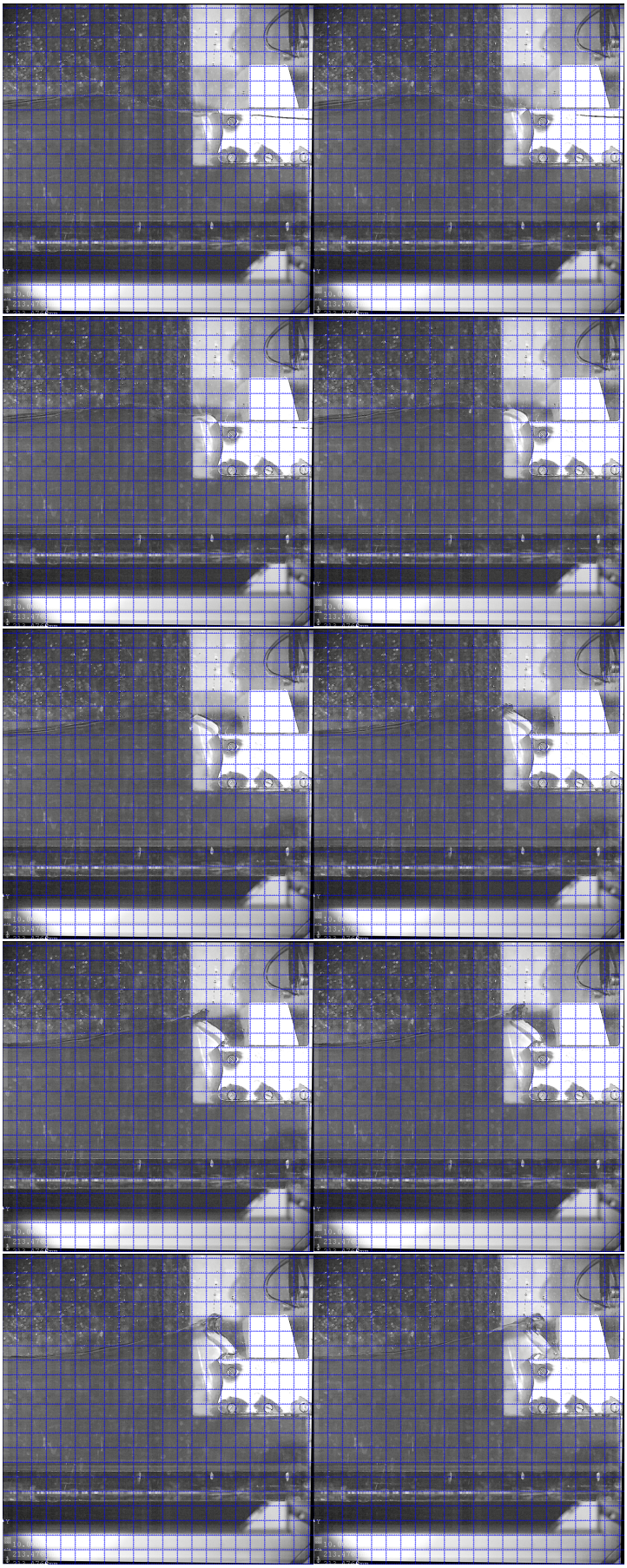

Figure 5.7: Timelapse of a PDB_{LC} greenwater event taken from the 19m wave sixth trial.

Additional to the visual classification of the shipping of waters events, the occurrences were categorized based on the incoming bore characteristics. In the previous literature two different methods had been used for classifying the type of greenwater event mentioned in (Sec.2). For these methods, the one proposed by Zhang et al. [56] was followed. The classification is based on the dimensionless values of the steepness, and the ratio of the wavelength divided by the vessel's draft (L_s/D).

These parametric classifications were chosen for two main reasons. First of all, the aforementioned classification method more clearly underscores the physics and parameters that were involved in each case of shipping of water, emphasizing the local effect of the structure on the wave field. Secondly, the main identification parameters coincided well with the main parameters that were given attention during the experimental trials. The draft remained the same for all the cases while the amplitude and wavelength were the variables that were tuned by adjusting the downstream to upstream water depth ratio of the tank. Moreover, with the classification method proposed by Greco et al. [15] a crucial parameter was the dimensionless ratio between the vertical component of the velocity at the bow divided by the theoretical value (W_w/W). Both of these values were deemed impossible to estimate accurately due to the geometry of the vessel and the measuring instruments. Therefore, the classification using the parameters suggested by Zhang et al. was followed.

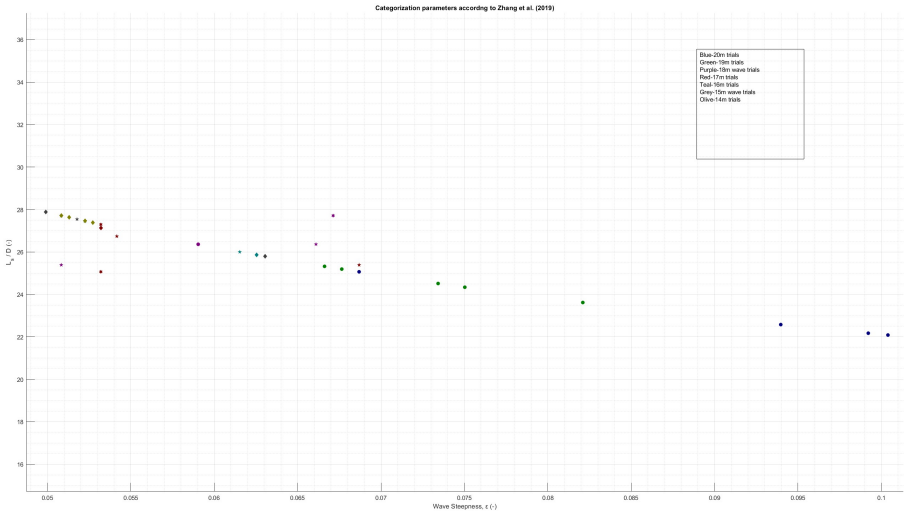

Figure 5.8: All the greenwater occurrences plotted(DB - $diamonds$, PDB - $star$, HF - $hexagon$, PDB_{LC} - dot.

As can be seen from the above graph (Fig.5.8) the plot followed an inverse soft root function. This was expected since with the dam-break method for generating the waves, the properties of the generated bores were directly connected with the water elevation, H_i, that was produced during each experiment. Combining the equations for wave steepness assuming that $H = 2H_i$, and (Eq.5.2), the dependence of the steepness and wavelength on the water elevation can bee seen shown below. With (Eq.5.8), it becomes apparent that the steepness, re-written eliminating the wavelength, followed a soft power curve as a function of the water elevation. By plotting the steepness on the horizontal axis the function is automatically inversed, which becomes a soft root curve (power of 2/3) which explains the decreasing almost linear trend.

$$\epsilon = \frac{\sqrt{3}\ H_i^{3/2}}{2\sqrt{2}\pi\ h_0^{3/2}} \tag{5.8}$$

Comparing the curve with the ones produced by Zhang et al. no strong correlation could be made whether the parameters identified by the researches in [56], could adequately describe the greenwater events during the experiments conducted for the current project. Unlike the figures produced by Zhang

et al. the greenwater cases observed overlapped in several parts, while no clear regions for each case could be identified using the classification parameters in [56]. Specifically for the region between $e = 6.0 - 7.0\%$ all four cases coexisted, with the only distinct regions of $e \approx< 5\%$ where predominately DB cases appeared, and for $e > 7.0\%$ where only PDB_{LC} were observed. Moreover, regions that were identified by Zhang et al. as regions of slamming occurrences (i.e $e > 3.5\%$ & $L_S/D > 20$), consisted several of the observations of the current project's experiments. This deviation could be attributed to the waves used by Zhang et al, since the freeboard to draft ration in the current project $f/D = 0.61$, fell within the rage tested by the researchers. During simulations conducted in [56] the incoming waves were generated with the concentrated wave group method, using waves which could could be described by the linear potential theory. The waves generated by Zhang et al. had inherently different shape, additionally ranged from $e = 1.2 - 5.6\%$, compared to the current experiments where the steepness ranged from $e = 4.8 - 10.2\%$, implying that steepness plays an important role during the behavior before the water exceeding the deck, while also affecting the type of greenwater event occuring.

Similarly to the researchers and the current project it was observed that the HF events started occuring for steepnesses around $e = 4.5 - 5.0\%$ (Fig.2.2 and Fig.5.8). Additionally, the asymptotic behavior presented in (Fig.5.8), could be implied also for the current project. The observations followed an inverse soft power curve, which mathematically leads to zero towards infinity, and towards infinity close to zero. However, for stronger correlations between the finding in [56] and the current project, more trials and thus more points would be needed for clearly defining a curve over a wider range, compared to the limited window of observations collected during the current project.

5.4. Recorded Signal Processing

After processing the data collected from the video feedback, the second type of data collected by the sensors was examimined. The force time series were stored in Technical Data Managing Streaming or "tdms" files specialized in storing large volumes of data. The force sensors were set to a sampling frequency of 10kHZ, which means that the sensors detected a wide variety of disturbances, ambient vibrations, and other types of interference, in addition to the shipping of water loading. For this reason, before the recorded time series were used, the signals were processed so that only the frequencies that were of scientific interest were kept.

For cleaning out the force sensor signals, two questions need to be answered simultaneously. Firstly, whether the frequencies utilized reflect the loading and the main mechanisms acting during greenwater events, and secondly, whether the frequencies contain high amounts of noise. Answering the first question the range of frequencies that present during the shipping of water events needed to be investigated.

5.4.1. Duration of sub-mechanisms

During greenwater impacts in most occurrences a two-phase flow is created which contains several different mechanisms involved. Regarding the gross body of water involved during impacts, a couple of related quantities can be identified. The first quantity is the rise time t_r, which is the time duration between the initial contact of the body of water with an object until the maximum pressure from the impact is exerted on that object. From previous literature the duration of rise time is in the order of $\mathcal{O}(10^{-1} - 10^{-2})sec.$ Buchner in [6] recorded the rise time that had a duration of 0.3-0.5sec while Song et al. [51] investigated the velocities and impact pressures on a fixed structure during the shipping of water events, verifying that the rise time during greenwater impacts is in agreement with the ones recorded by Buchner, while at the same time measuring rise times as low as 0.02 sec. Additionally, Song et al. , suggested an empirical relationship between the peak pressures and the rise time $p_{max} = at_r^b$. Several publications have verified this equation fitting the coefficients a, b according to their collected data. Hernandez et al.[21] using the formula from Song et al. suggested the range of $0.18 < t_r/t_d < 0.64$ where the relation between the rise time and the duration of greenwater impacts ,t_d can be estimated. Boon & Wellens [5], in the experiment they conducted found a larger range of

t_r/t_d, however they concluded that the most events appeared on the range specified in [21]. Using the above range, a reasonable estimate for the average duration of the greenwater impacts would be $t_d \approx 1.5sec - 2.0sec$ and a tise time of $0.2 < t_r < 1$. The second quantity is the duration of the maximum pressure t_{pmax}. The duration of the peak pressure is the time where a strong highly localized pressure takes place. These peak pressures can lead to singularities and pressure spikes, which are local maxima with significantly higher values than the mean pressure during each time-instance. These localized peak pressures have a very small duration $\mathcal{O}(10^{-3}sec)$ [41].

With regard to the behavior of the second phase in the flow, the trapped air, several stages in the sub mechanisms of the bubbles can be identified. After the air is trapped within the volume of water where the air-cavity shape rapidly changes shape leading to the maximum pressure built-up of the bubble, which results in radiation of acoustic waves translating into pressure changes through the surrounding liquid. Several parameters affect the behaviour and oscillations of the air cavities such as gravity, the fluid's viscosity, surface tension phenomena, size of the bubble, and the difference between the pressure of the liquid and the air cavity [11]. However, once the initial transient state comes to an end, the volume oscillates in specific modes contracting and expanding with the pressure at the boundaries retaining a uniform pressure, until the entrapped bubble is disturbed, bursting into fragments at high velocities that turn into smaller cavities and that get mixed with the flow. Jain et al. [25] conducted a series of experiments investigating the effect of trapped air during impact phenomena dropping a horizontal disk with several different velocities onto stationary water. The researchers were able to measure the duration of each of the aforementioned stages, concluding that the duration of the initial pressure build-up $> \mathcal{O}(10^{-4})$ sec, while the contraction stage as a duration $> \mathcal{O}(10^{-1} - 10^{-2})$ sec, and the rupture of the cavity $> \mathcal{O}(10^{-3})sec$.

5.4.2. Signal Filtering

Due to the high sensitivity of the force sensor recordings, the quality of the equipment used, and unpredictable random environmental circumstances, significant levels of noise were introduced into the system. The term noise refers to unintended changes that a signal may go through during capture and storage. Noise that infiltrates the recordings alters the shape of the recorded signal, making the results more difficult to interpret, while it provides no scientific interest.

Removing the noise from the recordings is an important aspect of signal processing engineering and can be rather challenging. The simplest and most reliable way is to use Fourier analysis to process the signal from the time to the frequency domain. Using Fourier analysis, the signal is broken down into a summation of finite discrete frequencies and amplitudes of harmonic components, which when combined are able to form the the original signal. A typical recorded signal during the experimental trials along with the decomposed signal in the frequency domain can be seen below:

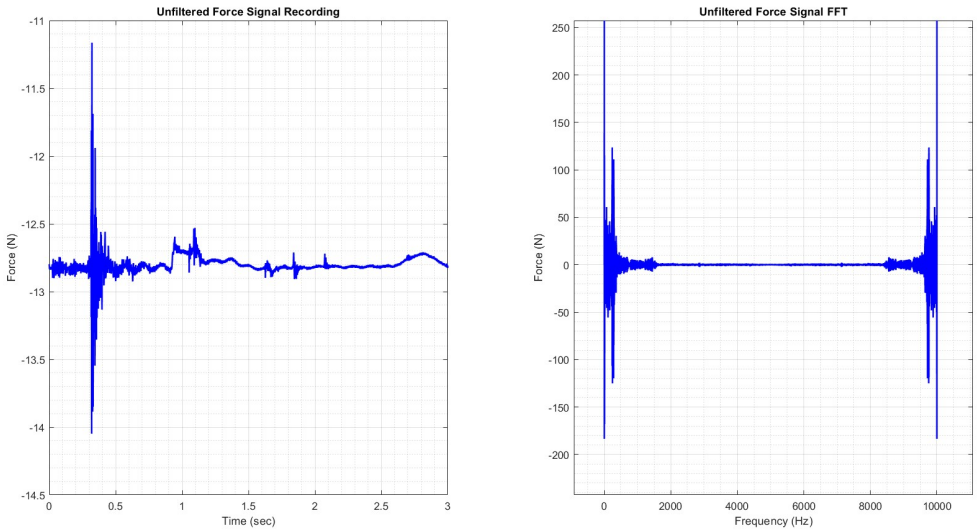

Figure 5.9: 1. Unfiltered force signal recording , 2. Fourier Transformation on the unfiltered signal (right).

For a more efficient and easy process of the recorded signal, an initial attempt to eliminate the noise in the signal was made. Once the layout was triggered by the data acquisition system to initiate a trial, the sensors were able to record for a short period of time, while the electric magnet released the weight conducting a free-drop until the rope that connected it with the water gate became taut and pulled the gate up sending an impulse to the whole system to vibrate as can be seen in (Fig. 5.9) before the large spike in the recorded values. During that time window, the sensors were able to record with no actual loading on the sensors caused by greenwater phenomena taking place, except for random ambient noise picked up by the force cells.

The FT was on the the time-series was implemented using Matlab built-in functions. However, the resulting graphs were further processed for two main reasons. Firstly, a mirroring effect is present, which is a characteristic of the Fourier Transform applied to real-valued signals, due to the property of conjugate symmetry of the Fourier Transform. This property states that the spectrum around a frequency component is half of the sampling frequency of the instruments.Secondly, the negative values that can be observed in (Fig. 5.9 -right) in the amplitude spectrum represent the phase information of the signal components. In the a time series ,and thus in FT both the magnitude and the phase provide important information about the original signal. Negative amplitudes correspond to certain phase shifts that occur at specific frequencies within the signal being analyzed. Resulting from the mathematical formulas of Fourier transformation there are always two equal-amplitude complex exponentials, rotating in opposite directions, so that their real parts combine and imaginary parts cancel out, leaving only a real sinusoid as the result. For the decomposed noise signal to be easier to interpret, the absolute value for all amplitude components was used, while only half of the frequencies are plotted. Additionally, due to transformation byproducts the value corresponding to a frequency of 0Hz or an infinite period was set to zero. The averaged noise signal and the FT plot for each sensor are observed below:

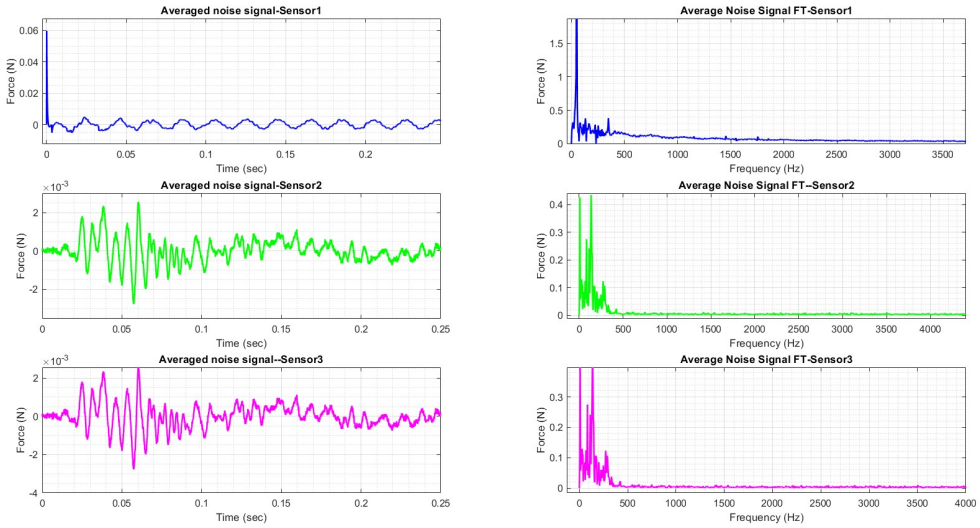

Figure 5.10: Extracted averaged noise signal (*left*) , Fourier Transformation on the averaged noise signal (*right*)- Sensor1 (blue), Sensor 2 (green), Sensor3 (magenta).

Additionally, for an easier interpretation a type of manual filter was applied, where the frequencies that contained less energy that a certain percentage (20%) of the frequency which contained the maximum energy could be set to zero and thus eliminated from the graphs. Using these segments of the recordings, valuable conclusions in both frequency and amplitude components about the noise could be drawn.

By analysing the processed time segments, in the frequency domain it was observed that signal affected a wide range of frequencies specifically from almost 0Hz up to 500Hz, with the higher frequencies showing small amplitudes which could be considered negligible initially. Long peaks which translated to high energy gathered were observed around the 50-250Hz for all three sensors. These peaks indicated that either these frequencies were often reappearing in the time-series or the contained a source of noise with high energy. A distinction could be made for the different sources of noise, comparing the the amplitude and their respective frequency between the sensors. Electrical interference was gathered around the frequency of 48.49Hz and its harmonics 113.48Hz and 230.39Hz which had a strong presence on all three sensors, whereas environmental noise possibly attributed to ambient noise and vibrations introduced to the sensors depending on their location within the experimental layout, their position on the model and their connection to it, manufacturing imperfections, and other causes. Environmental noise was observed in all sensors but the peaks appeared in neighbouring frequencies, with a strong noise source around 8Hz which can be attributed on mechanical properties of the system and vibrations caused by ambient environmental excitation. This does not imply that a frequency affecting a sensor was not picked up by the others, but signifies that a specific frequency affected a single sensor more compared to the others. It is worth mentioning that for Force-Sensor1 a strong noise presence in the order of*2.42N* for *48.49Hz*, five times higher than the ones that were observed compared to the others sensors *0.42N* for *8.01Hz* for Force-Sensor2 and Force-Sensor3 respectively, while being highly susceptible to electric noise.

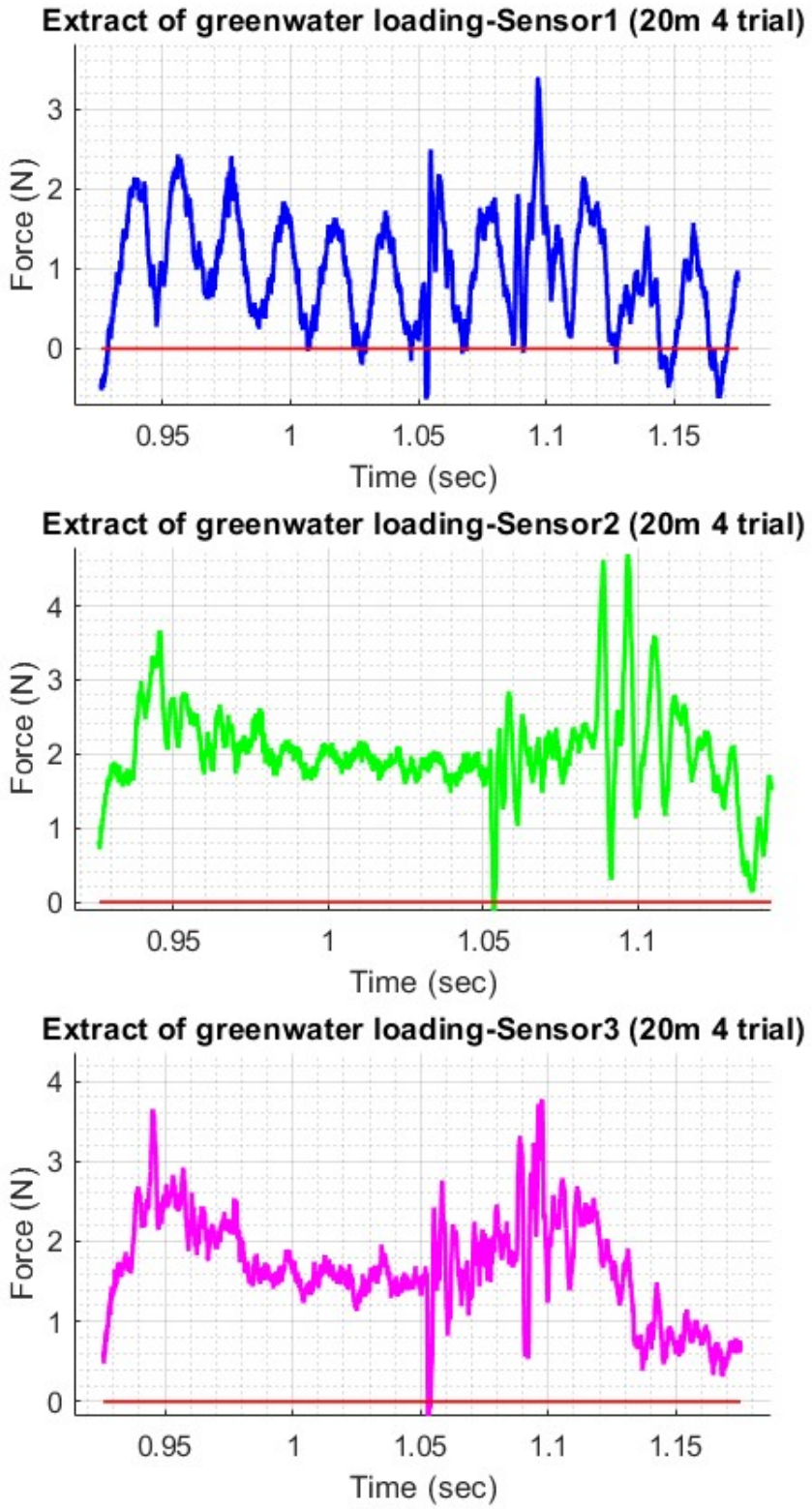

Figure 5.11: Extract of greenwater loading for 20m trial 4 - Sensor1 (blue), Sensor 2 (green), Sensor3 (magenta).

After a first estimation of the noise sources was established, a more detailed investigation of the signal recorded could be made. While inspecting the initial recording of all the sensors showed a static offset, which lead to a wrong estimation of the amplitude. This issue was fixed by averaging the amplitude of the recorded time-series before the impulse from the free falling weight was introduced to the system during each individual experiment, and then subtracting the value from the rest of the signal. Finally, using the video recordings and comparing the collected time-series a window containing the water impact on the the on deck structured was isolated from the rest of the signal (Fig.5.11).

With the extracted greenwater loading from each experimental trial, a Fourier transformation could be applied on the isolated signal. With the analysis in the frequency domain, the frequencies that corresponded to the mechanisms that took place during the shipping of water events could be identified as the frequencies that contained the largest amplitudes or amounts of energy. These frequencies were then compared to dominant sources of noise. As a final measure to reliably isolate the greenwater loading, the values of the averaged noise signal was then subtracted for each experimental trial for all three sensors so the absolute error could be used as index of the ambient noise infiltration. In this way a better correlation could be made between the greenwater loading and the noise in terms of relative size.

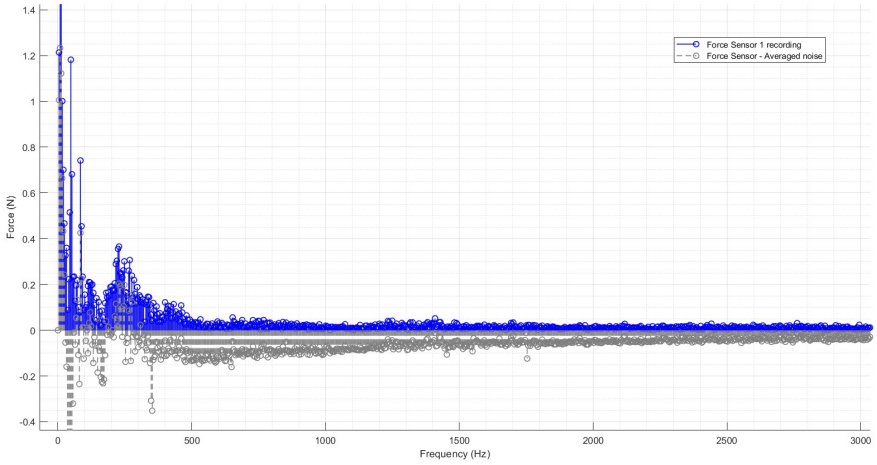

Figure 5.12: Comparison between the Force Sensor 1 signal recording (blue) and the Force Sensor recorded signal minus the average noise.

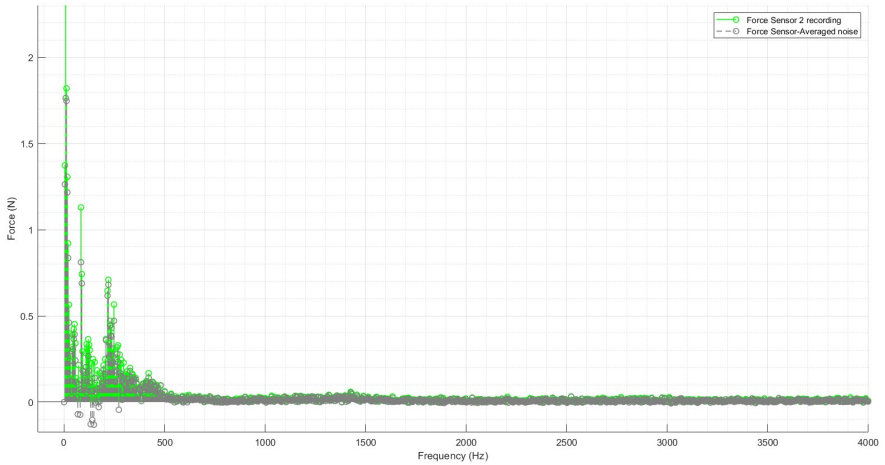

Figure 5.13: Comparison between the Force Sensor 2 signal recording (green) and the Force Sensor recorded signal minus the average noise.

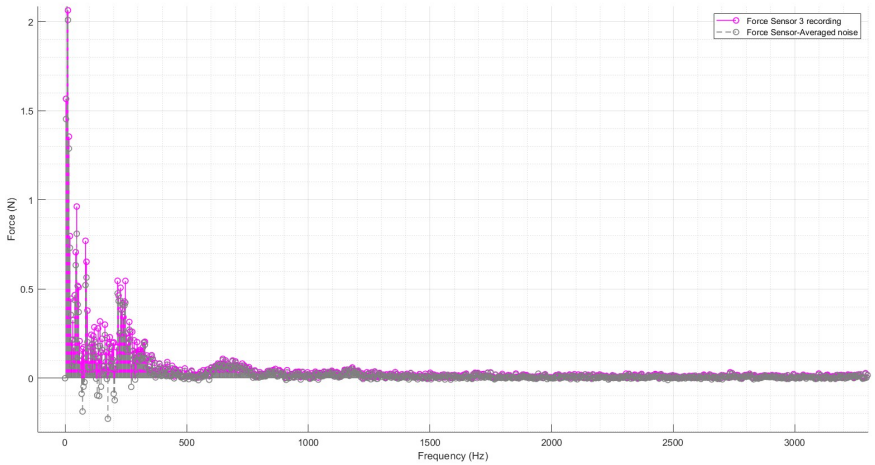

Figure 5.14: Comparison between the Force Sensor 3 signal recording (magenta) and the Force Sensor recorded signal minus the average noise.

The process described above was implemented, because examining only the noise sources is not an index fully capable for examining the intrusion of random noise within the recorded time-series. In the figures above the values of the force sensors' time-series extracts for the 4^{th} experimental trial of the 20m full scale wave height are shown with their respective colour. Blue represents the measurements of force sensor 1, green the recording for force sensor 2, and magenta for force sensor 3, while indicated by gray is the value of the average noise measured from each sensor subtracted from their respective green water loading recording.

From (Fig.5.12-5.14), two main observations were made. Firstly, the noise level affected the values of the loading signal to a different degree depending on the frequency value. In general, it was observed that higher frequencies were more affected by noise signal. By calculating the relative error by normalizing the absolute error by the force recording value for each sensor, no trend could be identified, as the relative error could greatly vary between neighbouring frequencies and between different experimental trial recordings. However, characteristically it was shown that for high frequencies (900Hz) the number of relative errors that had a negative value increased noticeably, meaning that the expected noise in the recordings for high and very high frequencies could potentially contain more energy from ambient

sources than the actual loading, thus considerably influencing the recorded time-series. In contrast, the opposite was observed as for the low frequencies, where for up to 38Hz all the recordings showed only positive values meaning that the recorded signal was always larger than the ambient noise for these frequencies, which was observed around $5-40\%$ with high variation between, experimental trials,and consecutive frequencies and signals coming from different sensors. An observation rather important, because these are the showed positive values ranging from $60-95\%$ showing that frequencies that according to theory were expected to hold most of the information about the greenwater loading were less affected by ambient noise in general.

Second observation was the ambient sound affected the force sensors differently. For a specific frequency the extracted signal and the ambient noise had different values for all three sensors. A trend although that held for all force sensor recordings was that for the frequencies which were identified as the main sources of noise, when the time window before the opening of the water gate were examined in the frequency domain, is that noise dominated that frequencies for all sensors. As can be seen in (Fig.5.12-5.14) for the main electric interference frequency and its harmonics the greenwater loading minus the ambient noise yielded negative values showing that in all cases noise was more governing than the actual recording.

Additionally, regarding the difference in noise signal infiltration into the collected time-series for all experiments for sensor 1, this was also observed when an investigation was conducted in the noise time-series where the noise recorded by force sensor 1 was significantly larger compared to force sensors 2 and force sensors 3. As shown in (Fig.5.12) for almost all the frequency ranges the values were below zero, showing the strong presence of noise. This observation could not be solely attributed to a single reason, as possible explanations could be issues in the installation of the sensor on the experimental setup, applied filtering through the data acquisition system, or faulty connection of the force sensor cabling with the rest of the system, or even small sensor defects. It is noted that defect of the sensor was excluded, since during the sensor's calibration process no abnormal readings could be observed which would raise suspicion. The large noise level was also amplified due to the weak loading as the experimental was designed in a scale of 1:400 and the forces recorded had a value less than one Newton.

For the all aforementioned reasons, it was decided that for greenwater loading that the whole frequency range of the recordings would not be used. Using a bandpass built-in function of Matlab which enables isolating a specific range of frequencies from the timeseries, only the range between 1-35Hz or 0.029sec-1sec in the time domain was used. The choice was based on several factors. Using that frequency range as expected and proven in practise contained the greenwater horizontal loading contained most of the impact mechanisms as was explained in the beginning of the subsection. The effect of the localized peak pressures or the behaviour and the different development stage of air pockets could not be captured using this range as both of these phenomena appear for very high frequency values. However, based on the goals of the current project emphasis was given in the mean forces and the gross behaviour during greenwater loading which could cause material failure in real life and not highly localized phenomena.

Moreover, this range provided recordings where the shipping of water loading was the dominant component in the time-series and were considered more reliable compared to high frequency components which were highly more susceptible to noise introducing significant unreliability in the results, without affecting the overall loading considerably. Finally, the frequencies below 1Hz were discarded, as were considered to be to long lasting to express dynamic phenomena taking place during impact, and mostly involved ambient vibrations, cause by the moving mass of water outside the model vessel and from the water that managed to leaked into the place where the force sensors were located. It is mentioned that some small frequency windows arbitrarily located between 200-900Hz frequencies were all the sensors had positive relative error values meaning that in the recordings green water loading was larger than the expected noise. However, these frequencies were not incorporated in the final filtering, because they were not consistent with each experimental trial so they had to be manually filtered for each case, and most importantly they did not correspond to a range where they could reveal mechanisms that affected the total impact loads considerably.

The typical processed shape of the force sensors signals that were used final result interpretation are presented on the figures below. The final graphs resemble closely the expected ”church roof” shape of greenwater loading as met in previous literature. The two peaks can be distinctively observed representing the initial impact of the the body of water until the maximum height of the jet in front of the deck structure and the gravitational force pulling back the body of water that streamed upwards converting the dynamic energy back to kinetic, before the body of water floats off deck.

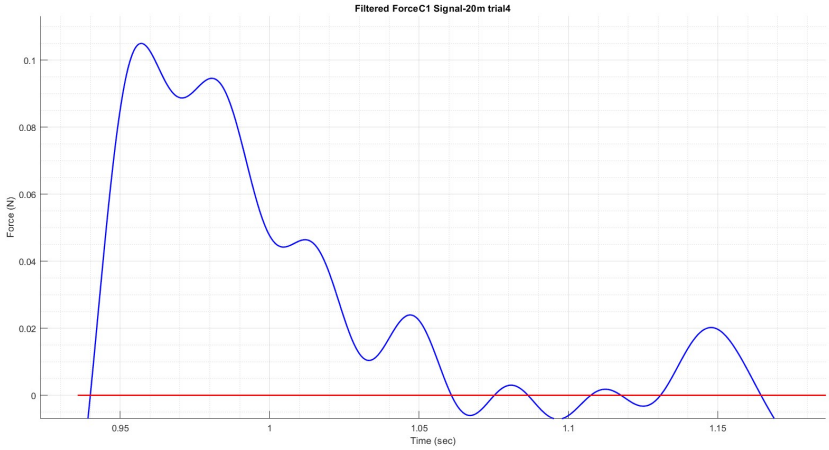

Figure 5.15: Filtered time series recording of force sensor 1 for the 20m wave height- trial4.

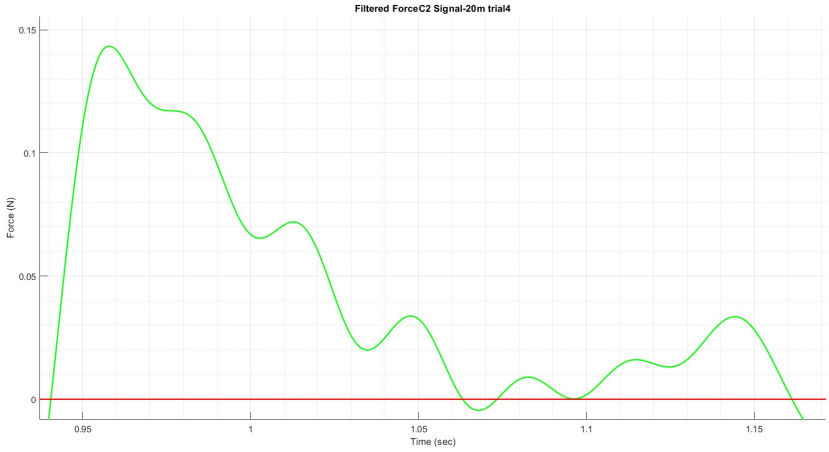

Figure 5.16: Filtered time series recording of force sensor 2 for the 20m wave height- trial4.

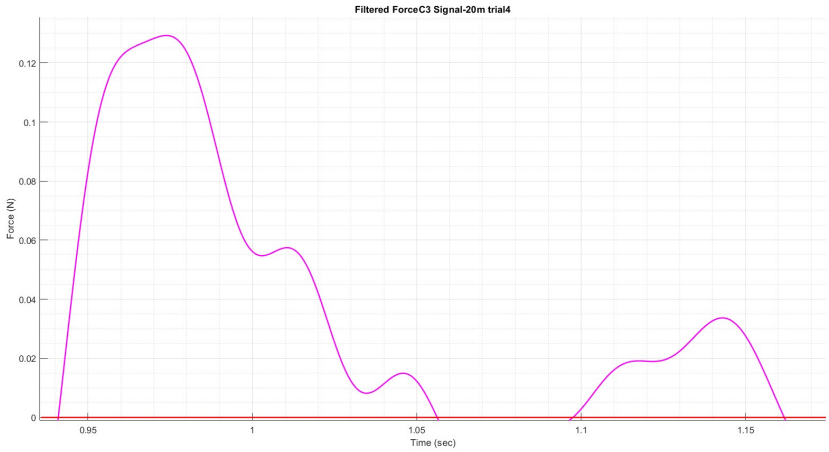

Figure 5.17: Filtered time series recording of force sensor 3 for the 20m wave height- trial4.

5.5. Force Measurements

Once the appropriate frequency range was selected and the force recordings for each experimental trial could be processed, the total force developed during the greenwater events could be calculated. As shown in (Sect. 3.2), the deck structure and its supporting plates were a separate mechanical system, which was suspended from the force sensors. The system could be simplified into a statically determined system, since the only reactions were the three horizontal forces at the position of the bolts connecting it to the force sensors. This means that knowing the forces of the supports, which were the force sensor recordings, the total horizontal force and moment created by the eccentricity can be easily calculated by solving the 2D system assuming a simply supported beam using the following equations (Eq. 5.9-5.10), where d_s is the distance between the supports, which is the length between the outer bolt slots that were used for connecting the sensors with the rigid support plate on one end, and the mechanical system on the other, which was equal to 70mm.

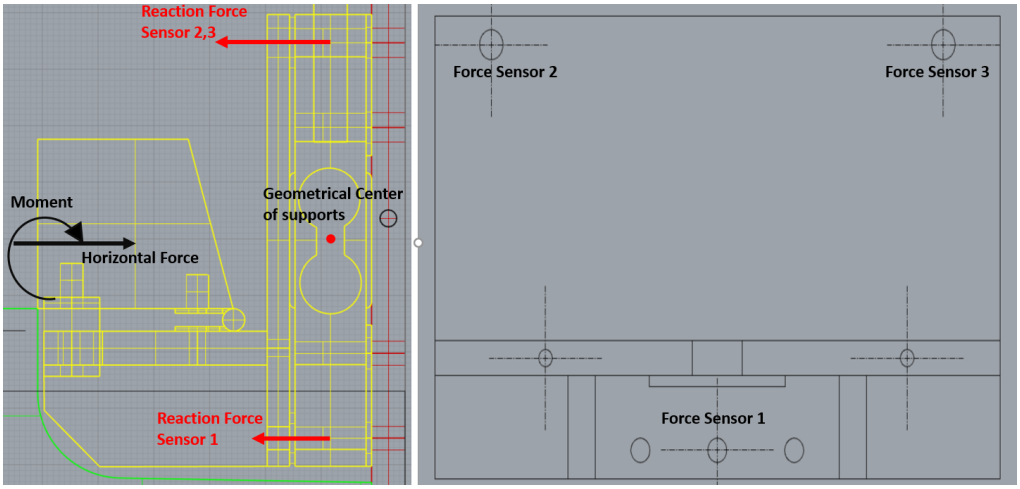

Figure 5.18: The mechanical system used for estimating the greenwater loads exerted on the deck structure from side (left) and cross section of the back plate (right).

$$F_{hor} = F_{Sensor1} + F_{Sensor2} + F_{Sensor3} \tag{5.9}$$

$$M = (F_{Sensor2} + F_{Sensor3} - F_{Sensor1}) \cdot d_s \tag{5.10}$$

$$a_{lev} = \frac{M}{F_{hor}} \tag{5.11}$$

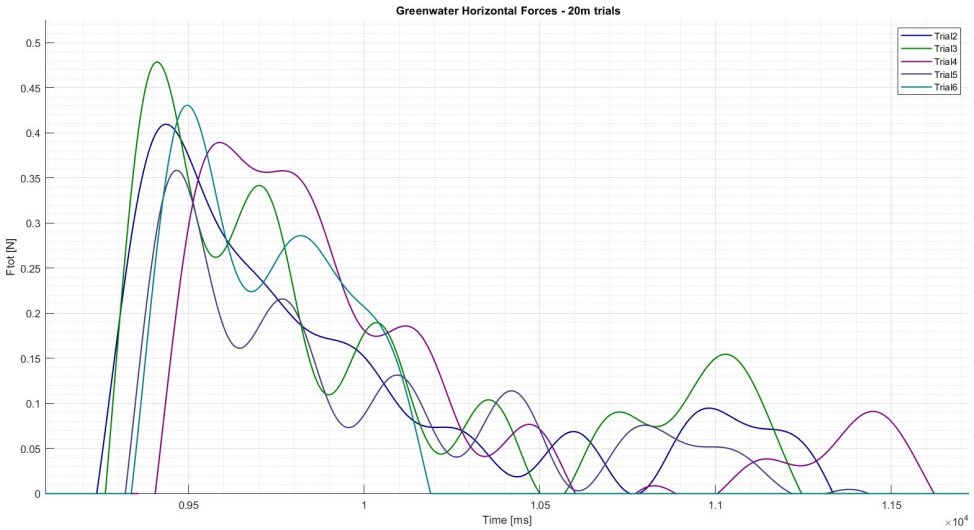

Figure 5.19: The timeseries of the total horizontal force for the 20m trials.

The peak force as recorded by each sensor, $F_{Sensor,i}$,the resulting peak force,F_{hor} ,the moment created from the eccentricity from the horizontal forces,M, and the lever-arm of the horizontal force to the center of the supports,a_{lev}, for all experiments used can be seen in (Table 5.5). Additionally, the processed time-series for the total horizontal greenwater loads for the 20m wave height trials are shown in (Fig. 5.19). The figure presented is intended for illustrative purposes show-casing the shape of the greenwater horizontal loads recorded.

Taking a close look at the values of the columns for the moment and the horizontal force lever-arm caution was raised. The skepticism in the results was initiated mainly from the values of the lever-arm. Examining the dimensions of the model, it can be seen that the distance of the center of the supports from which a_{lev} measured, range from [-12.1mm, 17.9mm] (Fig.5.20) measuring from the center of the supports as zero elevation (Fig.5.20). Therefore, the values of the lever-arm that did not belong in that range required further investigation, since the impact took place on the front surface of the on-deck box the application point of the equivalent total greenwater force should exist on a point along that surface. It is reminded that the static offset coming from the vertical dead weights of the all the model's components that were suspended from the force sensors, was removed during the stage of the signal processing. When the averaged value of the time-series before the water-gate had been released was removed from the rest of the signal, besides the ambient noise, the signal also contained the deflections caused by the static loads which took a steady value throughout the recordings. Thus, the force values corresponded purely on the greenwater events and transient phenomena , which was evident as the values measured from zero Newtons.

Trial	$F_{Sensor1}$ [N]	$F_{Sensor2}$ [N]	$F_{Sensor3}$ [N]	F_{hor} [N]	M [Nm]	a_{lev} [m]
20m - trial 2	0.0987	0.1454	0.1647	0.4087	0.0148	0.0362
20m - trial 3	0.1171	0.1781	0.1816	0.4769	0.0170	0.0356
20m - trial 4	0.1060	0.1450	0.1357	0.3867	0.0122	0.0316
20m - trial 5	0.0529	0.1548	0.1499	0.3576	0.0176	0.0493
20m - trial 6	0.1425	0.1600	0.1214	0.4238	0.0097	0.0229
19m - trial 1	0.0567	0.1279	0.1264	0.3111	0.0138	0.0445
19m - trial 3	0.1076	0.1296	0.1350	0.3721	0.0110	0.0295
19m - trial 4	0.0367	0.1373	0.1113	0.2853	0.0148	0.0520
19m - trial 5	0.1734	0.1335	0.1442	0.4511	0.0073	0.0162
19m - trial 6	0.1810	0.1237	0.1366	0.4414	0.0056	0.0126
18m - trial 1	0.0488	0.1229	0.1428	0.3144	0.0152	0.0483
18m - trial 2	0.1300	0.0876	0.0964	0.3141	0.0038	0.0120
18m - trial 3	0.1482	0.1056	0.1134	0.3672	0.0050	0.0135
18m - trial 6	0.0709	0.1040	0.1071	0.2819	0.0098	0.0348
18m - trial 7	0.1370	0.0960	0.1030	0.3360	0.0043	0.0129
17m - trial 2	0.1064	0.0648	0.0564	0.2276	0.0010	0.0046
17m - trial 3	0.0285	0.0556	0.0552	0.1393	0.0058	0.0414
17m - trial 4	0.0672	0.0656	0.0743	0.2072	0.0051	0.0246
17m - trial 5	0.1016	0.1000	0.0993	0.3009	0.0068	0.0227
17m - trial 6	0.0419	0.0459	0.0473	0.1351	0.0036	0.0266
16m - trial 2	0.0434	0.0642	0.0624	0.1700	0.0058	0.0343
16m - trial 3	0.0106	0.0566	0.0512	0.1183	0.0068	0.0575
16m - trial 4	0.0577	0.0714	0.0706	0.1997	0.0059	0.0295
16m - trial 5	0.0289	0.0714	0.0745	0.1748	0.0082	0.0469
16m - trial 6	0.0764	0.0573	0.0535	0.1872	0.0024	0.0129
15m - trial 1	0.0829	0.0702	0.0693	0.2225	0.0040	0.0178
15m - trial 2	0.0457	0.0545	0.0500	0.1501	0.0041	0.0274
15m - trial 4	0.0053	0.0237	0.0173	0.0463	0.0025	0.0539
15m - trial 5	0.0385	0.0366	0.0371	0.1122	0.0025	0.0219
15m - trial 6	0.0234	0.0398	0.0405	0.1036	0.0040	0.0385
14m - trial 1	0.0314	0.0589	0.0488	0.1391	0.0053	0.0384
14m - trial 3	0.0232	0.0275	0.0278	0.0785	0.0022	0.0286
14m - trial 4	0.0128	0.0235	0.0195	0.0559	0.0021	0.0379
14m - trial 5	0.0163	0.0269	0.0234	0.0666	0.0024	0.0358
14m - trial 6	0.0112	0.0186	0.0219	0.0517	0.0020	0.0396

Table 5.5: Peak forces recorded by each sensor and the resulting total horizontal force and moment for all experiments.

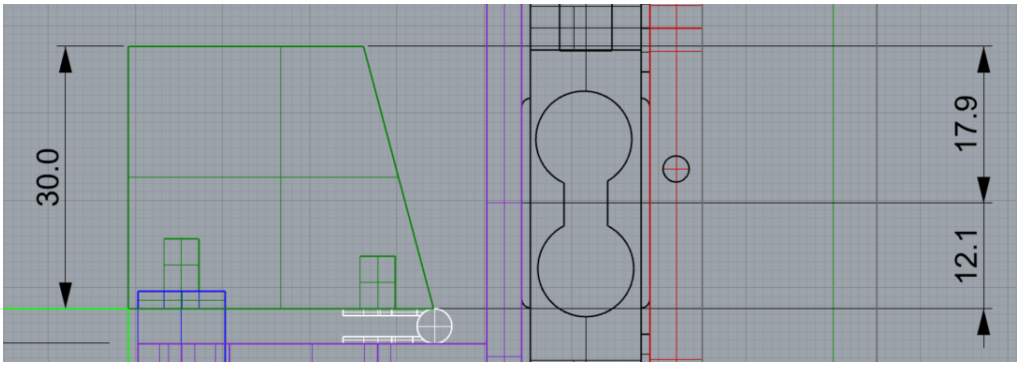

Figure 5.20: Distance between on deck box edges from the the center of the sensors' supports.

Focus was shifted on the generated moments for locating the reason of the abnormal values on the resulting horizontal greenwater leverarms. The first investigations took place for the higher rangens of the wave heights simulated. The original hypothesis was that judging from the experimental video feedback, the overtopping volume of water passed the deck box and got onto the supporting plating system, as can be seen in (Fig.5.21) from the camera feedback. At the time instance of the peak force, which was cross examined using the synchronised force sensors recordings, the fluid had not reached the rigid back-plate where the force sensors were supported, except for a few droplets. Thus, it could be assumed that the contribution on the total horizontal force was insignificant and not considered. However, the weight of the fluid on the box and the side flows around it, was ultimately transferred on the horizontal part of the support plate, and thus into the force sensors as an additional moment Assuming that the loading had an almost triangular distribution, which was support by (Fig.5.21), the equivalent resulting force could be roughly placed on the lower one third of the front side of the box. Examining (Fig.5.20) it was concluded that the point of application was lower than the center of the supports. This resulted in creating an anti-clockwise moment, which had the same direction as the extra moment created from the weight of the fluid on the horizontal part of the rigid plates, explaining the additional length when calculating the lever-arm.

The weight of the fluid overflowing the deck structure could explain the high wave ranges, since the the point of applications could only reduce in height from the 20m waves, meaning that the additional moment works together leading to an increased lever-arm length. However, the above hypothesis could not explain the cases when the wave heights were not strong enough to cause the fluid to overtop the deck structure. Examining (Fig.5.22) which depicts the 5th trial for the 14m wave height at the time instance when the sensors recorded the maximum horizontal force, the first thing stood out is the mass of water flowing underneath the ondeck box. Although, the time instant that the snapshot was taken was less than 0.3sec from the initial moment the overtopping of water first made contact with the deck structure. This time duration is very limited for a considerable amount of fluid to spill underneath the deck structure to result in any significant change in the lever arm length, therefore this hypothesis was discarded.

The second thing to be observed was that the mean water level on the sides was raised to a point higher than the lower support of the force sensor1. This could imply that the lever arm values were affected by measurements coming from force sensor1 that were being distorted by water leaking between the two rigid plates where the sensors were positioned and interacting with them specifically with the lower part of force sensor1 which coincided with its unrestricted end. This hypothesis was supported by the fact that smaller wave heights produced larger wavelengths. Moreover, the position of the model vessel was shifted a few millimeters upstream with each different wave-height range tested, meaning that the waves could potentially reach faster the model vessel than the shorter waves did, due to their size and the introducing body of water could affect the measurements faster than the higher wave-height ranges. However, this hypothesis was discarded after inspecting the force sensors recordings for the 14m wave heights which showed no abnormalities. The force sensor recordings for the 14m wave height fifth trial can be seen on the figures below (Fig.5.23-5.25).

In the end, the reason that a_{lev} acquired values that fell outside of the elevation ranges of the deck structure could not be identified for the whole range of waveheights tested. Lever arms lengths greater than the height of the wall are not physically possible, and were not used for any further result interpretation. As a consequence, no further investigations were conducted for the overturning moment of the box. Since no reliable estimation of the point of application for the horizontal greenwater loads could be established for the statically determined system, no reliable conclusions about the overturning moment could be drawn. Although, the force sensors' were considered reliable for interpreting, regarding the shipping of water loads, attention was tehn paid to the peak force acting during these events.

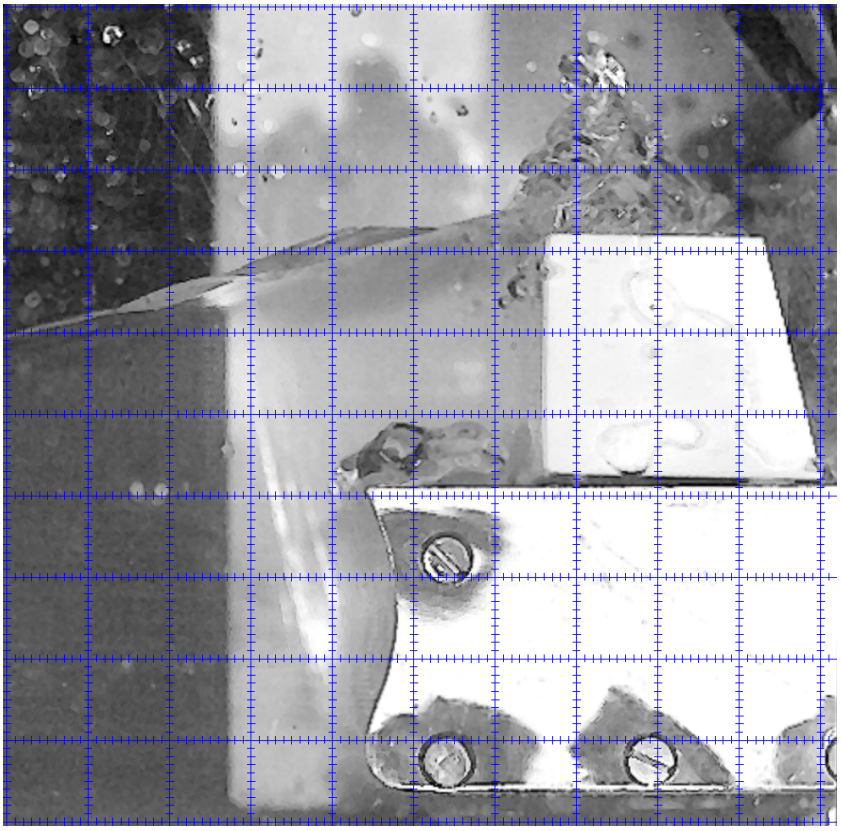

Figure 5.21: Greenwater impact during peak force time instance 20m-4trial.

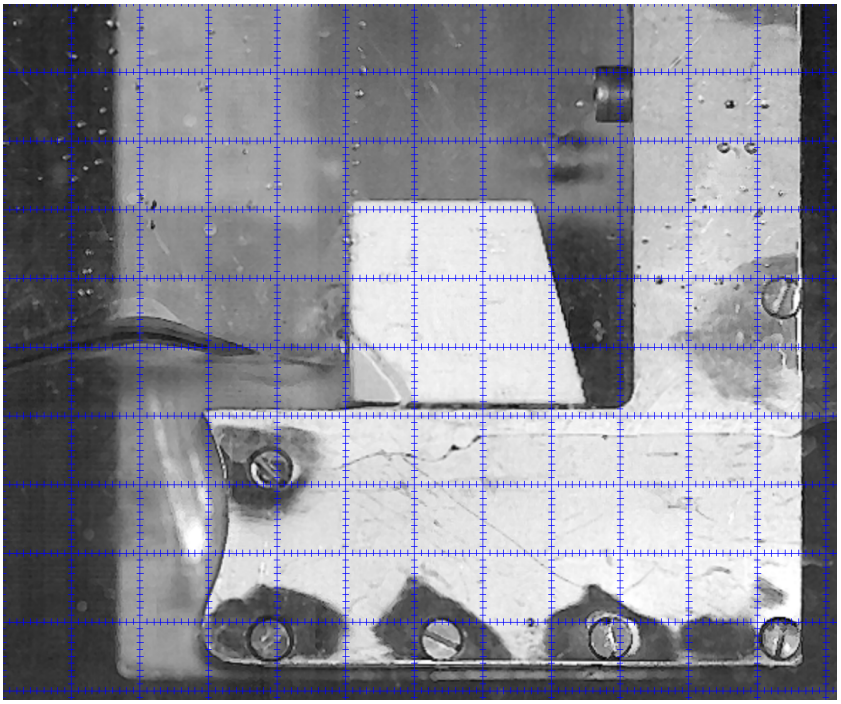

Figure 5.22: Greenwater impact during peak force time instance 14m-5 trial.

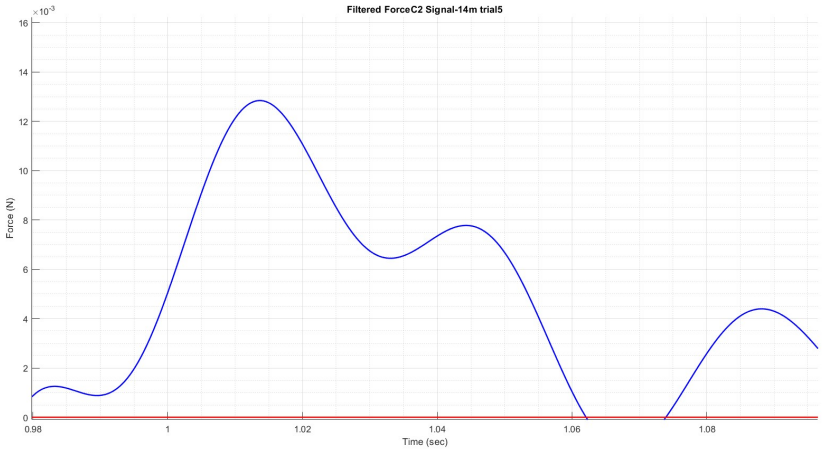

Figure 5.23: Force recording during greenwater event of sensor1 14m-5trial.

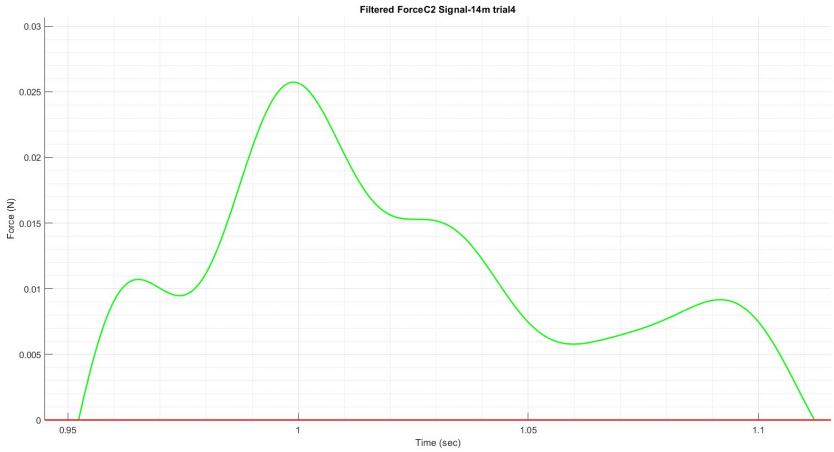

Figure 5.24: Force recording during greenwater event of sensor2 14m-5trial.

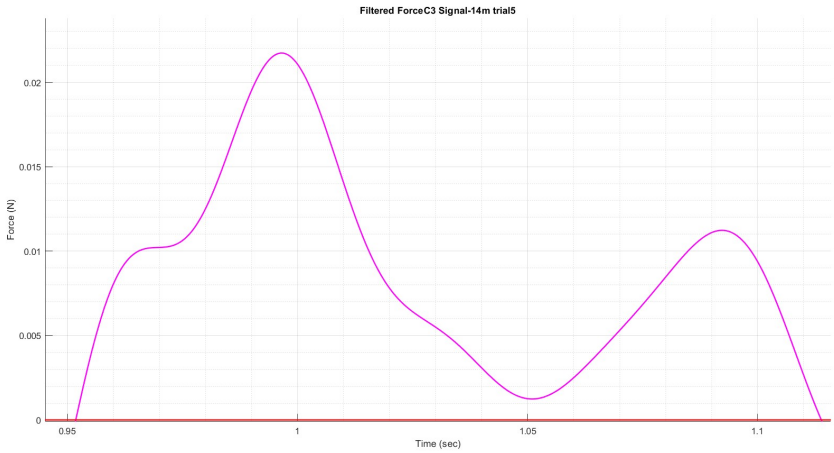

Figure 5.25: Force recording during greenwater event of sensor3 14m-5trial.

6

Discussion

This chapter involves a physical interpretation of the simulation results and an attempt to draw conclusions based on the measured quantities obtained from the experimental setup. Additionally, an examination is conducted on the outcomes of the primary objective set in current research, by identifying key parameters, and comparing between the results obtained from the CFD numerical simulations with those recorded in the experimental setup and analysing the differences.

6.1. Parametric study

After all the data collected from the recording instruments had been processed in the previous chapter, the investigations focused on looking into the intertwinement and the relationship of the parameters that affected the green water occurrences and that were controlled by the experimental configuration. Moreover, an effort was made to correlate the aforementioned quantities and their effect on the severity of certain aspects of the greenwater events which were captured during the experimental trials.

6.1.1. Resulting flow properties

Using the dam-break method for generating individual waves paired with the data gathering equipment that was used, there are limited parameters that are considered independent from each other, and at the same time can shape the greenwater phenomena. Parameters such as the the upstream water depth ,h_1, the downstream water depth ,h_0, the freeboard height ,f, and the draft D, even thought they either determine the properties of the generated wave or the greenwater event itself, they will not be examined.

This choice was based on as it was considered that further investigation of the aforementioned properties did not align with the main goals of the present research. The draft and the freeboard exceedance were measured with an accuracy of a tenth of a millimeter when the experiments were conducted. This variation would translate to a difference of 1cm in full scale. Considering the above this variance was considered negligible, and therefore these quantities were considered as constant, and provided no scientific interest into further investigating.

On the other hand the upstream and downstream water depth affect the waves generated and thus the greenwater events, however again with these quantities it was decided that examining these parameters falls better in the dam-break wave generation method. Investigating these properties stirs the focus more on the flow characteristics instead of the horizontal greenwater loading which is not the scope of the project. Instead, emphasis was given in the independent parameters of the wave elevation measured ,H_i, and the freeboard exceedance,h_e, as well as to the wave steepness ,ϵ, but to a lesser degree than the two former quantities.

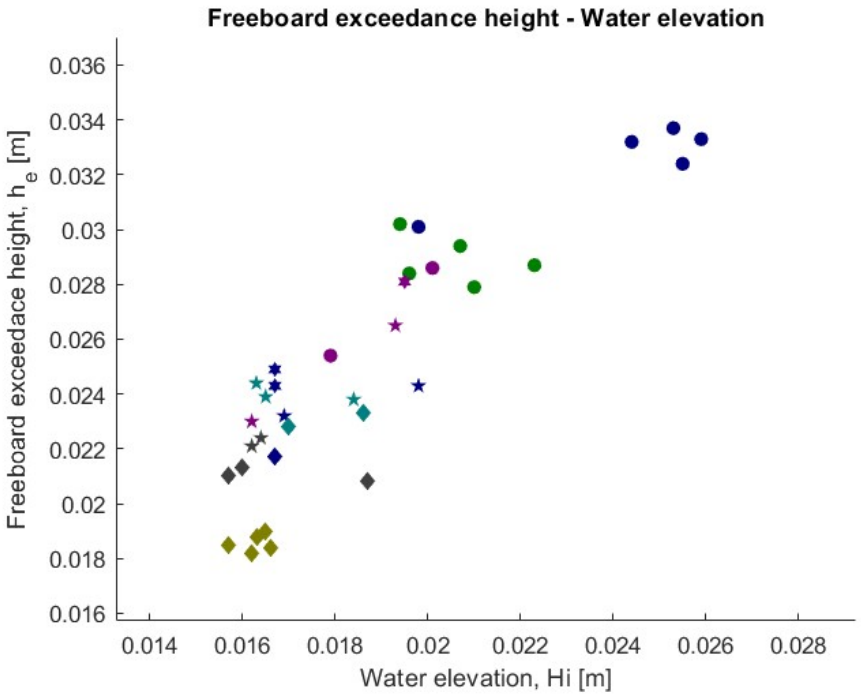

Figure 6.1: Scatter graph of the freeboard exceedance with the water elevations measurements from all experiments.

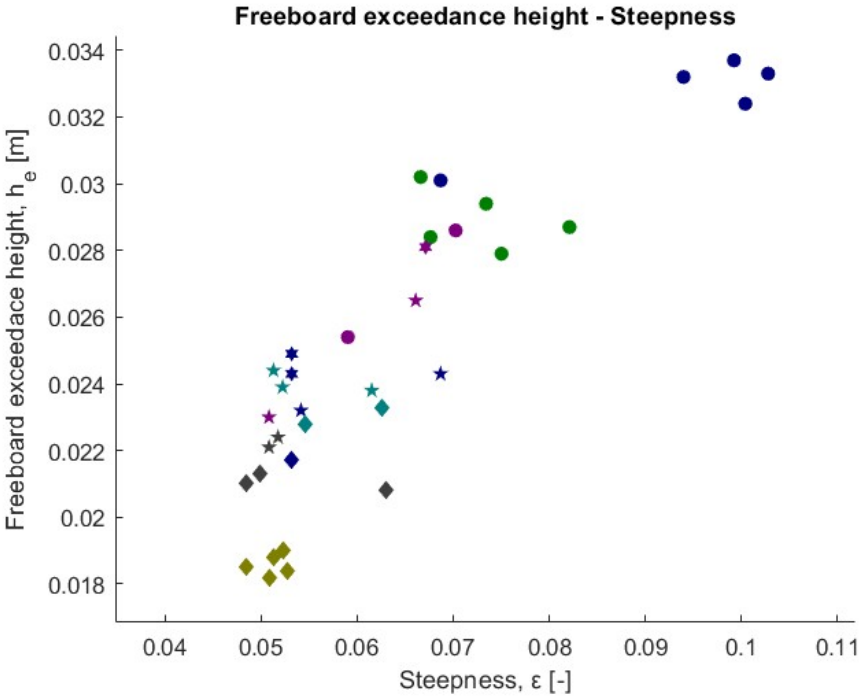

Figure 6.2: Scatter graph of the freeboard exceedance with the steepness measurements from all experiments.

In the (Fig.6.1-6.2) the scatter plots showing the correlation of the freeboard exceedance height with the measured water elevation at location 1 and the wave steepness of the generated wave. As can be seen, the trend that the points follow does not change for these two quantities. However, this was to be expected, as it was shown that with the wave generating method that was used, an equation can be derived that can describe the relationship between the H_i and ϵ parameters, (Eq.5.8).

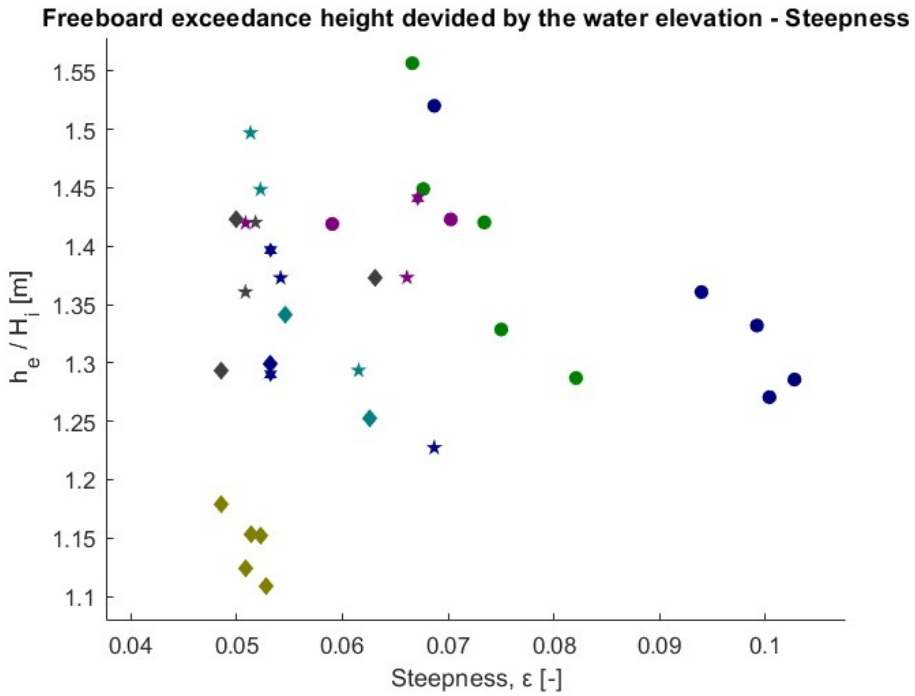

Figure 6.3: Scatter graph of the freeboard exceedance with the steepness measurements from all experiments

Trying to examine the relationship of the wave steepness and the maximum freeboard exceedance height an effort was made to eliminate the influence of the wave elevation from the freeboard exceedance measurements. This is why the dimensionless number h_e/H_i was used, where each freeboard exceedance measurement was divided with the corresponding wave elevation measurement for each experiment. The resulted scatter plot can be seen on (Fig.6.3). As can be seen, the scatter with the removal of H_i is rather high, and no clear conclusions could be made, between the correlation of the maximum freeboard exceedance and the incoming wave's steepness. The governing role of the water elevation in the freeboard exceedance became apparent, and thus focus was shifted to the relationship of the latter two quantities.

For examining the correlation between h_e and H_i the Matlab built-in Curve Fitter application was used. With the Curve Fitter app, several types of functions could be tested on the experimental data, while the application automatically fitted the desired function to match with the measurements. Additionally, this extension made possible to calculate automatically the coefficients of the functions selected for describing the measurements that produced the best fitting, while allowing to modify them, as well as to use custom functions to correlate the data. Moreover, the application calculated several indices, which described how successful was the function in correlating the measurements.

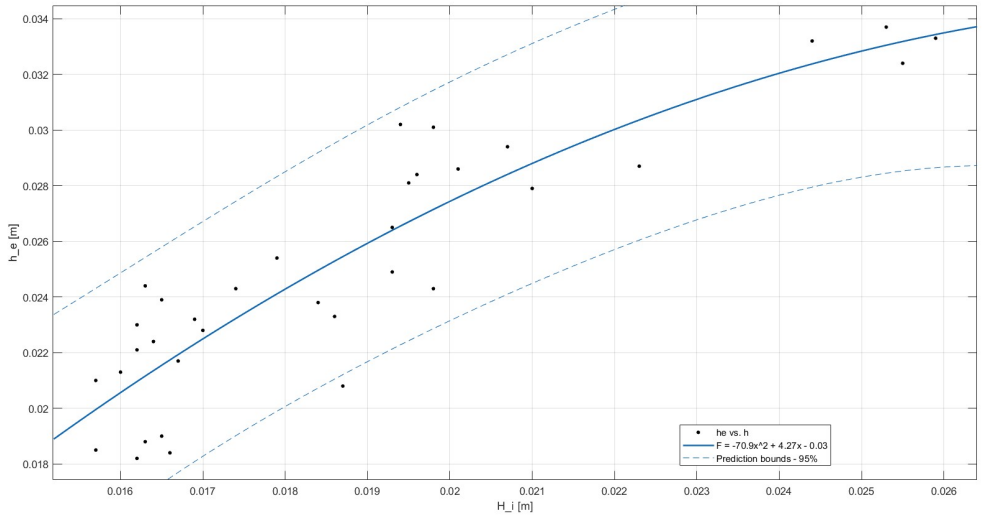

Figure 6.4: Correlation between the freeboard exceedance height and the water elevation.

In (Fig.6.4) the Curve Fitter extension was used to calculate the most appropriate curve for describing the correlation between h_e and the H_i, as well as the upper and lower 95% prediction bounds. The goodness of the fitted curve was evaluated from the R-square value calculated by the software, which is a statistical method that quantifies the proportion of the variance in the dependent variable that is predictable from the independent variable in a regression model. A second degree polynomial by visual examination, and by statistical based indices provided the best fit with an R-square value of $R^2 = 0.81$.

The literature focusing on the correlation between the incoming water elevation to the freeboard exceedance regarding greenwater events is not very extensive. In an investigation conducted by the Health and Safety Executive (HSE) of the United Kingdom in cooperation with MARIN, studied industry incidents where damaged was caused due to wave overtopping and greenwater events in 16 FPSOs and FSUs [4]. The research was conducted using 3D simulations in regular sea-states of several directions based on the vessels and had two main goals. Firstly, to analyze the greenwater susceptibility of the floating units, and secondly to perform a parametric study identifying the most crucial parameters and their effect on the greenwater loads. The freeboard exceedance was examined with waves with a significant wave heights (5m-14m) which showed an almost linear relationship.

Moreover, Hernandez et al. in [40] investigated the applicability and the benefits of using the dam-break wave generation method to create individual waves and thus individual greenwater events. On the series of experiments they conducted, the researches showed using the mean values of a group of trials that the h_e and H_i quantities are linearly correlated. However, caution should be given to the above findings, since the observations came from of trials with different upstream and water stream depth but with the same ratio, and also with different freeboard values. Therefore, the influence of additional parameters that affect shipping of water events cannot be confidently excluded.

The current findings could be partially in agreement with the above literature. Correlating the freeboard exceedance height with the water elevation using linear regression also yielded a good fit with a value of $R^2 = 0.79$, meaning that a linear relationship could also adequately describe the dependence between the h_e and H_i. As can been seen from (Fig.6.1 & Fig.6.4), the quadratic relationship becomes more fitting after incorporating the measurements from the 20m wave height where the values seem to ”distance” themselves from the trend that the rest of the observations followed.

This could imply that after a certain value of water elevation, or otherwise steeper waves $h_e > 0.09$, a break down of the linear relationship which can describe more precisely the correlation between the h_e and the H_i for lower steepness values. This could explain the observations of [4], where the highest

wave simulated corresponded to the lowest wave height produced in the experimental trials. For [40] similar claims cannot be made, since several parameters between the two setups and the measurements were different. To further support the above findings, a wider range of water heights tested, and thus water elevations would be required to broaden the range of measurements, so that a better understanding of dependence between the elevation and the freeboard exceedance could be provided.

6.1.2. Peak force parameters

After the properties of the generated incoming bore were investigated, the measurements taken from the force sensors were examined. The investigation focused on the horizontal peak force measured in each experiment, which was correlated with quantities deriving from the incoming wave. The scatter graphs of the horizontal peak force plotter against the water elevations, the wave steepness and the maximum freeboard exceedance can be see in (Fig.6.5 - 6.7) respectively.

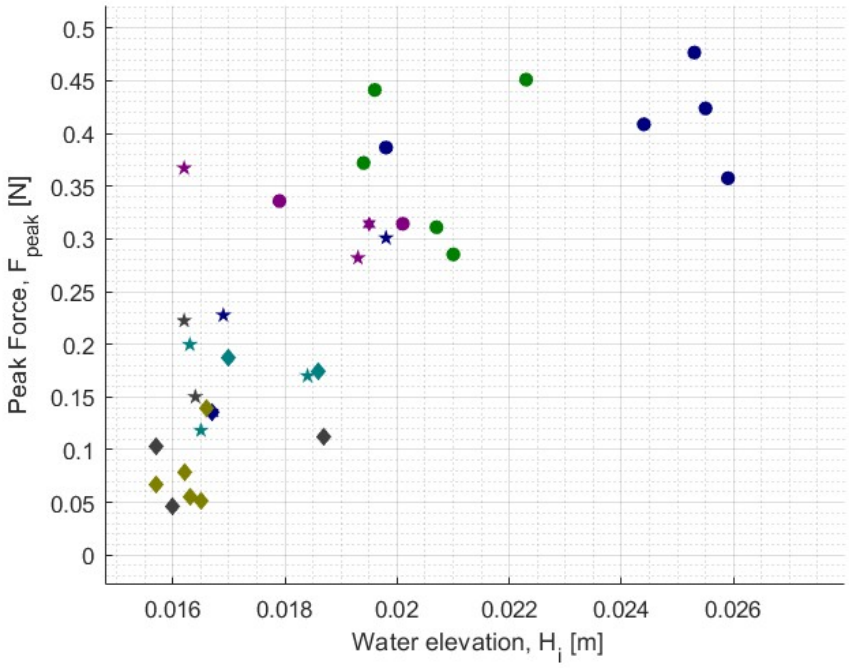

Figure 6.5: Scatter graph of the peak force with the water elevation.

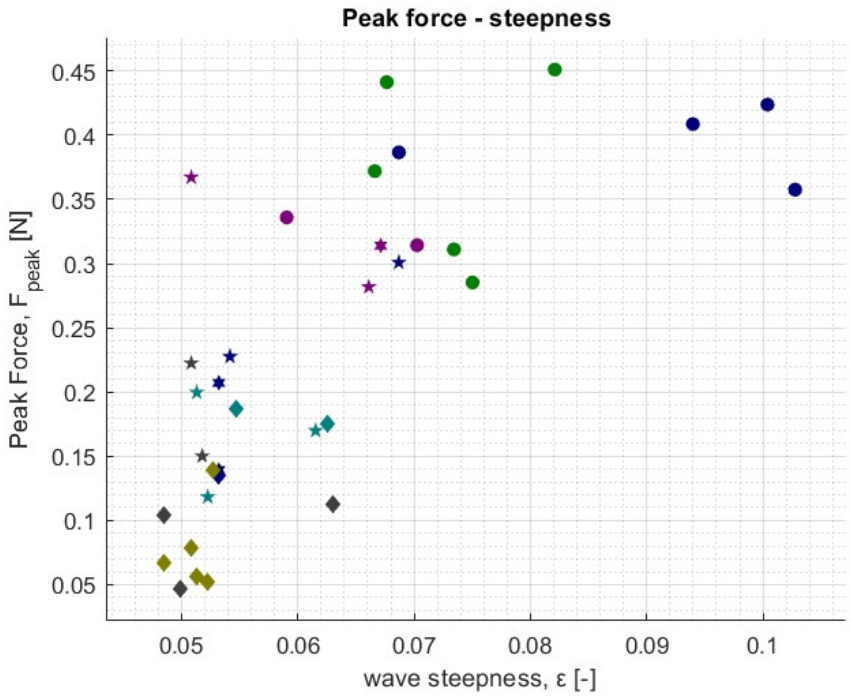

Figure 6.6: Scatter graph of the with the peak force with the incoming wave steepness.

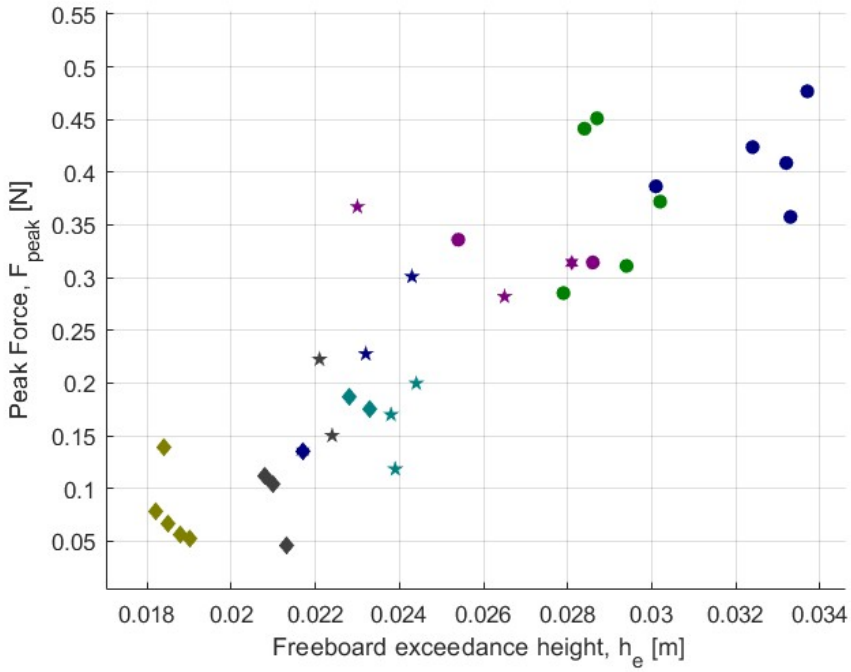

Figure 6.7: Scatter graph of the with the peak force and the maximum freeboard exceedance.

Observing the scatter graphs of the peak force with the water elevation and with the steepness, it became obvious that the horizontal loads followed the same trend for both of these quantities. This was also observed in the previous subsection examining the correlation between the freeboard exceedance with the incoming water elevation and the steepness of the generated wave. As a result, it was concluded that using the dam-break method, only limited parameters affecting the greenwater event can

be examined, since the wave length and wave steepness are heavily dependent on the water elevation which dominated the behavior of the properties of the incoming wave in the greenwater events. Therefore, the peak force was examined with regards to the the h_e and H_i measured values.

Peak force-incoming water height

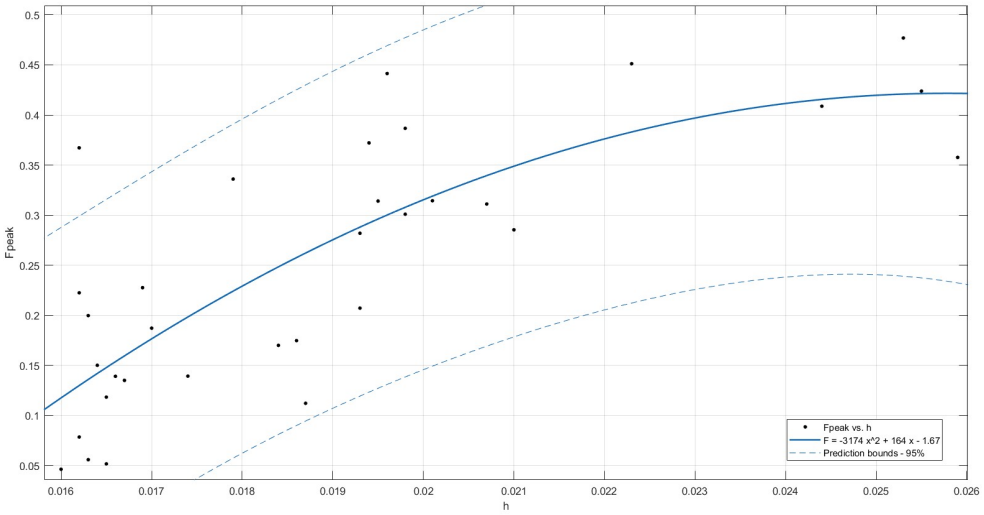

Figure 6.8: Correlation between the peak force height and the water elevation.

Similarly to the previous subsection the data collected from the experiments were used to conduct a regression analysis on the maximum horizontal loads. A quadratic function was found to provide the best description of the correlation between the maximum force and the wave elevation measured in the experimental trials, as can be seen in (Fig.6.8). The second order polynomial presented an adequate fit with an R-square value of $R^2 = 0.64$, which implied a quadratic relationship that the two quantities showed with the experimental setup that was used for the range of wave heights tested. It is noted that the model would require further validation due to the limited amount of data collected and the scarcity of measurements for several ranges of the incoming wave height.

Moreover, the curve at the end of the experimental measurements was observed to show that it reached a potential point of inflection. This could translate to the curve following a downward or upward path, or even reaching a plateau with additional measurements. Any one of the above options would create a different type of function that would best fit the correlation of the two quantities. However, upon examining the camera measurements, this trend could be explained.

For the upper range of waveheights tested from the video feedback large pockets of air were unable to escape and trapped between the bulk volume of water and the deck structure. As can be seen from (Fig.6.9), moments before the maximum horizontal force took place, two large cavities were captured within the overtopping wave. One large pocket formed at the fore aft of the bow, while another pocket formed at the mid-top part of the superstructure near the back end wall of the tank.

Closely examining the video feedback, it can be observed that from the lower part of the impacting flow a jet was developed travelling upwards. At the same time, the rapidly moving crest of the wave was able to catch up with the vertical flow trapping the large air cavity at the top part of the front wall, where the first few moments of this mechanism can be observed in (Fig.6.9). The upwards travelling jet prevailed managing to outrun the crest, while pushing the cavity towards the side. A few moments later, the accelerated crest pushed forward collapsing the pockets of air captured between the two veins of fluid, with the aerated flow and spray droplets shooting diagonally above the superstructure.

Chuang et al. [10] investigated the flow kinematics and the dynamic phenomena during wave impingement on a fixed platform during greenwater events. The researches concluded that for deck impacts the peak impact pressure decreased with higher levels of aeration, due to the cushioning effect. Similarly in the current application, it can be observed that after the top part of the wave overturned, gas was trapped near the contact area where the bulk part of the wave would later impinge, showing evidences of cushioning effects taking place during impact on the vertical wall of the superstructure.

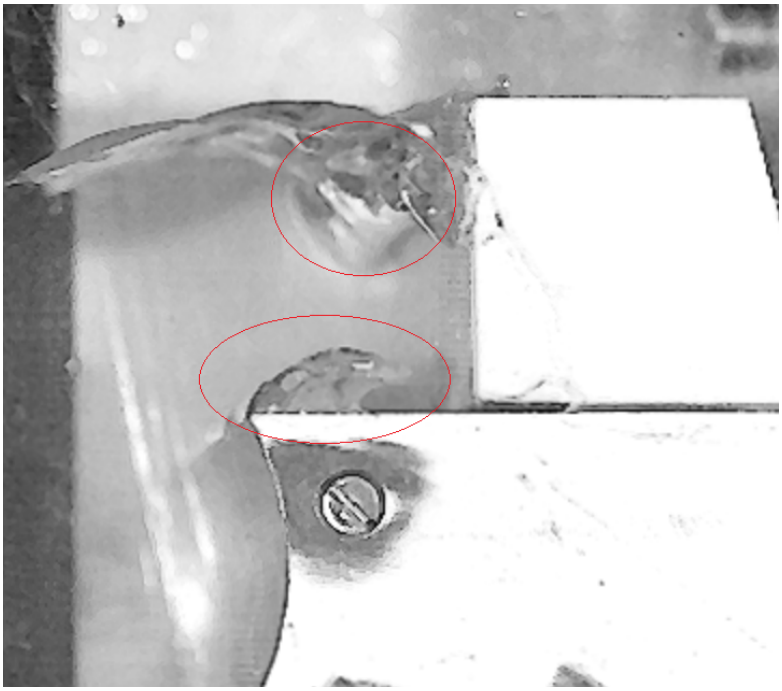

Figure 6.9: Snapshot of the horizontal impact of the on deck flow on the deck structure for the 20m-trial 4,

Additionally, as can be observed in (Fig.5.21) during the moment of the maximum horizontal load the maximum horizontal load was recorded, a part of the wave had risen higher than the deck structure overtopping it. This means that for the upper range of wave heights tested, the overtopping flow was capable of exceeding the vertical wall, thus part of the wave was unable to contribute to the total horizontal load. For larger waves this would be more evident, as a significant part of the wave would not be present, but the only increase in force would be the bulk body of water following the a trapezoid distortion from starting from the deck up to highest point of the box.

Considering both reasons, that for the larger wave heights more air entrapment took place leading to cushion effects, while the deficient vertical length of the wall lead to part of the wave not contributing to horizontal force, the point of inflection in the measurements could be interpreted. Therefore, the correlation presented in (Fig.6.8) could imply a quadratic relationship between the incoming wave height and the incoming wave height based on the experimental setup, although the findings should be treated with skepticism.

In past research more emphasis was given in wave properties like the steepness and wavelength for examining greenwater events. In the current investigation, neither quantity could be objectively examined due to the generation method of the waves, where both quantities were heavily depended on the waveheight which governed their influence over the greenwater events. Therefore, a direct comparison with previous literature cannot be applied.

From the experimental data that was gathered it can clearly be seen that increasing water elevation leads to increased horizontal greenwater loads. This is in agreement with numerous researches [8],[13], [28],[31] and other publications, in both experimental setups and simulations with various geometries

and sea-states, with all unable to provide clear conclusions regarding the correlation between water elevation and greenwater loads.

Lee et al. [32] conducted a series of experiments testing three different bow geometries of a fixed structure, in regular head waves. The researchers generated several greenwater incidents alternating either the wave height or the wave length of the incoming wave. It was observed that the peak pressures increased with an increase of the wave amplitude in all geometries and concluded, that the peak pressures increased significantly after a threshold values, which was not observed in the current trials.

Peak force-freeboard exceedance height

The correlation between the peak force and the freeboard exceedance for the experimental data from all the trials can be seen in (Fig.6.10). The data suggested a linear relationship between the quantities of h_e and F_{peak} with a coefficient of correlation equal to $R^2 = 0.78$. Both the R-squared value and the visual representation of the data shows that a linear relationship presented a good fit between the freeboard exceedance and the total force measurements gathered from the experimental setup of the current project.

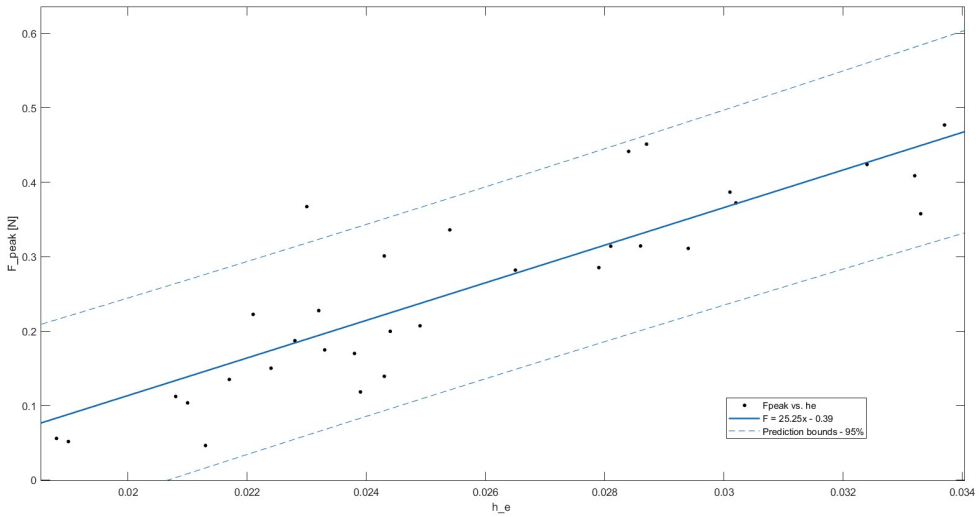

Figure 6.10: Correlation between the peak force and the maximum freeboard exceedance height.

Comparing the findings with previous literature no verification of the trend observed in the series of the experiments that were conducted could be made. Buchner in [7] conducted a series of experiments on 3D model vessels based on FPSO with elliptical and narrow bow geometries without bow flare in head-sea regular and irregular waves. The models simulated FPS0s in deep water water conditions during weathervaning conditions, and were restricted from moving. Buchner derived an empirical equations based on the data collected from the experimental trials which showed a quadratic relationship between the freeboard exceedance height and the maximum horizontal force.

Pham in his PhD Thesis [42] investigated the greenwater loads on high speed container vessels. Several experiments were conducted with three different generic container vessel geometries for deep water conditions in head sea regular waves. The model vessels were able to move in heave and pitch directions, while maintaining constant forward speed. Pham concluded that the relationship between the maximum horizontal force and the freeboard exceedance could not be determined due to the high scatter of the measured data.

Silva et al. [49] investigated the impact loads on FPSO vessels from several directions. They researchers conducted a series of experiments on a moored FPSO model vessel with three different drafts in deep water conditions. The incoming sea-state was based on recorded metocean data, and

was tested for the perpendicular and quarterly directions from the longitudinal axis of the model. Silva et al. derived an analytical equation of the horizontal force acting on deck objects that incorporated corrections coefficients and the flow velocity of the dambreak equation. The equations presented a quadratic dependency of the horizontal load to the freeboard exceedance of overtopping volume, which as the researchers concluded required further investigation, but adequately described the experimental data.

The difference between the current findings and the ones from previous literature could be attributed to several reasons as the greenwater loads are affected from several parameters including both the geometry of the vessel and the properties of the incoming flow. Firstly, in the current setup the geometry of the vessel presented more curvature compared to the simple geometries from the aforementioned literature. Additionally, in all the previous research the experiments were conducted to deep water conditions, where as in the current project the waves were in the intermediate domain. Thirdly, in the experimental trials isolated waves were used, where as in the past publications a train of waves generated by a wave maker was used. Finally, unlike previous literature the current experimental trials included 3D models, which inevitably introduced 3D phenomena.

Due to the complexity of the problem this deviation from the past findings could not be explained. However, it is noted that most possible explanations for the linear correlation observed in the experimental setup between the maximum horizontal force and the freeboard exceedance would be variables that simplified the resulting forces. Therefore, a first step for further investigations would be comparing the 2D vs 3D geometries, and then resulting relationship compared consecutive and individual greenwater occurrences.

Dimensionless study

As was underlined in previous sections greenwater is a rather complex phenomenon due to all different mechanisms taking place and variables that affect and alter its characteristics. With the dam-break method the wave height, the wavelength, and the steepness are all intertwined quantities, which at the same time are heavily dependent on the wave height. Thus, when interpreting the results and trying to make correlations between specific properties, it is really difficult to isolate the effect of a single quantity from the rest. This is why dimensionless analysis was used.

Dimensionless analysis has many different advantages. First of all it can be used to generalize results by converting physical quantities into dimensionless numbers. That way the results become more universal allowing the findings to be used in other applications with different dimensions and scales. Moreover, dimensionless analysis provides critical insights into which physical effects are governing a phenomenon, identifying dominant quantities, thus simplifying the problem and highlighting the underlying physics. The scatter plots of the dimensionless peak force with the dimensionless water elevations and maximum freeboard exceedance can be seen in (Fig.6.11-6.12) respectively.

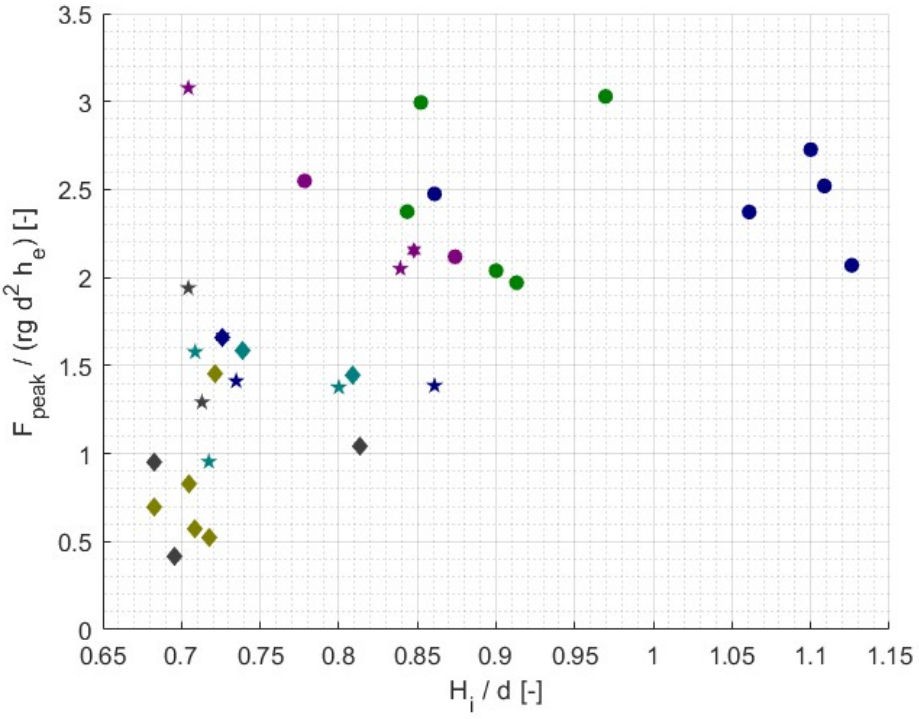

Figure 6.11: Dimensionless peak horizontal force plotted against dimensionless water elevation.

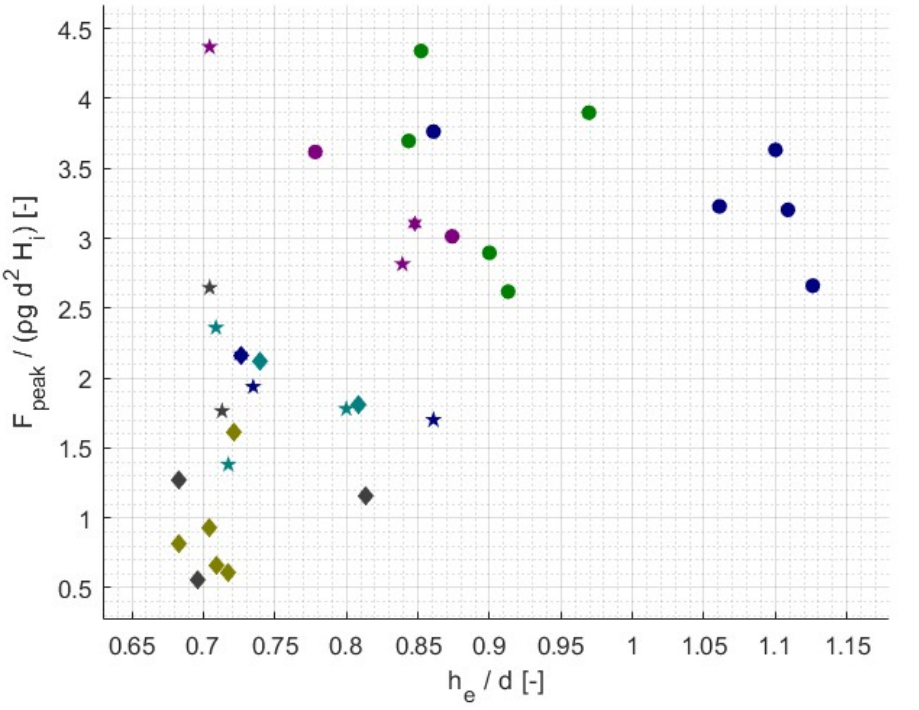

Figure 6.12: Dimensionless peak horizontal force plotted against the dimensionless maximum freeboard exceedance.

The are several different methods to make a quantity dimensionless, such as normalizing with a characteristic number of a quantity, using the Buckingham theorem, or scaling to name a few. In (Fig.6.11-

6.12) the quantities for the peak force were normalized using the liquids density ,ρ, the gravitational accelerations, the freeboard length, and then either the freeboard exceedance or the incoming water elevations, depending on the quantity plotted on the other axis.

The water density ,the gravitational acceleration and the other quantities related to length were chosen, since this way of making force dimensionless is common practice for hydrodynamic phenomena met in literature [6],[50],[22]. The freeboard was chosen for both axis since it was treated as a constant, meaning that it wouldn't affect the underlying physics of the dimensionless number, while for the other quantities was used for eliminating the influence of the freeboard exceedance height or the water height on the horizontal load while examining the other quantity.

As it can be observed from (Fig.6.11-6.12) eliminating the influence of either the h_e or the H_i parameter from the peak horizontal loads, a rather significant scattering was created. Examining both graphs, no clear correlations could be made as the data showed poor fitting for several types of curves. These observations underlined the complexity of greenwater phenomena. While the correlations of each quantity that was found in the previous subsection still holds, it was concluded that it is rather difficult to isolate the influence of specific properties in the resulting greenwater event and the generated loads as their effects complement each other and shape the final outcome of the greenwater events.

6.2. Material failure

The main goal of the current project was to investigate failure caused by greenwater loads acting on the deck structure of the model vessel. Using the experimental setup material failure could be identified as the opening of the box structure that was held by hinge supports placed at the leeward side of the superstructure. If the box opened the incident would be marked as material failure. However, no observation of the box opening was recorded besides slight rotation of the box in a few instances for the 20m waves. This leads to the conclusion that the main goal of the current research was not achieved. For further examination of the causes that led to this outcome the main mechanisms that were expected to lead to material failure during shipping of water events were put under the microscope.

As it was mentioned in previous chapters, typically during the first stages of greenwater events a large body of water will exceed the freeboard. In general, depending of the type of shipping of water scenario taking place, the fluid will present an initial impact on the deck of the structure with a jet forming, while the bulk body of water will follow propagating further inwards toward the deck. Then, a first direct impact will take place on the deck structure from the fast moving jet. As the event unfolds the impact surface increases in height as the main body of the fluid reaches the superstructure. Due to the small compressibility of the water, the momentum transfer of fluid will lead to pressure built-up which is released by a second jet shooting upwards along the deck structure. The fluid will reach its final height when all the kinetic energy is transformed into potential energy and the gravitational pull will dominate the behaviour of the flow forcing the water to impinge once more onto the deck. Throughout the duration of all these different stages, strong gas-fluid interactions will take place which affect the peak pressures as well as the resulting force exerted on the superstructure.

Material failure in real life application occurs when the strength of the material is exceeded. In an controlled experimental setup such as the current research failure can also occur after the values of the generated forces surpass a certain design threshold. For the configuration that was used the design value was expected to be exceeded during the peak forces of the upper range of the wave heights tested. The distribution of the total pressure and forces during shipping of water occurrences follows a distinct "church roof" shape distinctive which often met in other impact phenomena. The time instance where the maximum global forces may appear depends on case specific characteristics, as the maximum pressures might appear at the later stages of the greenwater loading when the fluid is accelerated by the gravitational pull downwards towards the deck [17]. In the present application during the series of experiments conducted, after force sensors' measurements had been processed and examined, it was observed that for all trials the horizontal force took place during the direct impact of the jet on the deck structure, while the jet surface was increasing in height, with the time instance differing between

experiments depending on the wave height tested and the type of greenwater event that was recorded. Therefore, the deviance in the expected behaviour between the design and the experimental phases should focus on that time window.

6.2.1. Numerically estimated and measured forces comparison

First suspect for material failure not being able to be observed during the experimental trials is the peak forces recorded in situ and their diffence between the corresponding numerical values that were expected. In the table below (Tabl.6.1) the values of the mean peak horizontal forces measured by the sensors, the numerical values, and the relative error between these quantities are shown. The resulting moments were not compared because of the high variance and uncertainty of the experimentally recorded values, as was mentioned in the previous chapter.

Wave height	Mean max. horizontal force	Simulation horizontal forces	Relative error
Abbrev.	$F_{hor,mean}[N]$	$F_{sim}[N]$	e_{rel} [%]
20m	0.411	1.85	350
19m	0.31	1.50	384
18m	0.323	1.40	334
17m	0.202	1.27	529
16m	0.170	0.92	441
15m	0.127	0.72	467
14m	0.100	0.51	412

Table 6.1: Mean max peak forces recorded during trials and estimated peak forces from the numerical simulations.

Calculating the relative error between the simulations and the experimental values it can be easily observed that ComFLOW overestimated the forces for all the wave ranges tested. Numerical values were 330-530% larger showing that the simulations were unable to adequately capture greenwater loading mechanisms. This deviation between the estimated and the recorded values was expected to a certain degree, as the greenwater multi-phase flow, flow instabilities,cavity behaviour and fluid compressibility effects could not be fully captured by CFD simulations,as has been concluded in previous literature [17],[1].The high variation between experimental and numerical values could be attributed to multiple reasons.

Scaling effects

Heller et al. [20] investigated scale effects in subaerial landslide generated impulse waves. A series of two-dimensional experiments with different scales (1:1 - 1:4) were conducted where the researchers investigated the surface tension and influence of the boundary layer during wave generation and wave attenuation phases in a long prismatic tank with horizontal bottom. The results of the above research could correlate to the current experimental setup, as the dambreak and the landslide generated impulse wave generation methods share the same principle, where a heavy mass falls on a body of water acting as a piston producing an undular bore type of waves. Additionally, both experiments took place in intermediate waters and for describing the waves the solitary wave theory was used.Heller et al. concluded that for small experimental scales Froude similitude may significantly affect the results as fluid viscosity and surface tension become more predominant. The researchers observed that scale effects were responsible for reducing the relative generated wave amplitude. Furthermore, they concluded that the boundary layer and the surface tension through the dispersion of the waves affected the wave attenuation, and the fluid viscosity mostly affected the wave propagation zone.

In the numerical simulations, a 2D domain was used where only the cross-section of the midline of the model vessel was modeled, as the three-dimensional effects were considered negligible for the experimental setup. When defining the boundary conditions thus, the solid boundaries were set for the left and right hand side and the bottom surface of the simulation tank. This means that the flow was able only to only experience the friction effects from the bottom plate and not the side walls which

doubled the surface with which the liquid was in contact, thus significantly increased the effects of the boundary layer in the resulting flow, especially in a much smaller scale (1:400) as the current experimental configuration.

To further test the hypothesis that significant energy losses were caused by viscous effects, the Reynolds numbers for both the simulations and the experiments were calculated for the 20m wave heights. Using the ComFLOW output and the camera feedback the undular bore's celerity and water elevation could be reassured, and therefore Reynold's number $Re = \frac{vD}{\nu}$, where v the wave's celerity, D the water depth measuring from the bottom of the tank until the top of the crest, is the kinematic viscosity. The values of all the quantities can be seen in (Tabl. 6.2). For the experimental measurements the average value of the water elevation and the wave celerity measured for each trial were used. Moreover, the values were sampled from the second monitoring point as defined in (Sect.5) at the time instant where the crest top passed from that location in both simulation and experimental trials.

Measurements	v $[m/s]$	D $[m]$	ν x10^{-6} $[m^2/s]$ $(20°)$	*Re* [-]
20m - simulation	0.94	0.853	1.0034	779,103
20m - trials	0.80	0.872	1.0034	695,236

Table 6.2: Reynold numbers calculated for the numerical simulations and the mean values from the 20m experimental trials

Reynolds number shows the ration expresses the ratio between the inertial forces and the viscous forces acting on a flow. From the *Re* values estimated above it was shown that as expected the Reynold's number for the simulations was higher than the experimental trials, meaning that the inertial forces had a stronger influence in the resulting flow than in situ. However, the difference between the two Reynolds numbers calculated equal to 12.5% does not justify the large deviations between the simulations and the experimental measurements, so focus was stirred on the freeboard exceedance and the resulting deck flow.

Miller in [37] conducted a series of experiments to investigate the role of surface tension in the breaking of waves. He tested several different types of waves breaking such as solitary waves, periodic waves, and standing waves in two dimensional prismatic tanks with steady and sloped bottom using a generating piston. In the experiments different solutions were used to alter the surface tension between consecutive experiments. Miller observed that for smaller surface tension values, the solitary waves showed an increase in the steepness limit as well as the limit crest angle; smaller angles than 120deg.

Figure 6.13: Freeboard exceedance height estimated for the 20m-simulation.

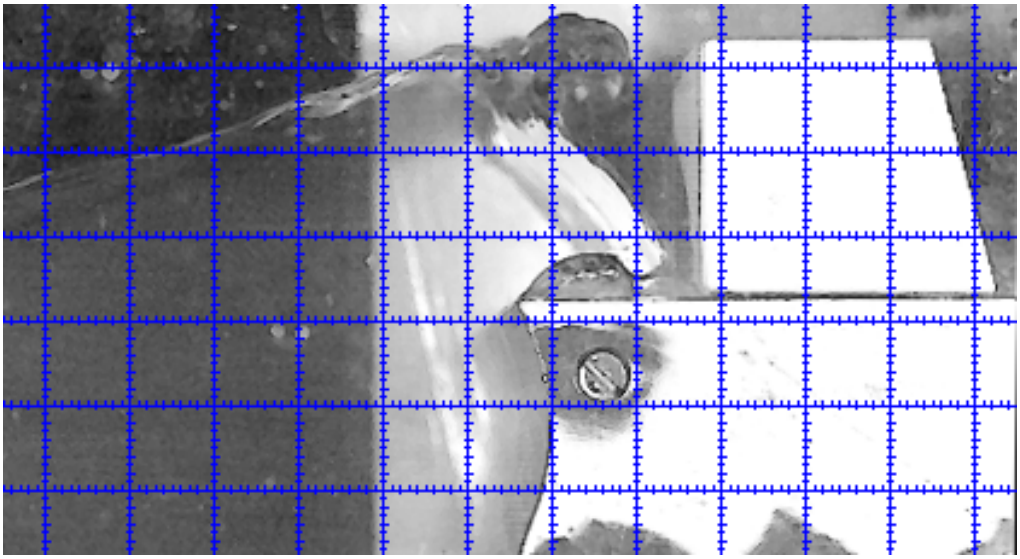

Figure 6.14: Freeboard exceedance height captured from the 20m-trial 4.

Examining the shape of the overtopping body of water, it can be seen from (Fig. 6.13-6.14) that ComFLOW was not fully able to capture the curvature during the maximum freeboard exceedance. The simulation was able to capture the deviating vein of liquid and the large air pocket trapping below the main body of water. However, ComFLOW was not able to simulate the large accelerations from the reflected pushing the wave upwards keeping it from breaking [40]. The large inertial forces dominated the behavior of the overtopping liquid against the surface tension forces, allowing the body of water to reach steep crest angles as observed by Miller, a mechanism observed throughout the range of the generated wave heights.

Nevertheless, the numerical simulation was able to capture adequately the water elevation from deck. In general, ComFLOW slightly under-predicted the maximum freeboard exceedance height which can be seen for both the simulations and the experiments for the 20m wave (Fig. 6.13-6.14). Although, the difference in freeboard exceedance elevation and the difference in curvature of the overtopping may lead to some difference between the experimental and the simulations' results, these parameters were deemed not responsible for causing the high variance observed in results.

Gas-Liquid phase interaction

Another reason between the deviation between the results was possibly attributed to the behavior of the gas pockets and and the cushioning effects that took place, especially for the upper wave heights tested. As it was more explained in detail in the previous subsection, the vertical jet created after the initial impingement of the flow onto the front wall of the box structure, managed to outrun the fluid travelling at the crest of the wave, trapping an air cavity between these two volumes. As a result, the trapped air absorbed the impact of the fluid at the mid-top part of the superstructure, which is the one that responsible for the larger proportion of the overturning moment acting on the hinge support due to the large lever-arm.

The effect of cushioning in peak pressures due to air cavities has also been observed in previous literature [10], [25]. This hypothesis could be further supported by previous literature where it was observed that the computational tools still lack the means to accurately simulate the complex behaviour and interaction of the air pockets in the two-phase deck flows [11]. As it can be seen in (Fig. 6.15), ComFLOW was able to simulate the general behaviour of the flow, although it did not accurately capture the entrapped air, and the aerated flow overtopping the superstructure. Thus, it was not capable of estimating the reduction in the overall horizontal force acting on the box structure, overestimating the expected forces, which the experimental configuration design was based of.

It is noted, that even though the presence of cushioning effects is strongly correlated with reduction

in the overall loading, it does not solely explain the large deviation between the numerical and the recorded values. Since it did not affect the bottom part of the impacting fluid profile, which included the majority of the overtopping volume, the effect of the gas-fluid interaction could not single-handedly support a deviation in results of over 350%.

Figure 6.15: Fully developed impact during the 20m-simulation.

Manufacturing imperfections

As it was mentioned before, the main mechanism that was expected to force open the box, thus indicate failure in the experimental setup, was the direct impact from the on-deck flow of the overtopping mass. This mechanism is based on the momentum transfer of the rapidly moving fluid, which due to the incompressability of water leads to pressure built-up. In the construction of the experimental setup small gaps were introduced on the sides of the deck structure and along the bottom between the superstructure and the model's deck. These gaps even thought they were equal to or less than a millimeter or 40cm or less full scale, allowed for a small percentage of the flow to escape reducing therefore the pressure build-up.

Moreover, besides the pressure losses on the contour of the box structure, the escaping mass of water with the aerated flow could possibly cause suction effects. The trapped body of water was in contact with the atmospheric pressure on one side, with the vibration caused by the small scale dynamic phenomena taking place during impact and the overturning motion of the box, the volume beneath the box-structure tended to increase. This increase in volume combined with the non-pressurized front surface of the flow, could potentially create a suction force which spanned throughout the width of the experimental setup, therefore considerably hindering the work of the destabilizing greenwater forces.

In summary, without being able to identify a main source that led to the main goal of the Thesis to not be met, there were several sources that to a certain extent affected the experimental trials. When all the aforementioned reasons are added up, there are strong evidences that the large differences observed between the estimated and the recorded forces can be reasoned with, as to why a different outcome than the one expected to be achieved with the present research did result in the end. However, it is highlighted that with supplementary modifications in the existing experimental setup, which are going to be discussed in the following chapter, material failure caused by greenwater loads could be captured under a controlled environment such as the present laboratory experiments and critical conclusions to be drawn.

7

Recommendations

In this section several aspects of the graduation project are evaluated and further suggestions are provided based on the methods utilized in several different stages of the research. In the meanwhile, aspects that could be further investigated in the future are mentioned.

Experimental Scale

First topic is the experimental scale. The scale of the experiment was based in the pre-existing tank that was used for hosting the experiments. The idea behind this decision was that a small scale experiment would be easily manipulated in aspects such as resetting the experiments,and automating all components of the experimental setup from the trigger mechanisms to the data gathering instruments. Moreover, a small scale experimental configuration would provide a time-wise efficient practise to run additional experiments if needed,and gather larger amount of data for further investigations.

However, the small scale used for designing the experiment lead to hindrances which could not be identifying a priori. The post processing of the results gathered from the force sensors, was susceptible to significant level of ambient noise, not based on the instruments used, but due to the weak forces exerted on the experimental setup from the small scale of the experiments. In order, to avoid high noise pollution and uncertainty several frequencies had to be removed and the resulting forces to ultimately show smaller values that the ones actually taking place.

Furthermore, the small scale of the experiment also made reproduced phenomena more susceptible to scale effects like boundary layer effects and surface tension effects. Small imperfections like small tilts and opening in the experimental setup would affect the recordings, which are aspects, f.e smaller forces that did not lead to failure of the setup, which could not be anticipated in advance even when using numerical simulations for the design process.

For this a larger scale than the one used (1:200, 1:100) where the maximum generated wave of 20m is reproduced as a 10cm or 20cm wave respectively would eliminate a lot of uncertainties and improve the quality of the experimental results gathered.

Wave Generation

For the wave generation the dam break method was used. The dam-break method presents several advantages when producing greenwater events. Firstly, it is an easy to use and inexpensive method to create individual waves. By adjusting the water depth upstream and dowstream of the water gate, a wide range of several types of flows can be generated (undular bores, breaking waves, hydraulic jumps). Moreover, by creating individual waves, single greenwater events can be created where the interaction between the wave and the structure is not affected by residual flows, thus allowing for an easier and more profound investigation into the greenwater events. Finally, the dambreak method is a proven method which has been used in several researchers, contains analytical equations expressing the characteristics of the resulting flow and has an extensive literature where it has been used.

The downside of the dambreak method is that the main parameter affecting the properties of the wave is the generated wave amplitude. The wave's amplitude thereof determines the wavelength and period of the generated flow along with its steepness. Even thought dam-break as a wave generation method, is very reliable in reproducing experiments under similar conditions and generating all the observed types of greenwater events, being ideal for examining the characteristics of each greenwater scenario, presents limited applicability when examining how different parameters that determine and alter greenwater events affected the phenomenon, due to the small variability in can offer in the generated waves' characteristics.

For this reason the focused wave method is suggested. The focused wave method is a technique used to generate waves, where wave components are set up using the different combined waves. These components can represent different wave types (such as regular waves, irregular waves, or solitary waves) with specific frequencies, amplitudes, and directions. This is achieved by focusing the energy of these wave components at a specific location within the tank.
By adjusting the phase relationships and amplitudes of the individual components, the resulting wave field converges at the desired (focal) point. The advantages of this method include customizability, where the generated waves can me modified to keep several wave properties steady while altering a single property, which can be highly utilized when conducting a parametric study on how these parameters affecting the greenwater events if altered, while focusing an a single parameter per greenwater type.

Experimental Setup

The experimental setup used, contained several different components that required designing and configuration. However, the experimental setup was considered successful in generating the phenomenon at hand, recording several aspect of greenwater events that could be used for drawing results and in general capable for achieving the core goals that were set for the current project.

Some aspects that could be further improved or modified in the future, would be the length of the tank. The generated flow being in a confined short span space showed strong reflection influences the back of the tank, especially for the larger wave heights simulated. At the same time for the smaller wave heights the length of the wave shortly after it had been generated would reach the length of the tank. Emphasis could be given in a larger tank where the effects of the wave length would be minimized or could be investigated, along with the effects of the length in the wave propagation, and also the effect of the reflection caused by the model structure.

Another aspect that could be further improved would be the deck structure and the mounting mechanism. As it was observed during the experimental trials, the overtopping fluid of volume would exceed the height of the deck structure, leading to a mass of water transferring its weight on the supporting plates, and thus generating additional moments which could not be measured during the trials affecting the deflections and therefore the recordings of the force sensors. Furthermore, as the incoming body of water after the initial jet impact on the vertical wall of the deck fracture was increasing in height, the vertical dimension of the wall was fully utilized and a part of the incoming wave could not contribute anymore to the greenwater loading as there was not surface to come in contact with.

For this reason two alternative solutions are presented. Firstly, a longer vertical L shaped superstructure with wedge type stiffeners, which could capture all of the impacting water's profile, while being able to transfer the loads to the supports plate using the same magnet-hinge supports statically determined system, while remaining light enough, so that the weight of the box structures has the minimum impact on the shipping of water loads . That way the restoring force of the box could almost solely rely on electric magnet introducing a vertical reaction, leading again to system where all the loads could be estimated by simple hand calculations from the force sensors' measurements.

Finally, a 2D dimensional setup was deemed rather successful focusing on the main aspects of the greenwater events that needed investigating, collecting all the required data that would be used for later for later examination, while providing ease of application and simplicity in the experimental trials. However, a wider field of view would be recommended as the characteristics of the incoming flow were

limited, especially for the smaller waveheights simulated where the model vessel was shifted in a forward position.

Furthermore, it is suggested utilizing the wide applications of the high speed-camera, and the advantages of camera feedback in measuring quantities such as velocities, waveheights, freeboard exceedance elevation and others, coupled with an image post processing software. This way a reliable estimate of the quantities such as the overtopping volumes, combined with the cameras inherit time measuring, could provide useful insight in further investigation about the momentum and volume of the overtopping fluid, the contour profiles of the deck flow, which are properties which could shed light into further understanding of the phenomenon, and the complex interaction of its submechamisms.

References

[1] Omar S. Areu-Rangel et al. “Green water loads using the wet dam-break method and SPH”. In: *Ocean Engineering* 219 (Jan. 2021). ISSN: 00298018. DOI: 10.1016/j.oceaneng.2020.108392.

[2] M. Barcellona et al. “An experimental Investigation on Bow Water Shipping”. In: *Journal of Ship Research* 47.4 (Dec. 2003), pp. 327–346.

[3] *Experimental And Numerical Investigations On the Green Water Effects On FPSOs*. Vol. All Days. International Ocean and Polar Engineering Conference. May 1998, ISOPE-I-98–043.

[4] BOMEL Limited. *Analysis of Green Water Susceptibility of FPSO/FSU’s on the UKCS*. Offshore Technology Report 2001/005. Ledger House, Forest Green Road, Fifield, Maidenhead, Berkshire SL6 2NR, United Kingdom: Health and Safety Executive, 2001.

[5] A.D. Boon, N.P.M. van der Molen, and P.H.A.J.M. van Gelder. “Probability and distribution of green water events and pressures”. In: *Ocean Engineering* 264 (2022), Page Range. DOI: DOI.

[6] B Buchner. *The Impact of Green Water on FPSO Design*. 1995. URL: http://onepetro.org/OTCONF/proceedings-pdf/95OTC/All-95OTC/OTC-7698-MS/1962126/otc-7698-ms.pdf/1.

[7] Bas Buchner. *Green Water on Ship-type Offshore Structures*.

[8] Bas Buchner and Arjan Voogt. “The Effect of Bow Flare Angle on FPSO Green Water Loading”. In: *Proceedings of ETCE/OMAE2000 Joint Conference Energy for the New Millenium February 14-17, 2000, New Orleans, LA OMAE 00-4092*. Maritime Research Institute Netherlands (MARIN). 2000.

[9] Subrata Kumar Chakrabarti. *Offshore Structure Modeling*. Vol. 9. Advanced Series on Ocean Engineering. Chicago Bridge & Iron Tech. Svcs. Co., Feb. 1994. Chap. 2. DOI: 10.1142/2127. URL: https://doi-org.tudelft.idm.oclc.org/10.1142/2127.

[10] Wei-Liang Chuang, Kuang-An Chang, and Richard Mercier. “Kinematics and dynamics of green water on a fixed platform in a large wave basin in focusing wave and random wave conditions”. In: *Experiments in Fluids* 59 (2018), p. 100. DOI: 10.1007/s00348-018-2554-8.

[11] G. Colicchio, M. Greco, and O.M. Faltinsen. “Domain-decomposition strategy for marine applications with cavity entrapments”. In: *Journal Name* Volume Number (Issue Number 2011), Page Range. DOI: DOI.

[12] O. M. Faltinsen, M. Greco, and M. Landrini. “Green water loading on a FPSO”. In: *Journal of Offshore Mechanics and Arctic Engineering* 124 (2 May 2002), pp. 97–103. ISSN: 08927219. DOI: 10.1115/1.1464128.

[13] Nuno Fonseca and C. Guedes Soares. “Experimental investigation of the shipping of water on the bow of a containership”. In: *Journal of Offshore Mechanics and Arctic Engineering* 127 (4 Nov. 2005), pp. 322–330. ISSN: 08927219. DOI: 10.1115/1.2087527.

[14] K. Goda, T. Miyamoto, and T. Yamamoto. “On Deck Wetness and Impulsive Water Pressure Acting on the Deck in Head Seas (in Japanese)”. In: 140 (1976).

[15] M. Greco, G. Colicchio, and O. M. Faltinsen. “Shipping of water on a two-dimensional structure. Part 2”. In: *Journal of Fluid Mechanics* 581 (June 2007), pp. 371–399. ISSN: 14697645. DOI: 10.1017/S002211200700568X.

[16] M. Greco, O. M. Faltinsen, and M. Landrini. “Shipping of water on a two-dimensional structure”. In: *Journal of Fluid Mechanics* 525 (Feb. 2005), pp. 309–332. ISSN: 00221120. DOI: 10.1017/S0022112004002691.

[17] Marilena Greco. “A Two-Dimensional Study of Green-Water Loading”. Doctoral thesis. Fakultet for ingeniørvitenskap og teknologi, 2001. URL: http://hdl.handle.net/11250/231252.

[18] "Green water loading on a floating structure with degree of freedom effects". In: *Journal of Marine Science and Technology (Japan)* 19 (3 2014), pp. 302–313. ISSN: 09484280. DOI: 10.1007/s00773-013-0249-7.

[19] B Hamoudi and K S Varyani. *Load prediction due to green water on deck mounted equipment for floating bodies*. 1994. URL: www.witpress.com,.

[20] Valentin Heller, Willi H. Hager, and Hans-Erwin Minor. "Scale effects in subaerial landslide generated impulse waves". In: *Exp Fluids* 44 (2008), pp. 691–703. DOI: 10.1007/s00348-007-0427-7.

[21] Jassiel V. Hernández-Fontes et al. "A Detailed Description of Flow-Deck Interaction in Consecutive Green Water Events". In: *Journal Name* Volume Number (Issue Number Year), Page Range. DOI: 10.1115/1.4049121.

[22] Jassiel V. Hernández-Fontes et al. "Assessing shipping water vertical loads on a fixed structure by convolution model and wet dam-break tests". In: *Applied Ocean Research* 82 (Jan. 2019), pp. 63–73. ISSN: 01411187. DOI: 10.1016/j.apor.2018.10.022.

[23] Jassiel V. Hernández-Fontes et al. "Green water on a fixed structure due to incident bores: Guidelines and database for model validations regarding flow evolution". In: *Water (Switzerland)* 11 (12 Dec. 2019). ISSN: 20734441. DOI: 10.3390/w11122584.

[24] Leo H. Holthuijsen. *Waves in Oceanic and Coastal Waters*. Cambridge University Press, 2015.

[25] Utkarsh Jain, Patricia Vega-Martínez, and Devaraj van der Meer. "Air entrapment and its effect on pressure impulses in the slamming of a flat disc on water". In: *Journal Name* Volume Number (Issue Number 2021), Page Range. DOI: DOI.

[26] Joint Committee for Guides in Metrology. *JCGM-WG2-CD-01: International vocabulary of metrology: Fourth edition – Committee Draft (VIM4 CD), 11 January 2021*. Tech. rep. Joint Committee for Guides in Metrology, 2021.

[27] K.M.T. Kleefsman et al. "A Volume-of-Fluid based simulation method for wave impact problems". In: *Journal of Computational Physics* 206.1 (2005), pp. 363–393. ISSN: 0021-9991. DOI: https://doi.org/10.1016/j.jcp.2004.12.007. URL: https://www.sciencedirect.com/science/article/pii/S0021999104005170.

[28] Ravindra Babu Kudupudi, A. Bhattacharyya, and R. Datta. "A parametric study of green water impact on a container ship". In: *Ships and Offshore Structures* 15 (3 Mar. 2020), pp. 318–324. ISSN: 17445302. DOI: 10.1080/17445302.2019.1615728.

[29] Ravindra Babu Kudupudi and Ranadev Datta. "Numerical investigation of the effect due to vessel motion on green water impact on deck". In: vol. 7A-2017. American Society of Mechanical Engineers (ASME), 2017. ISBN: 9780791857731. DOI: 10.1115/OMAE2017-61054.

[30] Guido Lauber and Willi H. Hager. "Experiments to dambreak wave: Horizontal channel". In: *Journal of Hydraulic Research* 36.3 (1998), pp. 291–307. DOI: 10.1080/00221689809498620.

[31] Gang Nam Lee et al. "Experimental study on flow kinematics and pressure distribution of green water on a rectangular structure". In: *Ocean Engineering* 195 (2020), p. 106649. DOI: 10.1016/j.oceaneng.2020.106649.

[32] Hyun-Ho Lee, Ho-Jeong Lim, and Shin Hyung Rhee. "Experimental investigation of green water on deck for a CFD validation database". In: *Ocean Engineering* 42 (2012), pp. 47–60. DOI: 10.1016/j.oceaneng.2011.12.021. URL: http://www.elsevier.com/locate/oceaneng.

[33] Per A Madsen, David R Fuhrman, and Hemming A Schäffer. "On the solitary wave paradigm for tsunamis". In: *Journal of Geophysical Research* 113.C12012 (2008). DOI: 10.1029/2008JC004932.

[34] Offshore American Society of Mechanical Engineers. Ocean. *ASME 2017 36th International Conference on Ocean, Offshore and Arctic Engineering : June 25-30, 2017, Trondheim, Norway.* ISBN: 9780791857731.

[35] M. van Meerkerk et al. "Gas flow dynamics over a plunging breaking wave prior to impact on a vertical wall". In: *European Journal of Mechanics, B/Fluids* 91 (Jan. 2022), pp. 52–65. ISSN: 09977546. DOI: 10.1016/j.euromechflu.2021.09.008.

[36] Mike van Meerkerk, C. Poelma, and J. Westerweel. “Scanning stereo-PLIF method for free surface measurements in large 3D domains”. In: *Experiments in Fluids* 61 (1 Jan. 2020). ISSN: 14321114. DOI: 10.1007/s00348-019-2846-7.

[37] Robert L. Miller. “The Role of Surface Tension in Breaking Waves”. In: (), pp. 433–449. DOI: 10.1061/9780872620490.025. eprint: https://ascelibrary.org/doi/pdf/10.1061/9780872620490.025. URL: https://ascelibrary.org/doi/abs/10.1061/9780872620490.025.

[38] H. Nakagawa et al. “Generation and Development of a Hydraulic Bore Due to the Breaking of a Dam (1)”. In: *Bulletin of the Disaster Prevention Research Institute* 19.2 (Nov. 1969), pp. 1–17. URL: http://hdl.handle.net/2433/124774.

[39] International Society of Offshore and Polar Engineers. *The proceedings of the twenty-second (2012) International Offshore and Polar Engineering Conference : Rhodes, Greece, June 17-22, 2012.* International Society of Offshore and Polar Engineers, 2012. ISBN: 9781880653944.

[40] “On the generation of isolated green water events using wet dam-break”. In: *Journal of Offshore Mechanics and Arctic Engineering* 140 (5 Oct. 2018). ISSN: 1528896X. DOI: 10.1115/1.4040050.

[41] D. H. Peregrine. “Water-wave impact on walls”. In: *Annual Review of Fluid Mechanics* 35 (2003), pp. 23–43. ISSN: 00664189. DOI: 10.1146/annurev.fluid.35.101101.161153.

[42] Xuan Phuc Pham. “Green Water and Loading on High Speed Containerships”. PhD thesis. Glasgow, Scotland: University of Glasgow, Dec. 2007.

[43] H. Qin et al. “Numerical Study of Nonlinear Freak Wave Impact underneath a Fixed Horizontal Deck in 2-D Space”. In: *Applied Ocean Research* 64 (2017), pp. 155–168. DOI: 10.1016/j.apor.2017.02.007.

[44] E. Renzi, Y. Wei, and F. Dias. “The pressure impulse of wave slamming on an oscillating wave energy converter”. In: *Journal of Fluids and Structures* 82 (Oct. 2018), pp. 258–271. ISSN: 10958622. DOI: 10.1016/j.jfluidstructs.2018.07.007.

[45] “Ritter’s dry-bed dam-break flows: positive and negative wave dynamics”. In: *Environmental Fluid Mechanics* 17 (4 Aug. 2017), pp. 665–694. ISSN: 15731510. DOI: 10.1007/s10652-017-9512-5.

[46] P. J. Roache. “Perspective: A Method for Uniform Reporting of Grid Refinement Studies”. In: (1994). P.O. Box 9229, Albuquerque, N.M. 87119.

[47] S.Takezawa, K. Kobayashi, and K. Sawada. “On Deck Wetness and Impulsive Water Pressure Acting on the Deck in Head Seas (in Japanese)”. In: *Zosen Kiokai, SNAJ* 141 (1977).

[48] Leonard E. Schwer. “Is Your Mesh Refined Enough? Estimating Discretization Error using GCI”. In: *LS-DYNA Anwenderforum*. Bamberg, Germany: DYNAmore GmbH, 2008, Chapter 7.

[49] Daniel F.C. Silva, Alvaro L.G.A. Coutinho, and Paulo T.T. Esperança. “Green water loads on FPSOs exposed to beam and quartering seas, part I: Experimental tests”. In: *Ocean Engineering* 140 (2017), pp. 419–433. ISSN: 0029-8018. DOI: 10.1016/j.oceaneng.2017.05.033. URL: https://www.sciencedirect.com/science/article/pii/S0029801817304483.

[50] Carlos Guedes Soares and Other Author. “Experimental Study of the Probability Distributions of Green Water on the Bow of Floating Production Platforms”. In: *Journal of Offshore Mechanics and Arctic Engineering* (2005). DOI: 10.1115/1.1951773. URL: https://www.researchgate.net/publication/245363606.

[51] Youn Kyung Song et al. “Surface velocity and impact pressure of green water flow on a fixed model structure in a large wave basin”. In: *Ocean Engineering* 104 (2015), pp. 40–51. ISSN: 0029-8018. DOI: 10.1016/j.oceaneng.2015.04.086. URL: https://www.sciencedirect.com/science/article/pii/S0029801815002377.

[52] P.K. Stansby, A. Chegini, and T.C.D. Barnes. “The initial stages of dam-break flow”. In: *Journal of Fluid Mechanics* 374 (1998), pp. 407–424.

[53] J.J. Stoker. *Water Waves, the Mathematical Theory with Applications*. New York: Interscience Publishers Inc., 1957.

[54] Rik Wemmenhove. “Numerical Simulation of Two-Phase Flow in Offshore Environments”. PhD thesis. May 2008.

[55] Shaolin Yang et al. “Experimental and numerical study on the evolution of wave front profile of dam-break waves”. In: *Ocean Engineering* 247 (Mar. 2022). ISSN: 00298018. DOI: 10.1016/j.oceaneng.2022.110681.

[56] Xiantao Zhang et al. “Eliciting features of 2D greenwater overtopping of a fixed box using modified dam break models”. In: *Applied Ocean Research* 84 (2019), pp. 74–91. DOI: 10.1016/j.apor.2018.12.001. URL: https://www.sciencedirect.com/science/article/pii/S0141118718302987.

[57] Xiantao Zhang et al. “Numerical investigation of effects of bow flare angle on greenwater overtopping a fixed offshore vessel”. In: vol. 1. American Society of Mechanical Engineers (ASME), 2018. ISBN: 9780791851203. DOI: 10.1115/OMAE2018-77487.